UNIVERSITY OF SOUTHAMPTON

Fine tuning in non-minimal supersymmetric models

by

Maien Yahya M Binjonaid

A thesis submitted in partial fulfillment for the degree of Doctor of Philosophy

in the

Faculty of Physical Sciences and Engineering

School of Physics and Astronomy

June 2015

UNIVERSITY OF SOUTHAMPTON

ABSTRACT

FACULTY OF PHYSICAL SCIENCES AND ENGINEERING

SCHOOL OF PHYSICS AND ASTRONOMY

Doctor of Philosophy

`Fine tuning in non-minimal supersymmetric models`

by Maien Yahya M Binjonaid

This thesis is based on work that investigates the fine tuning in low scale non-minimal supersymmetric models. We present a comparative and systematic study of the fine tuning in Higgs sectors in three scale-invariant NMSSM models: the first being the standard Z_3-invariant NMSSM; the second is the NMSSM plus additional matter filling $3(5+\overline{5})$ representations of $SU(5)$ and is called the NMSSM+; while the third model comprises $4(5+\overline{5})$ and is called the NMSSM++. Naively, one would expect the fine tuning in the plus-type models to be smaller than that in the NMSSM since the presence of extra matter relaxes the perturbativity bound on λ at the low scale. This, in turn, allows larger tree-level Higgs mass and smaller loop contribution from the stops. However we find that LHC limits on the masses of sparticles, especially the gluino mass, can play an indirect, but vital, role in controlling the fine tuning. In particular, working in a semi-constrained framework at the GUT scale, we find that the masses of third generation stops are always larger in the plus-type models than in the NMSSM without extra matter. This is an RGE effect which cannot be avoided, and as a consequence the fine tuning in the NMSSM+ ($\Delta \sim 200$) is significantly larger than in the NMSSM ($\Delta \sim 100$), with fine tuning in the NMSSM++ ($\Delta \sim 600$) being significantly larger than in the NMSSM+.

Moreover, supersymmetric unified models in which the Z' couples to the Higgs doublets, as in the E_6 class of models, have large fine tuning dominated by the experimental mass limit on the Z'. To illustrate this we investigate the degree of fine

tuning throughout the parameter space of the Constrained Exceptional Supersymmetric Standard Model (cE$_6$SSM) that is consistent with a Higgs mass $m_h \sim 125$ GeV. Fixing $\tan\beta = 10$, and taking specific values of the mass of the Z' boson, with $M_{Z'} \sim 2 - 4$ TeV. We find that the minimum fine tuning is set predominantly from the mass of Z' and varies from $\sim 200 - 400$ as we vary $M_{Z'}$ from $\sim\ 2 - 4$ TeV. However, this is lower than the fine tuning in the Constrained Minimal Supersymmetric Standard Model (cMSSM), of $\mathcal{O}(1000)$, arising from the large stop masses required to achieve the Higgs mass. Finally, it was found that varying $\tan\beta$ below and above 10 does not correspond to lower fine tuning in the cE$_6$SSM, nor does lowering the mass of the Z' by lowering its associated coupling g'.

Contents

List of Figures

List of Tables

Nomenclature

Metric	$-+++$
SM	The Standard Model
QFT	Quantum Field Theory
DM	Dark Matter
LH	Left handed
RH	Right handed
QED	Quantum Electrodynamics
EWSB	Electroweak Symmetry Breaking
VEV	Vacuum Expectation Value
RGE	Renormalisation Group Equation
SUSY	$\mathcal{N} = 1$ Supersymmetry
MSSM	Minimal Supersymmetric Standard Model
NMSSM	Next-to-minimal Supersymmetric Standard Model
E_6SSM	Exceptional Supersymmetric Standard Model
GUT	Grand Unification Theory
LSP	Lightest Supersymmetric Particle

Author's Declaration

I declare that this thesis has been written by myself. Chapters two and three contain literature review material that is well known in the main textbooks and pieces of work by others, which have been cited.

Chapter four is based on original work carried out by myself under the supervision of my supervisor Prof. Stephen F. King. Sections 4.1 to 4.6 are published in:

- PHYSICAL REVIEW D, Volume: 90, Issue: 5, Article Number: 055020, Published on SEP-22-2014 under the title: "Naturalness of scale-invariant NMSSMs with and without extra matter". By: Maien Y. Binjonaid, and Stephen F. King.

Section 4.7, which is work carried out by myself under the supervision of Prof. Stephen F. King, is original to this thesis.

Chapter five is based on original work carried out by myself under the supervision of Prof. Stephen F. King and Dr. Peter Athron. Sections 5.1 to 5.5 are published in:

- PHYSICAL REVIEW D, Volume: 87, Issue: 11, Article Number: 115023, Published on JUN-21-2013 under the title: "Fine tuning in the constrained exceptional supersymmetric standard model". By: Peter Athron, Maien Binjonaid, and Stephen F. King.

Section 5.6.1, which is work carried out by myself under the supervision of Stephen F. King, is based on work that was presented in the 7th Saudi Students Conference in the

UK, held in Edinburgh between 1-2 Feb 2014. The abstract is published in the proceedings of the conference (ISBN: 9780956904522), under the title: "More on the naturalness of the constrained exceptional supersymmetric standard model". By: Maien Y. Binjonaid and Stephen F. King.

Section 5.6.2, which is work carried out by myself under the supervision of Stephen F. King, is original to this thesis.

Signed:

Date:

Acknowledgements

First, I'd like to thank my parents, wife, and family for their constant encouragement, and especially my wife for her patience and understanding throughout my PhD journey.

I am very grateful to my supervisor Prof. Steve King for his support and guidance.

I'd like to thank my collaborator Peter Athron for his guidance throughout the work we have carried out together, along with Steve.

I'd like to thank Tadeusz Janowski, Marc Thomas, Miguel Romao, and Venus Keus for our many discussions on QFT and SUSY. And thanks to Prof. Stefano Moretti, Dr. Alex Merle, and Dr. Alex Stewart for the pieces of advice they gave to me during my PhD.

Finally, I acknowledge sponsorship by King Saud University in Riyadh (Saudi Arabia).

To my parents and my wife.

Chapter 1

Introduction

The SM of particle physics is a remarkably successful theory describing Nature at the smallest distance scales accessible to experiments. However, the SM is believed to be an incomplete description of Nature due to a number of observational and theoretical issues. One such issue is the hierarchy problem associated with the Higgs. The quadratic sensitivity of the Higgs mass-squared parameter (m_H^2) to the scale of new physics, be it the Planck scale at 10^{19} GeV or a scale at which heavy masses may exist (e.g. the GUT scale $M_{GUT} = 10^{16}$ GeV) means that in the absence of new physics at the low scale ($\mathcal{O}(1)$ TeV), the parameter m_H^2 will need to be carefully fine tuned, order by order in perturbation theory, against the cut-off of the new scale (or any heavy mass), thereby destabilizing the electroweak scale. For example, if new heavy states exist at the GUT scale, then the degree of tuning is roughly 1 part in 10^{32}.

Naturalness, which can be understood as the requirement that observable quantities in a given model does not possess large and unexplained fine tuning, has been a leading motivation for developing theories beyond the SM in order to overcome that huge fine tuning.

Supersymmetry is a well motivated extension of the SM. It predicts the existence of a new sector of particles in Nature at the energy scales currently probed by the Large Hadron Collider (LHC) experiment at CERN. These particles are related to the ordinary particles of the SM by a symmetry principle that flips the quantum spin by a

unit of half an integer. This means that any scalar particle in the SM (spin zero) will have a supersymmetric fermion partner (spin half), any fermion particle in the SM (spin half) will have a scalar supersymmetric partner (spin zero), and finally, any vector boson in the SM (spin 1) will have a supersymmetric fermion partner (spin half). The lightest supersymmetric particle could be neutral and stable, and have the properties of dark matter.

Finding supersymmetry is one of the major goals of particle physics experiments, and in particular the LHC. So far, the LHC has been running since 2009, it has achieved centre-of-mass energy of 8 TeV, and accumulated more than 20 fb^{-1} of data. However, there are no signs of supersymmetry yet. Moreover, the discovery of a scalar boson that resembles the Higgs predicted by the SM at the LHC is a major triumph of the SM. However, considering the hierarchy and the fine tuning problems associated with the SM, this discovery may be an indication of new physics at the $\mathcal{O}(1)$ TeV scale since such a SM-like Higgs is generally predicted by supersymmetric models.

Supersymmetric models differ in the way they predict observables, such as the mass of the Higgs and the Z bosons (m_Z), since these are derived quantities. While some models require large contributions from radiative corrections as in the MSSM, other models can, in principle, accommodate a 126 GeV Higgs at tree-level.

However, the absence of supersymmetric particles at the LHC leads to a tension between the electroweak scale and the supersymmetry scale (the little hierarchy problem). As a result, a given model becomes less attractive from the point of view of naturalness if its parameter space require large fine tuning. It is important, then, from model building point of view to learn the degree of fine tuning within a given model and whether or not it is possible to find regions in the parameter space that have low fine tuning along with correct predictions for the values of observables. This in turn enables testing the predictions of Naturalness at the LHC.

In this thesis, we review some aspects of the SM of particle physics in Chapter two. We start by discussing quarks and leptons, and their experimentally observed properties and interactions. Next, we discuss gauge symmetries that are associated with the forces of electromagnetism, and weak and strong nuclear interactions. The Higgs

mechanism of breaking the electroweak symmetry is reviewed. Next, the hierarchy problem in the SM is explained. Finally, other issues with the SM are covered.

In Chapter three, we introduce Supersymmetry and its algebra. We briefly discuss superfields. Next, we review the minimal supersymmetric standard model, and use it to layout the main concepts needed in later Chapters. These include, electroweak symmetry breaking, soft supersymmetry breaking, renormalisation group equations, and the hierarchy problem. Next, quantifying the fine tuning is discussed. Finally, non-minimal supersymmetric extensions are motivated, and the next-no-minimal and the exceptional supersymmetric standard model are briefly introduced.

In Chapter four, the fine tuning in the parameter spaces of three scale-invariant NMSSM models is considered. We discuss the main motivation to add extra vector-like states to the NMSSM. Next, we outline our procedure of calculating and implementing the RGEs of the new models in the public tool NMSSMTools. Then we present our results in six different parameter spaces. Finally, we discuss dark matter relic density constraints on the parameter space of the NMSSM with three extra $SU(5)$ states.

In Chapter five, the fine tuning in the exceptional supersymmetric standard model is discussed. A brief motivation to the E6SSM is outlined. Next, the properties of the E6SSM are introduced, and the electroweak symmetry breaking conditions are presented. Then a fine tuning master formula is presented, and the procedure to implement this formula in a private spectrum generator is presented. The results are presented for five different parameter spaces corresponding to different masses of the Z' boson. Finally, the results are discussed and conclusions are presented.

In Chapter six, we conclude the thesis.

Chapter 2

The Standard Model of Particle Physics

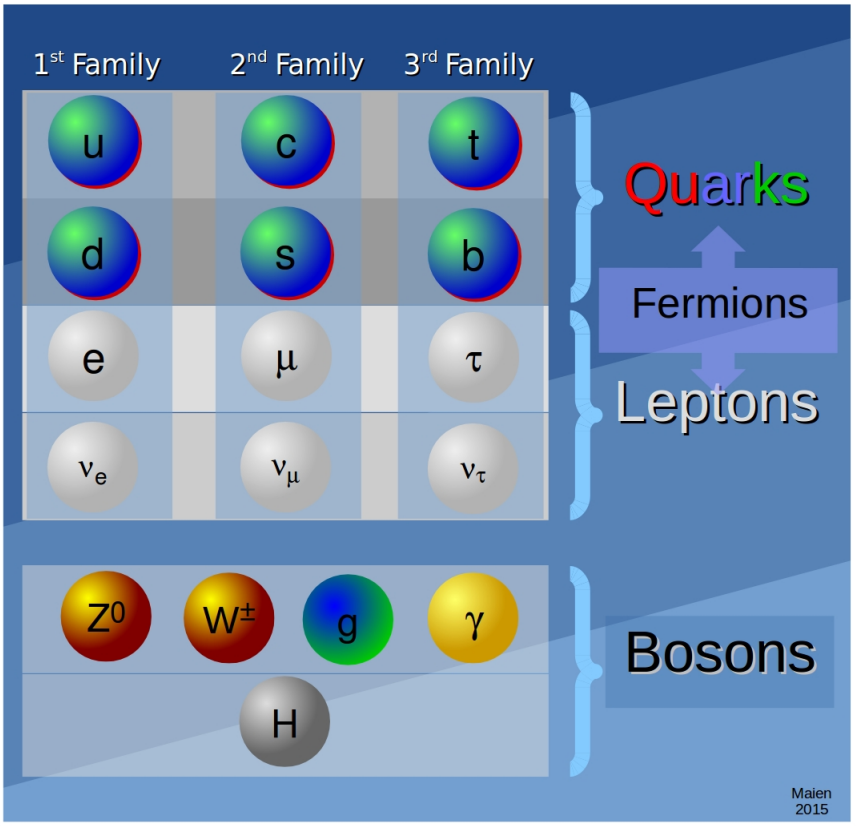

FIGURE 2.1: The Content of the Standard Model

The SM Particle Physics is a quantum gauge field theory describing quarks and leptons, and their electromagnetic, weak, and strong interactions through the exchange of gauge bosons (photons, $W^{\pm}$ and Z, and gluons). QFT consistently combines Einstein's special theory of relativity and quantum mechanics. Quantum fields are operators that satisfy canonical commutation (or anti-commutation) relations, and are non-unitary representations of the Lorentz group (rotations and boosts). These fields are Fourier expanded in terms of creation and annihilation operators, which are infinite unitary representations of the Poincare group (the combination of the Lorentz group with translations). Elementary particles found in Nature are excitations of such quantum fields. For each type of particle, there exists an antiparticle with the opposite additive quantum numbers (e.g. charge, lepton number, etc.).

The area of particle physics tries to confront these theoretical constructs with experiments and observations. Up to the date of writing this thesis, the SM is in an exceptional agreement with experiments, but there are reasons to believe that the SM does not constitute a complete description of the realm of particle physics. It is, however, believed by some to be an effective field theory that is only valid up to the $\mathcal{O}(1)$ TeV energy scale.

In this Chapter, we explore the matter content of the SM, gauge symmetries, the Higgs mechanism, the Higgs boson, and shortcomings of the SM. In particular the hierarchy problem and the fine tuning problem associated with it.

Along with the original SM papers and reviews cited, more details on the SM can be found in e.g. Refs. [1, 2, 3, 4, 5].

2.1 Matter content

As far as experiments and observations are concerned, the Universe is made of fermions and bosons. Fermions are spin $\frac{1}{2}$-n entities obeying anti-commutation relations, while bosons are spin n entities obeying commutation relations, where n is an integer. The set of spins observed in elementary particles contains: $\{0, \frac{1}{2}, 1\}$.

According to their interactions, fermions are divided into two categories: quarks and leptons. Quarks interact strongly, weakly, and electromagnetically. There are two types of quarks: up-type quarks comprising the up (u) [6, 7, 8], charm (c) [9], and top (t) [10] quarks with masses[1],

$$m_u = 2.3^{+0.7}_{-0.5}\ \text{MeV} << m_c = 1.275 \pm 0.025\ \text{GeV} << m_t = 173.21 \pm 0.51 \pm 0.71\ \text{GeV}, \tag{2.1}$$

and electric charge $q_u = \frac{2}{3}e$. Next, down-type quarks comprising the down (d) [6, 7, 8], strange (s) [6, 7, 8], and bottom (b) [10] quarks with masses

$$m_d = 4.8^{+0.5}_{-0.3}\ \text{MeV} << m_s = 95 \pm 5\ \text{MeV} << m_b = 4.18 \pm 0.03\ \text{GeV}, \tag{2.2}$$

and electric charge $q_d = -\frac{1}{3}e$. Moreover, each quark comes in three distinct quantum numbers called colours and denoted: red, green, and blue. And each quark has an anti-quark with the opposite additive quantum numbers, such as the electric charge.

On the other hand, leptons (and antileptons) are only weakly and electromagnetically interacting. They comprise three electron-like particles: the electron (e), muon (μ), and tau (τ) [12] particles with masses

$$\begin{aligned} m_e &= 0.510998928 \pm 11 \times 10^{-9}\ \text{MeV} << \\ m_\mu &= 105.6583715 \pm 35 \times 10^{-7}\ \text{MeV} << \\ m_\tau &= 1776.82 \pm 0.16\ \text{MeV}, \end{aligned} \tag{2.3}$$

and three neutrinos: the electron-neutrino (ν_e), muon-neutrino (ν_ν), and tau-neutrino (ν_τ) with extremely small masses ($m_\nu < 2$ eV). However, in the SM, these neutrinos are massless.

The previous physical particles are viewed as excitations of the corresponding quantum fields. Depending on how these fields transform under the Lorentz group, they are classified into: scalars, spinors, vectors, and tensors. For spinors, it is the two-component Weyl fermion fields that form irreducible representations of the

[1] All values of masses, couplings, and limits cited in this Chapter are from [11].

Lorentz group. Moreover, it is well-known that there is an equivalence between the Lorentz algebra and the algebra $su(2) \otimes su(2)$ [2]. Therefore, it is possible to denote fields transforming differently under Lorentz transformations by two numbers that are multiples of one-half. Specifically,

- $(0, 0) \rightarrow$ Scalar fields.
- $(\frac{1}{2}, 0) \rightarrow$ LH spinors.
- $(0, \frac{1}{2}) \rightarrow$ RH spinors.
- $(\frac{1}{2}, \frac{1}{2}) \rightarrow$ Vector fields.

A four-component Dirac fermion can be expressed in terms of two Weyl fermions as follows,

$$\psi = \begin{pmatrix} \chi_\alpha \\ \overline{\eta}^{\dot{\alpha}} \end{pmatrix}, \tag{2.4}$$

where $\alpha, \dot{\alpha} = 1, 2$, and $\overline{\eta}^{\dot{\alpha}} = (\eta^\alpha)^\dagger$.

As mentioned at the beginning of this Chapter, elementary particles interact through the exchange of gauge bosons. Table 2.1 shows some experimentally observed processes exemplifying such fundamental interactions:

Finally, it turns out that weak interactions are only communicated to LH particles and RH antiparticles. An interesting consequence is that, only LH neutrinos (RH anti-neutrinos) are found in Nature according to the SM and current observations. The possibility of RH neutrinos (LH anti-neutrinos) is the subject of new physics beyond the SM.

2.2 Gauge symmetries

Gauge field theories, such as the SM, are theories in which the free Lagrangian (i.e. non-interacting) is invariant under certain global gauge transformations of the form:

$$\psi(x, t) \rightarrow e^{iM\alpha}\psi(x, t), \tag{2.5}$$

[2] Lower case letters denote the algebra, whereas upper case letters, e.g. $SU(N)$ denote the group

Interaction	Process	Diagram
QED	$f\bar{f} \to f\bar{f}$	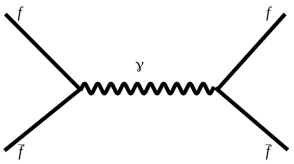
QCD	$q\bar{q} \to q\bar{q}$	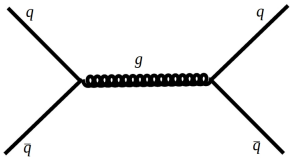
Weak	$\mu^- \to e^- \ \overline{\nu}_e \ \nu_\mu,$ $\overline{\nu}_\mu \ \ e^- \to \overline{\nu}_\mu \ \ e^-$	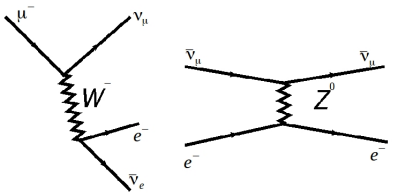

TABLE 2.1: Processes and Interactions

where α is an arbitrary parameter that is spacetime-independent, and M is the generator of the group representing the gauge transformation. Additionally, M is a number if the group under consideration is Abelian, such as $U(1)$, and a matrix if the group is non-Abelian, such as $SU(N)$ where $N > 1$.

Demanding the invariance of such Lagrangians under certain local gauge transformations (sometimes referred to as: gauging) by allowing α to be spacetime-dependant leads to the introduction of gauge bosons that interact with the matter fields. These gauge bosons are strictly massless and are self-interacting if the group is non-Abelian.

In the SM, there are three types of gauge interactions, we briefly describe them in this section.

2.2.1 $U(1)_{EM}$

QED [13, 14, 15, 16] is based on local $U(1)_{EM}$ symmetry, which is a symmetry of the vacuum. The QED Lagrangian comprises mass terms of fermionic fields, kinetic terms

of fermionic and gauge fields, and interaction term between fermions and gauge fields. It reads,

$$\mathcal{L}_{\text{QED}} = -\overline{\psi}(x)(\not{D}_\mu + m)\psi(x) - \frac{1}{4}A_{\mu\nu}(x)A^{\mu\nu}(x), \tag{2.6}$$

where $\not{D} = \gamma^\mu D_\mu$, and D_μ is the covariant derivative.

Under $U(1)_{EM}$, the field transformation is,

$$\psi(x) \to e^{iQ\alpha(x)}\psi(x), \tag{2.7}$$

where Q is the charge (zero component of the current J^μ_{em}). And $\alpha(x)$ is a spacetime-dependent (local) parameter.

The covariant derivative takes the form:

$$D_\mu = \partial_\mu + ieQA_\mu, \tag{2.8}$$

and the gauge field transforms as,

$$A_\mu(x) \to A_\mu - \frac{1}{e}\partial_\mu\alpha(x), \tag{2.9}$$

whereas the field strength tensor,

$$A_{\mu\nu} = \partial_\mu A_\nu - \partial_\nu A_\mu, \tag{2.10}$$

transform as,

$$A_{\mu\nu} \to e^{iQ\alpha(x)}A_{\mu\nu} \tag{2.11}$$

Finally, the strength of QED interactions is determined by the fine structure constant:

$$\alpha_{QED}(m_Z) = \frac{1}{128}. \tag{2.12}$$

2.2.2 $SU(3)_C$

The gauge symmetry associated with the strong interactions is the non-Abelian $SU(3)_C$ group [17] (also see [18] for a concise review), which is a symmetry of the vacuum. The Lagrangian of QCD (in terms of quarks) reads,

$$\mathcal{L}_{\text{QCD}} = -\sum_q \overline{\psi}_q(x)(\not{D}_\mu + m)\psi_q - \frac{1}{4}G^a_{\mu\nu}G^{\mu\nu}_a, \tag{2.13}$$

where ψ is a vector in colour space, q denotes quark flavours, and a is the colour index.

The quark fields transformation as,

$$q(x) \to Uq(x), \tag{2.14}$$

and

$$U = e^{i\frac{\lambda^a}{2}\alpha^a(x)}, \tag{2.15}$$

where, λ^a are the eight Gell-Mann matrices. They are the generators of the $SU(3)_c$ group, and obey the following algebra:

$$\left\{\frac{\lambda^a}{2}, \frac{\lambda^b}{2}\right\} = if^{abc}\frac{\lambda^c}{2} \tag{2.16}$$

where f^{abc} are the structure constants.

The covariant derivative takes the form,

$$D_\mu = \partial_\mu - ig_s\frac{\lambda^a}{2}G^a_\mu, \tag{2.17}$$

and by introducing the matrix notation $[G_\mu]_{\alpha\beta} = \left(\frac{\lambda_a}{2}\right)_{\alpha\beta} G^a_\mu$, the gauge fields transform as,

$$G_\mu \to U^{-1}G_\mu U + \partial_\mu U U^{-1}, \tag{2.18}$$

while the field strength tensor transforms as,

$$G_{\mu\nu} \to UG_{\mu\nu}U^\dagger, \tag{2.19}$$

where,

$$G_{\mu\nu} = \frac{\lambda^a}{2} G^a_{\mu\nu} = \frac{\lambda^a}{2} \left(\partial_\mu G^a_\nu - \partial_\nu G^a_\mu - g_s f^{abc} G^b_\mu G^c_\nu \right) \tag{2.20}$$

Finally, the strength of QCD interactions is measured in terms of the fine structure:

$$\alpha_s(m_Z) \approx 0.1184 \tag{2.21}$$

.

2.2.3 $SU(2)_L \otimes U(1)_Y$

The gauge theory of Electroweak interactions is more involved than QCD and QED. First, the mediators of the weak interaction are massive. Second, these mediators only couple to LH particles and RH antiparticles. Third, a mass term for the matter fields is not allowed since it mixes left and right chiral fields, which in turn would lead to explicit breaking of the gauge invariance.

Here, we will discuss the Electroweak theory with massless matter particles and gauge bosons. Only in Sec. 2.4 we will address the issue of giving masses to these fields.

As far as the electroweak interaction is concerned, a LH electron and a LH electron-neutrino form an $SU(2)_L$ doublet (similarly for LH up and down quarks),

$$\begin{pmatrix} \nu_e \\ e^- \end{pmatrix}_L, \quad \begin{pmatrix} u \\ d \end{pmatrix}_L \tag{2.22}$$

The Lagrangian before Electroweak symmetry breaking is:

$$\mathcal{L}_{EW} = -\overline{\psi}_L \not{D}_\mu \psi_L - \overline{\psi}_R \not{D}_\mu \psi_R - \frac{1}{4} B_{\mu\nu} B^{\mu\nu} - \frac{1}{4} W^i_{\mu\nu} W^{\mu\nu}_i \tag{2.23}$$

where only LH particles (or RH antiparticles) interact with the gauge bosons in the covariant derivative.

LH fields will transform as:

$$\psi_L \to U_L U_Y \psi_L, \tag{2.24}$$

where the $SU(2)_L$ transformation is,

$$U_L = e^{i\frac{\sigma^i}{2}\alpha}, \tag{2.25}$$

where σ^i are the three Pauli matrices that generate the $SU(2)$ group, while the $U(1)_Y$ transformation is,

$$U_Y = e^{i\frac{Y}{2}\beta}, \tag{2.26}$$

where Y is the hypercharge that generate the $U(1)$ group. Both α and β are spacetime-independent parameters.

The $su(2)_L$ algebra obeys,

$$\left[\frac{\sigma^i}{2}, \frac{\sigma^j}{2}\right] = i\epsilon^{ijk}\frac{\sigma^k}{2}, \tag{2.27}$$

where ϵ^{ijk} is the totally antisymmetric symbol.

On the other hand, RH fields are singlets under $SU(2)_L$, hence will only transform under $U(1)_Y$.

$$\psi_R \to U_Y \psi_R. \tag{2.28}$$

The electric charge is related to the hypercharge and the third component of the weak isospin, denoted T^3, by,

$$Q = T^3 + Y. \tag{2.29}$$

Moreover, the covariant derivative is written generically as,

$$D_\mu = \partial_\mu - c_L i g \frac{\sigma^a}{2} W_\mu^a - i g' \frac{Y}{2} B_\mu \tag{2.30}$$

where,

$$c_L = \begin{cases} 1 & \text{for LH fields} \\ 0 & \text{for RH fields} \end{cases}$$

After introducing the matrix notation $W_\mu = \frac{\sigma^i}{2} W^i_\mu$, gauge fields transform as,

$$W_\mu \to U_L W_\mu U_L^\dagger - \frac{1}{g} \partial_\mu U_L U_L^\dagger, \tag{2.31}$$

while B_μ transform as,

$$B_\mu \to B_\mu - \frac{1}{g'} \partial_\mu \beta \tag{2.32}$$

The field strength tensors of the electroweak interaction transform as (in matrix notation),

$$\begin{aligned} W_{\mu\nu} &\to U_L W_{\mu\nu} U_L^\dagger \\ B_{\mu\nu} &\to B_{\mu\nu}, \end{aligned} \tag{2.33}$$

where,

$$W_{\mu\nu} = \frac{\sigma^a}{2} W^a_{\mu\nu} = \frac{\sigma^a}{2} \left(\partial_\mu W^a_\nu - \partial_\nu W^a_\mu - g f^{abc} W^b_\mu W^c_\nu \right), \tag{2.34}$$

and

$$B_{\mu\nu} = \partial_\mu B^a_\nu - \partial_\nu B^a_\mu. \tag{2.35}$$

Given these gauge symmetries, the SM gauge group is the direct product of,

$$SU(3)_C \otimes SU(2)_L \otimes U(1)_Y, \tag{2.36}$$

which is a rank-4 group. This group will reduce to

$$SU(3)_C \otimes U(1)_{EM}, \tag{2.37}$$

after breaking the Electroweak symmetry as will be discussed in Sec. 2.4.

Finally, the SM fields and their symmetry properties are compiled in Table 2.2.

	Field	$SU(3)_C \times SU(2)_L \times U(1)_Y$	$SL(2,\mathbf{C})$
Quark doublets and Singlets	$\binom{u}{d}_L$	$(3,2,\frac{1}{6})$	$(\frac{1}{2},0)$
	u_R	$(3,1,\frac{2}{3})$	$(0,\frac{1}{2})$
	d_R	$(3,1,-\frac{1}{3})$	$(0,\frac{1}{2})$
Lepton doublets and Singlets	$\binom{\nu}{e}_L$	$(1,2,-\frac{1}{2})$	$(\frac{1}{2},0)$
	e_R	$(1,1,-1)$	$(0,\frac{1}{2})$
Higgs	H	$(1,2,\frac{1}{2})$	$(0,0)$
Gauge Bosons	G	$(8,1,0)$	$(\frac{1}{2},\frac{1}{2})$
	W	$(1,3,0)$	
	B	$(1,1,0)$	

TABLE 2.2: Matter content of the SM (first generation) and quantum numbers. The last column indicates how SM fields transform under the Lorentz group as discussed at the end of Sec.2.1.

2.3 Accidental Symmetries

As mentioned at the beginning of this Chapter, the SM is believed by some to be an effective theory and that a more complete description of the Universe at energy scales larger than $\mathcal{O}(1)$ TeV is yet to be formulated, and experimentally verified. A common aspect of effective field theories is that some symmetries appear to be respected even though such symmetries are not necessarily respected by a more complete and underlying theory. Here we will describe two of these symmetries, namely, baryon (B) and lepton (L) number conservation. The symmetry group takes the form,

$$U(1)_e \otimes U(1)_\mu \otimes U(1)_\tau \otimes U(1)_B, \tag{2.38}$$

The generators of these symmetries are: $L_{e,\mu,\tau}$, and B. Table 2.3 lists the values of these numbers for the fermion content of the SM.

(Particles),(Antiparticles)	L_e	L_μ	L_τ	B
(e,ν_e),$(\bar{e},\bar{\nu}_e)$	(1),(-1)	0	0	0
(μ,ν_μ),$(\bar{\mu},\bar{\nu}_\mu)$	0	(1),(-1)	0	0
(τ,ν_τ),$(\bar{\tau},\bar{\nu}_\tau)$	0	0	(1),(-1)	0
(q),$(\bar{q})$	0	0	0	$(\frac{1}{3})$,$(-\frac{1}{3})$

TABLE 2.3: Lepton and Baryon numbers of SM fermions.

A remarkable fact is that such symmetries in the SM forbid all processes violating the conservation of Lepton ($L = L_e + L_\mu + L_\tau$) and Baryon numbers. Up to the date of

writing this thesis, there is no experimental evidence for the contrary. Any observation of violation of these two numbers will be evidence for new physics beyond the SM. However, due to neutrino masses, the individual lepton numbers are not conserved.

2.4 The Higgs mechanism and EWSB

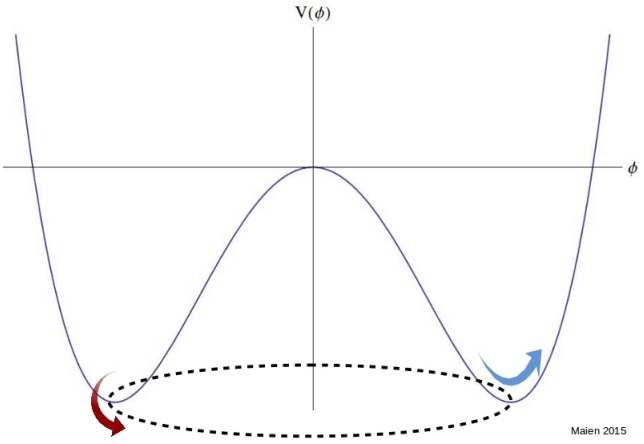

FIGURE 2.2: Schematic Higgs potential

At energy scales below 100 GeV, the $SU(2)_L \otimes U(1)_Y$ symmetry is spontaneously broken [3] into $U(1)_{EM}$. An issue arise here, according to the Goldstone theorem [19], such continuous global symmetry when spontaneously broken gives rise to a massless and chargeless scalar boson, called the Goldstone boson, for each broken generator (e.g. the modes circulating the trough of the potential in Fig. 2.2).

Moreover, it is not possible to add mass terms to the intermediate vector gauge bosons ($W^{\pm}$, and Z^0) by hand since gauge invariance will be explicitly broken.

These two issues are resolved by the Higgs mechanism [20, 21, 22] that combines spontaneous symmetry breaking with local gauge invariance. The result is that the Goldstone modes will contribute as the longitudinal component of the intermediate vector bosons thereby turning them from massless into massive fields.

[3] The vacuum of the theory is not invariant under the symmetry

In the SM, the Higgs mechanism involves introducing an $SU(2)_L$ doublet ($T^3 = \frac{1}{2}$ and $Y = \frac{1}{2}$) of two complex scalars,

$$\mathbf{\Phi} \equiv \begin{pmatrix} \phi^+ \\ \phi^0 \end{pmatrix}, \tag{2.39}$$

where $\phi^+ = \frac{1}{\sqrt{2}}(\phi_1 + i\phi_2)$, $\phi^0 = \frac{1}{\sqrt{2}}(\phi_3 + i\phi_4)$, $\phi^- = (\phi^+)^*$, and $\overline{\phi^0} = (\phi^0)^*$.

The Higgs potential is designed to provide spontaneous symmetry breaking of $SU(2)_L \otimes U(1)_Y$,

$$V(\mathbf{\Phi}, \mathbf{\Phi}^\dagger) = -m_\phi^2 \left|\mathbf{\Phi}^\dagger \mathbf{\Phi}\right| + \lambda \left|\mathbf{\Phi}^\dagger \mathbf{\Phi}\right|^2 \tag{2.40}$$

where m_ϕ^2 is a squared-mass parameter, and λ is a quartic self-coupling. The minimum of this potential occurs at $\Phi^\dagger\Phi = \frac{m_\phi^2}{2\lambda} = v_\Phi$.

Under the electroweak gauge symmetry, the Higgs doublet transforms as,

$$\mathbf{\Phi} \rightarrow e^{i\frac{\sigma^a}{2}\alpha} e^{iY\beta} \mathbf{\Phi}. \tag{2.41}$$

One can use the gauge freedom to select a certain direction that fixes the gauge symmetry, and where the three Goldstone bosons ($\phi_{1,2,4}$) disappear. This is the so-called unitary gauge in which the vacuum is,

$$\langle \mathbf{\Phi} \rangle \equiv \frac{1}{\sqrt{2}} \begin{pmatrix} 0 \\ v_h \end{pmatrix}, \tag{2.42}$$

where

$$v_h \equiv \sqrt{2} v_\Phi \approx 246\text{GeV} \tag{2.43}$$

is the VEV of the Higgs field.

This process of acquiring a non-zero VEV by one of the components of the Higgs doublet, namely the Higgs field, will result in giving rise to mass terms to the gauge bosons of the weak interaction, to fermion matter fields, and to the Higgs boson; the quantum excitation of the Higgs field around v_h. That is, $\phi_3 = v_h + h$, where h corresponds to the Higgs boson.

Now if we examine the kinetic term of the Higgs field at excitations above the minimum (in the unitary gauge) we find,

$$\begin{aligned}\mathcal{L}_H &\supset (D_\mu \mathbf{\Phi})^\dagger (D^\mu \mathbf{\Phi}) \\ &= \left[\left(\partial_\mu - \frac{ig}{2}\sigma^i W_\mu^i - \frac{ig'}{2}B_\mu\right)\frac{1}{\sqrt{2}}\begin{pmatrix}0\\ v_h+h\end{pmatrix}\right]^\dagger \left[\left(\partial^\mu - \frac{ig}{2}\sigma^i W_i^\mu - \frac{ig'}{2}B^\mu\right)\frac{1}{\sqrt{2}}\begin{pmatrix}0\\ v_h+h\end{pmatrix}\right] \\ &= \frac{1}{2}\partial_\mu h \partial^\mu h + (v+h)^2\left(\frac{g^2}{4}W_\mu^+ W^{-\ \mu}\right) + \frac{(v+h)^2}{8}\left(gW_\mu^3 - g'B_\mu\right)^2, \end{aligned} \tag{2.44}$$

where $W^\pm \equiv \frac{1}{\sqrt{2}}\left(W^1 \mp iW^2\right)$.

By rotating the neutral gauge eigenstates in the last term of Eq. 2.44, we obtain the neutral mass eigenstates,

$$\begin{pmatrix}Z_\mu\\ A_\mu\end{pmatrix} = \begin{pmatrix}\cos\theta_W & -\sin\theta_W\\ \sin\theta_W & \cos\theta_W\end{pmatrix}\begin{pmatrix}W_\mu^3\\ B_\mu\end{pmatrix}, \tag{2.45}$$

where θ_W is so-called Weinberg angle,

$$\begin{aligned}\cos\theta_W &= \frac{g}{\sqrt{g^2+g'^2}}, \\ \sin\theta_W &= \frac{g'}{\sqrt{g^2+g'^2}}. \end{aligned} \tag{2.46}$$

Therefore, both the $W^\pm$, and Z bosons acquired masses,

$$\begin{aligned}m_W^2 &= \frac{v_h^2 g^2}{4}, \\ m_Z^2 &= \frac{v_h^2 \overline{g}^2}{4}, \end{aligned} \tag{2.47}$$

where $\overline{g}^2 \equiv g^2 + g'^2$.

The application of the Higgs mechanism to the Electroweak theory and the first estimation of m_W and m_Z was carried out by Weinberg [23] and Salam (cited in [24]).

Similarly, the coupling of the Higgs boson, h, to the weak gauge bosons can be read off from Eq. 2.44.

Before discussing Yukawa interactions between the Higgs field and fermions, we note that, indeed the generators of $SU(2)_L$ and $U(1)_Y$ will not annihilate the vacuum state,

that is,

$$\begin{aligned} \sigma^i\langle\Phi\rangle &= \left\{\begin{pmatrix}0 & 1\\ 1 & 0\end{pmatrix}, \begin{pmatrix}0 & -i\\ i & 0\end{pmatrix}, \begin{pmatrix}1 & 0\\ 0 & -1\end{pmatrix}\right\}\frac{1}{\sqrt{2}}\begin{pmatrix}0\\ v_h\end{pmatrix} \neq 0, \\ Y\langle\Phi\rangle &= \frac{1}{2\sqrt{2}}\begin{pmatrix}0\\ v_h\end{pmatrix} \neq 0, \end{aligned} \tag{2.48}$$

while the combination corresponding to the electromagnetic charge, Q, does annihilate the vacuum,

$$\left(\frac{\sigma^3}{2} + Y\right)\langle\mathbf{\Phi}\rangle = 0, \tag{2.49}$$

and hence $U(1)_{\rm EM}$ is a symmetry of the vacuum.

Next, we turn to the Yukawa coupling between the Higgs field and fermions. The presence of this coupling will generate masses for fermions once the Higgs field acquires a VEV. However, an issue will arise when dealing with quark $SU(2)_L$ doublets, since $\langle\Phi\rangle$ can only give mass to the lower entry (c.f. Eq. 2.22). Overcoming this issue can be accomplished by introducing:

$$\Phi^c \equiv i\sigma^2\Phi^* = \begin{pmatrix}\overline{\phi^0}\\ -\phi^-\end{pmatrix}. \tag{2.50}$$

The Yukawa Lagrangian takes the form (for quarks):

$$\mathcal{L}_F = \mathbf{h}_d Q_L^\dagger \Phi D_R + \mathbf{h}_u Q_L^\dagger \Phi^c U_R + \text{h.c.}, \tag{2.51}$$

where $\mathbf{h}_{d,u}$ are 3×3 Yukawa matrices.

After EWSB, mass terms of the form $m_q q\bar{q}$ will arise, where

$$m_q = \frac{h_q v_h}{\sqrt{2}}. \tag{2.52}$$

Note that the Yukawa coupling is proportional to the mass. Since the top quark is by far the heaviest of all fermions in the SM (see Eq. 2.1), its Yukawa coupling to the Higgs is by far the largest and of $\mathcal{O}(1)$. An important consequence of this is that

quantum corrections to the Higgs propagator will be dominated by the contribution from the top quark. This will be further discussed in the Sec. 2.5.

The quantum excitation of the Higgs field, the Higgs boson (h), will also acquire a mass of the form

$$m_h^2 = 2\lambda v_h^2 = 2m_\phi^2. \tag{2.53}$$

Finally, in 2012, ATLAS and CMS experiments at CERN discovered a scalar particle that is consistent with a SM Higgs boson [25, 26]. One of the discovery channels is the process

$$gg \to h \to \gamma\gamma \tag{2.54}$$

where g, h, and γ stand for the gluon, Higgs, and photon. Fig. 2.3 shows the Higgs discovery plots by the CMS experiment for this particular channel.

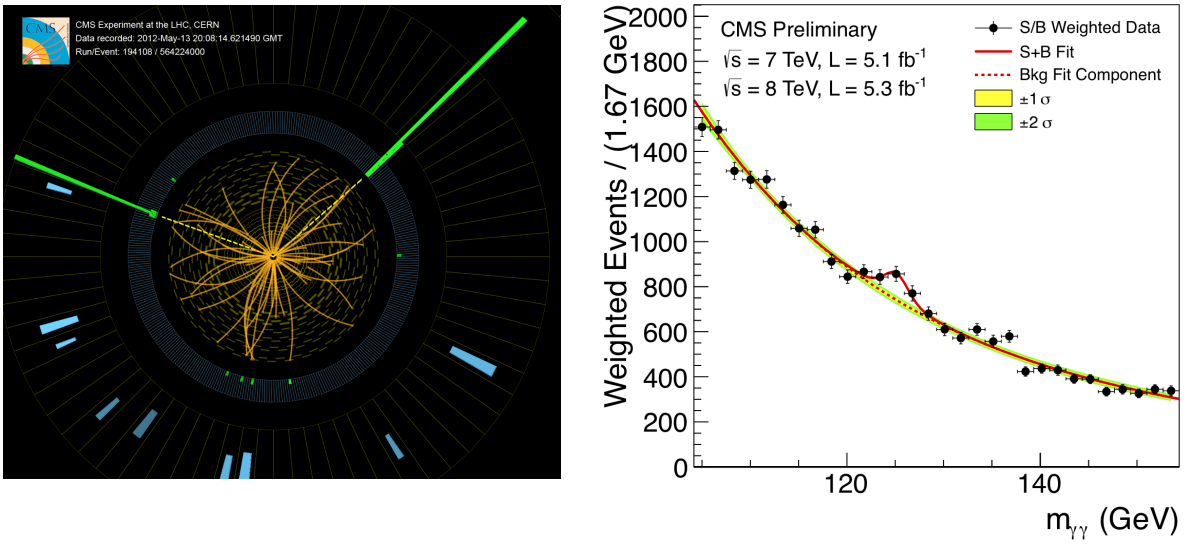

FIGURE 2.3: Left panel shows a di-photon event at the CMS detector, while the right panel shows the invariant mass distribution (by CMS) where a peak occurs at around 126 GeV corresponding to the Higgs mass.

2.5 Beyond tree-level and the hierarchy problem

The cross-section of the interaction between elementary particles is perhaps one of the most important quantities to be calculated in particle physics. This is because it can

be directly related to experiments, thereby enabling the verification of theoretical predictions of the SM. The cross-section is determined in terms of what is called the scattering matrix ($\hat{S}$-matrix) that contains the dynamical information of the theory. The $\hat{S}$-matrix is a perturbative expansion of the interacting Hamiltonian in powers of the relevant coupling where the interaction is dictated by the symmetries of the theory.

For instance, given an initial state $|\psi(t = -\infty)\rangle$ of free particles and asking what the possible finial states $|\psi(t = +\infty)\rangle$ due to a certain interaction are, we have,

$$|\psi(t = +\infty)\rangle = \hat{S}|\psi(t = -\infty)\rangle. \tag{2.55}$$

Furthermore, the $\hat{S}$-matrix can be expressed in terms of interacting and non-interacting parts,

$$\hat{S} = 1 + i\hat{T}, \tag{2.56}$$

where the matrix elements of the $\hat{T}$-matrix will contain delta functions that enforce the conservation of the four-momentum. It is the convention in most of the literature to separate the purely dynamical part from the purely kinematic part in the $\hat{T}$-matrix. The dynamics is then encoded in the so-called invariant amplitude $\mathcal{M}$. Schematically,

$$S_{fi} \sim 1 + \delta(\dots)i\mathcal{M}_{fi}. \tag{2.57}$$

The cross-section will be proportional to $|\mathcal{M}|^2$, which in turn can be calculated using the method of Feynman diagrams.

The diagrams shown in Table 2.1 represent interactions to lowest order in perturbation theory (referred to as tree-level or leading order). In order to obtain more precise predictions, it is necessary consider radiative corrections (e.g. loop diagrams in Fig.2.4) that represent higher order terms in the perturbative expansion of the $\hat{S}$-matrix.

However, by inspecting such loop diagrams, it is found that they involve integrals over internal momenta of virtual particles, which take the generic form (up to certain

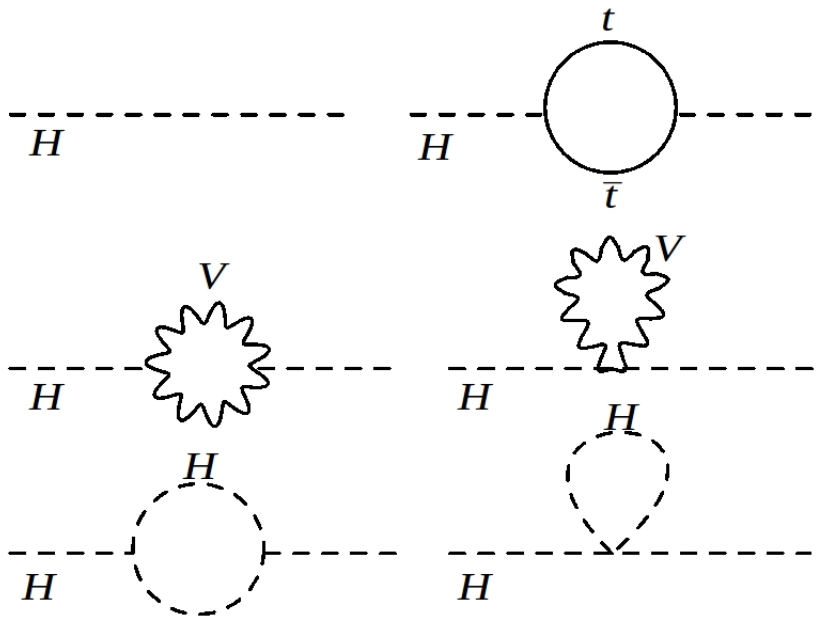

FIGURE 2.4: Possible 1-loop corrections to the Higgs field propagator.

factors):

$$\int_0^\infty k^n dk, \tag{2.58}$$

where k is an internal 4-momentum, and $n \geq -1$. This is problematic since such integrals are ultra-violet divergent.

In QFT, the procedure to tackle these divergences is to introduce a certain regularisation scheme, which involves the introduction of a parameter with a mass dimension. Three common schemes are the methods of dimensional regularisation, dimensional reduction, and Pauli-Villars. In dimensional regularisation, one calculates the ultra-violet divergent integrals in D-dimensions, where $D = 4 - 2\epsilon$. Then the results will turn out to be separated into finite parts, and divergent parts in the form of powers of $\frac{1}{\epsilon}$ poles as the limit $\epsilon \to 0$ is taken. As far as dimensional reduction is concerned, the procedure is the same as in dimensional regularisation expect that the algebra of the fields is taken to be four dimensional. This will prove crucial for preserving supersymmetry, which will be introduced in Ch. 3. Finally, the Pauli-Villars procedure involves adding auxiliary massive fields such that the integrals become convergent. In Sec. 2.5.2 we will apply a simple version of the Pauli-Villars

regularisation scheme to calculate the one-loop correction to the Higgs mass parameter m_ϕ^2.

Once a divergence is isolated, it is subtracted by the introduction of counter-terms at a certain renormalisation scale. However, it will turn out that the couplings and masses will be scale dependent. This dependence is determined using the RGEs of the model (also called β functions). In the SM, the one-loop β functions of the three gauge couplings are,

$$16\pi^2 \frac{\partial g_{(1,2,3)}}{\partial t} = \left(\frac{41}{10}, -\frac{19}{6}, -7\right) g^3_{(1,2,3)}(t), \tag{2.59}$$

where $t = \log(Q)$, and Q is the renormalisation scale.

The solution to Eq. 2.59 for each coupling (in terms of $\alpha_i = \frac{g_i^2}{4\pi}$) takes the general form,

$$\alpha(Q) = \frac{\alpha(Q_0)}{1 - \frac{c_{g_i}}{2\pi}\alpha(Q_0)\log(\frac{Q}{Q_0})}, \tag{2.60}$$

where $\alpha(Q)$ is the running coupling, Q_0 is some energy scale at which the coupling is measured, and c_{g_i} is the corresponding coefficient in Eq. 2.59. A remarkable property of the QCD running coupling is that it decreases with the increase of the energy scale. This is called Asymptotic freedom, and was discovered in [27, 28].

2.5.1 The SM is anomaly free

In QFT, an anomaly refers to an explicit breaking of a symmetry (e.g. gauge symmetry) due to the transition from classical to quantum fields. A theory that has anomalies is inconsistent since claims about the symmetries of the theory, and hence conserved quantities will be invalid. Therefore, it is vital for a theory that is intended to describe Nature to be anomaly free. In the SM, there are sources of anomalies, such as the triangle diagram in Fig. 2.5, but fortunately they cancel once all of them are taken into account.

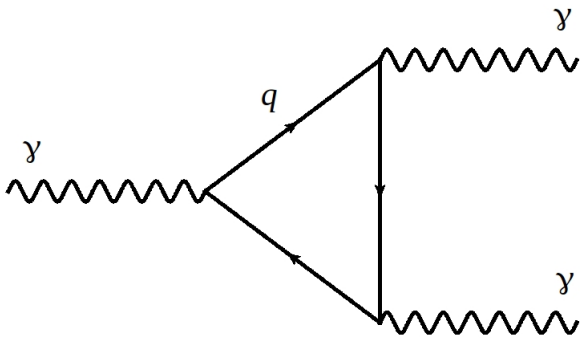

FIGURE 2.5: Chiral anomaly

In particular, it is possible to check if the theory is anomaly free by calculating the so-called: anomaly coefficient defined as,

$$\mathrm{Tr}\left[T_a\{T_b, T_c\}\right], \tag{2.61}$$

where $T_{a,b,c}$ are the generators of the symmetries, and the trace is over all fermions in the theory. An anomaly free theory must have Eq. 2.61 equal to zero, which is the case in the SM.

2.5.2 The hierarchy problem in the SM

In this section we describe the well-known hierarchy problem that is considered one of many important arguments for the incompleteness of the SM.

As described in Sec. 2.4, the Higgs doublet and the Higgs potential (Eq. 2.40) are introduced in order to break the electroweak symmetry spontaneously, thereby introducing masses to vector gauge bosons and to fermions. The Higgs mass parameter receives quantum corrections from all particles in the SM. However, the dominant contribution comes from the heaviest particle, the top quark. The interaction term is shown in Eq. 2.51. This interaction term leads to the following loop integral (top right loop diagram in Fig. 2.4),

$$I = -(-i)^2 y_t^2 \int \frac{d^4k}{(2\pi)^4} \frac{i(-i(\not{p}+\not{k}))\; i(-i\not{k})}{[(p+k)^2 - i\epsilon][k^2 - i\epsilon]}, \tag{2.62}$$

where we have denoted the coupling of the Higgs field to the top quark by y_t. p, and k are external and internal momenta, respectively. Using Feynman parametrisation (described in [3]) one obtains:

$$I = y_t^2 \int_0^1 dx \int \frac{d^4l}{(2\pi)^4} \frac{l^2 - \Delta}{[l^2 + \Delta - i\epsilon]^2} \tag{2.63}$$

where $\Delta = x(1-x)p^2$ and k was shifted $k = l - xp$.

We have two integrals. Only the first one will give rise to quadratic divergence,

$$I_A = \int \frac{d^4l}{(2\pi)^4} \frac{l^2}{[l^2 + \Delta - i\epsilon]^2} \tag{2.64}$$

This integral is divergent, which can be seen by power counting. One can use a Pauli-Villars regularisation by making the following replacement,

$$\frac{1}{[l^2 + \Delta - i\epsilon]^2} \longrightarrow \frac{1}{[l^2 + \Delta - i\epsilon]^2} - \frac{1}{[l^2 + \Lambda^2 - i\epsilon]^2}, \tag{2.65}$$

where $\Lambda^2 >> \Delta$ is of dimension $[mass]^2$. As l becomes large the term involving Λ^2 renders the integral finite.

Finally we have,

$$I_{SM} = \delta m_H^2(SM) = i\frac{3}{16\pi^2} y_t^2 [\Lambda^2 + \dots] \tag{2.66}$$

where the dots represent log-divergent and finite terms, and the factor of 3 is a colour factor.

The fact that the Higgs squared-mass parameter is quadratically divergent leads to the destabilising the electroweak scale since, as discussed in Sec. 2.4, it is related to the Higgs VEV and physical mass (Eq.2.53). The former being indirectly measured via measuring the Z boson mass and the gauge couplings g_1, and g_2, while the latter has been directly measured.

If the energy scale at which the SM fails is of $\mathcal{O}(M_{\text{Planck}})$, then the squared-mass parameter has to be tuned to order $\sim 10^{30}$ in order to bring it down to the weak scale where the physical Higgs mass is observed.

The huge amount of fine tuning makes the parameter m_H "unnatural". In fact, a general feature of scalar masses is that they lead to quadratic divergences. By contrast, fermions and gauge bosons do not introduce such divergences because they are protected by chiral and gauge symmetries. That is, the limit where the masses goes to zero results in restoring some symmetries. This is the definition of a natural parameter according to the $'$t Hooft Naturalness criteria [29].

In this thesis, we take this fine tuning problem as an indication that the SM is only an effective field theory, and that some new physics is expected to appear around and above the weak scale in order to solve this technical hierarchy problem.

2.6 Scalar partners and the hierarchy problem

A possible solution to the hierarchy problem described in the previous Section is the existence of scalar partners to top quarks (labelled with a tilde) as this will lead to the cancellation of quadratic divergences. In particular, consider the following interaction terms,

$$\mathcal{L} \ni Y_u |H_u \tilde{Q}_L|^2, \; Y_u |H_u \tilde{t}_R|^2. \tag{2.67}$$

where Y_u is the coupling of the left scalar quark doublet (third generation), $\tilde{Q}_L$, and the right top scalar quark singlet, $\tilde{t}_R$, to the Higgs doublet, H_u. Eq. 2.67 leads to the loop diagrams in Fig. 2.6.

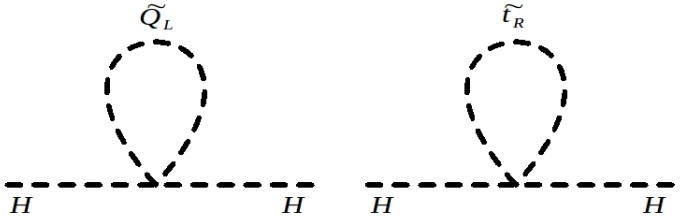

FIGURE 2.6: Correction to the Higgs squared-mass parameter from $\tilde{Q}_L$ and $\tilde{t}_R$.

The loop integrals are,

$$I_1 = -iY_u \int \frac{d^4k}{(2\pi)^2} \frac{-i}{[k^2 + m_{\tilde{t}}^2 - i\epsilon]}$$

Using similar techniques as before and introducing PV regulator one obtains,

$$I_1 = -i\frac{3}{32\pi^2} Y_u [\Lambda^2 - 2m_{\tilde{t}}^2 \; log(\frac{\Lambda^2}{m_{\tilde{t}}^2}) - m_{\tilde{t}}^2]$$

Similarly, the second diagram reads,

$$I_2 = -i\frac{3}{32\pi^2} Y_u [\Lambda^2 - 2m_{\tilde{Q}}^2 \; log(\frac{\Lambda^2}{m_{\tilde{Q}}^2}) - m_{\tilde{Q}}^2]$$

Combining the two results we have,

$$I = \delta m_H^2 = -i\frac{3}{16\pi^2} Y_u \Lambda^2 + \dots \tag{2.68}$$

We notice that this quadratic divergence is similar to the one obtained in Eq. 2.66, but with the opposite sign due to the different nature of the particles running in the loops (fermions in the SM, while scalars in this extension of the SM). Therefore, as long as $Y_u = y_t^2$, the quadratic divergences in the Higgs squared-mass parameter will cancel. Remarkably, supersymmetry (discussed in the next Chapter) introduces such scalar partners with the required relation between the couplings. This means that supersymmetry enable the stabilisation of the weak scale against radiative corrections to the Higgs squared-mass parameter, which in turn becomes technically natural.

2.7 Other issues beyond the SM

In this section we summarise some of the issues that provide evidence of the incompleteness of the SM in its current form, and that some new physics beyond the SM must exist. A more extensive list of issues can be found in [30].

Dark matter

There is an overwhelming evidence supporting the existence of a type of matter that is:

- Non-Baryonic
- Electrically neutral
- Slow (i.e non-relativistic)
- Stable (i.e. lifetime longer than the age of the Universe)

This unknown matter is called Dark Matter (DM), and it constitutes about 80% of the *matter* content of the Universe today. SM particles fail to account for DM (e.g. neutrinos are relativistic particles) and hence a new kind of particle that lies beyond the SM is required (if DM is really a particle and not a modification of gravity).

Assuming a particle dark matter, the relic density of dark matter, $\Omega_D h^2$, is related to the cross-section, σ, and velocity, v, by

$$\Omega_D h^2 \sim \frac{3 \times 10^{27}}{\langle \sigma v \rangle}, \tag{2.69}$$

where h is the Hubble parameter, and $\langle \dots \rangle$ denotes thermal averaging. Therefore, given the expansion rate of the Universe, a large cross-section and velocity is inconsistent with observations $\Omega_D h^2 \approx 0.1$. A common candidate is a called the weakly interacting massive particle (WIMP) [31]. A WIMP that has an interaction cross-section of order $10pb$, velocity of $0.1c$, and a mass between 10 GeV and 1 TeV can, in principle, account for cosmological observations (see [32] and references therein). In fact, in supersymmetic extensions of the SM, as will be seen in Sec. 4.7, a stable LSP can account for the observed DM relic density.

Matter-antimatter asymmetry

Another issue is the the asymmetry between matter and antimatter. Our observed Universe seems to have matter but not antimatter. It is commonly assumed that the

Universe started with an equal amount of matter and antimatter. However, at some point, and due to some mechanism, there was an excess of matter over anti-matter that lead to our baryonic Universe. The ratio between matter and anti-matter should be,

$$\frac{n_m - n_{\bar{m}}}{n_m + n_{\bar{m}}} \sim 10^{-10}, \tag{2.70}$$

where n_m and $n_{\bar{m}}$ is the number density of matter and anti-matter respectively. Eq. 2.70 indicates that at some point in the history of the Universe, there was an excess of one matter particle for each 10^{10} matter-antimatter pairs. In order to reach this situation, three conditions have to be met (Sakharov conditions):

1. Baryon number violation.
2. CP violation.
3. Thermal non-equilibrium.

Although these three conditions can be met in the SM, the amount of matter-antimatter asymmetry produced in the SM is not sufficient to account for the ration in Eq. 2.70. Therefore, some mechanism due to physics beyond the SM has to take place.

Neutrino mass

We have seen in Sec.2.4 that generating masses for fermions require mixing left and RH states. However, due to the fact that the weak force only couples to LH particles and RH antiparticles, RH neutrinos are not present. Therefore, the SM predicts that neutrinos are massless. However, this turned out to be wrong. Neutrinos oscillate, which is a strong indication that they are massive. This is considered as a direct evidence that the SM is incomplete and that new physics exists.

Finally, these issues, and other open questions in the SM, motivate the introduction of new theories and concepts beyond the SM. In the reminder of this thesis we consider low energy scale Supersymmetry.

Chapter 3

Supersymmetry

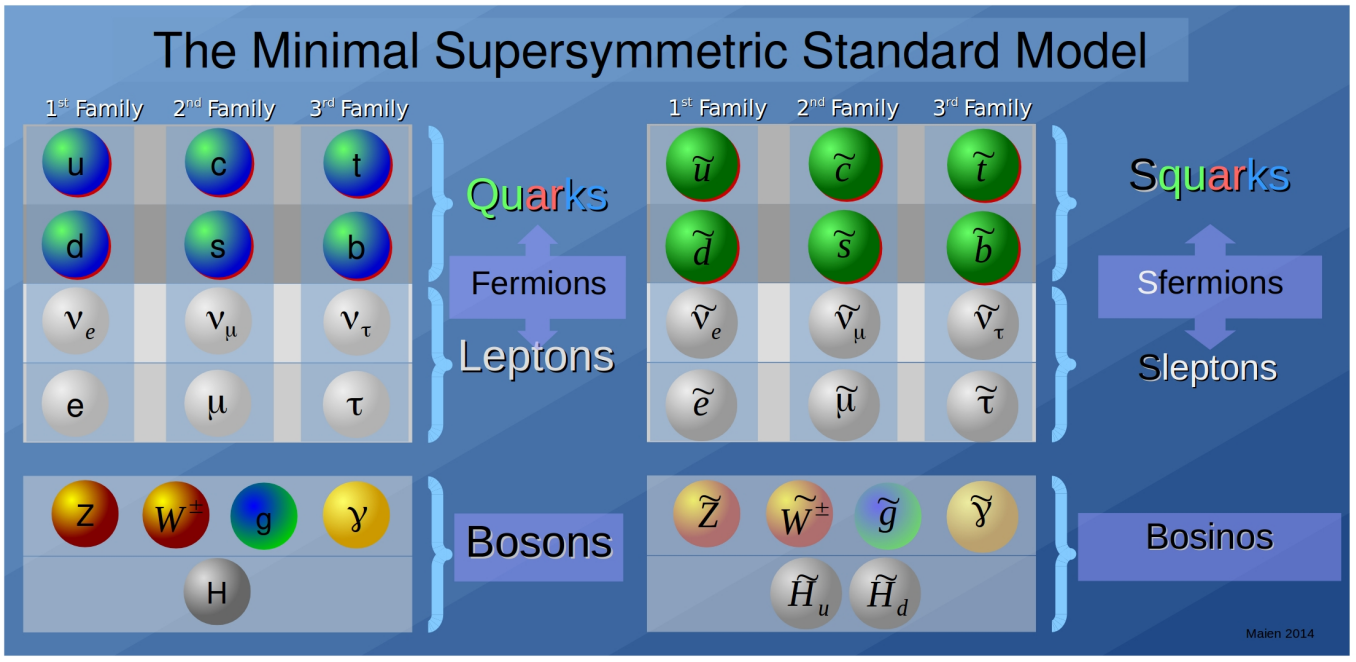

In the previous Chapter, we have briefly introduced the SM of particle physics. We discussed some issues that motivate replacing the SM with a more complete theory. In this Chapter we will introduce $\mathcal{N} = 1$ Supersymmetry (SUSY), and discuss the minimal supersymmetric extension of the SM, called the MSSM. Next, we consider the little hierarchy and fine tuning problems in the MSSM. Finally, the transition to non-minimal supersymmetric extensions of the SM will be motivated. Two models that are relevant to the thesis will be introduced, namely, the Next-to-minimal supersymmetric SM (NMSSM), and the Exceptional supersymmetric SM (E_6SSM).

3.1 Supersymmetry and its algebra

SUSY links bosons and fermions via fermionic generators Q_α and $\overline{Q}_{\dot{\alpha}}$, where $\alpha, \dot{\alpha} = 1, 2$ are spinor indices, and $(Q_\alpha)^\dagger = \overline{Q}_{\dot{\alpha}}$. Schematically,

$$Q_\alpha \big|\text{Boson}\rangle \to \big|\text{Fermion}\rangle_\alpha, \tag{3.1}$$

$$Q_\alpha \big|\text{Fermion}\rangle^\alpha \to \big|\text{Boson}\rangle. \tag{3.2}$$

This means that there is a non-trivial relation between internal and external (spacetime) symmetries encoded in the super-Poincare algebra (or superalgebra). Formally,

$$\{Q_\alpha, \bar{Q}_{\dot{\beta}}\} = 2(\sigma^\mu)_{\alpha\dot{\beta}} P_\mu, \tag{3.3}$$

$$\{Q_\alpha, Q_\beta\} = \{\bar{Q}_{\dot{\alpha}}, \bar{Q}_{\dot{\beta}}\} = 0, \tag{3.4}$$

$$[P^\mu, Q_\alpha] = \left[P^\mu, \bar{Q}_{\dot{\alpha}}\right] = 0 \tag{3.5}$$

$$[M^{\mu\nu}, Q_\alpha] = -i(\sigma^{\mu\nu})^\beta_\alpha Q_\beta. \tag{3.6}$$

Eq. 3.3 shows that the anti-commutation between elements of Q_α and $\bar{Q}_{\dot{\alpha}}$ are elements of translation in spacetime. This establishes the fact that SUSY is a spacetime symmetry. Eq. 3.5 shows that the commutation between elements of supersymmetric

transformations and spacetime translations vanishes. This relation establishes the fact that particles and their superpartners share the same mass if supersymmetry is exact. Additionally, Eq. 3.6 shows that the commutation between elements of Lorentz transformations and supersymmetric transformations are elements of supersymmetric transformations. This establishes the fact that supersymmetric generators are Lorentz spinors.

As discussed in the previous Chapter, the SM is a chiral theory since LH fields are treated differently from RH fields. SUSY establishes a realistic extension of the SM since it preserves this distinction between fields of different chirality, as opposed to *extended* SUSY where additional supersymmetic charges are present. This in turn means that there is a superpartner (sparticle) for each chiral state present in the SM, along with superpartners of SM vector fields. In particular, particles and their sparticles form supermultiplets. These are chiral supermultiplets containing,

$$\begin{pmatrix} \text{spin-0} \\ \text{spin-}\frac{1}{2} \end{pmatrix}, \tag{3.7}$$

and vector supermultiplets containing,

$$\begin{pmatrix} \text{spin-}\frac{1}{2} \\ \text{spin-1} \end{pmatrix}. \tag{3.8}$$

A given supermultiplet contains the same number of bosonic and fermionic degrees of freedom, and its members share the same quantum numbers and the same mass.

3.2 Superfields

While it is possible to formalise Supersymmetric models in ordinary spacetime, it is desired to use a formalism that enables writing terms that are manifestly supersymmetric (in analogy to 4-vector notation that makes Lorentz invariant manifest). Superspace is such a formalism (See [33, 34, 35]). It is an extension of spacetime that introduces fermionic coordinates, $\theta^{\alpha}, \overline{\theta}^{\dot{\alpha}}$. Fields that live in superspace

are functions of $\{x^\mu, \theta^\alpha, \overline{\theta}^{\dot{\alpha}}\}$. Such fields are called *general* superfields. A superfield that is only a function of $\{x^\mu, \theta^\alpha\}$ is called a *chiral* superfield and satisfies $\overline{D}^{\dot{\alpha}}\Phi = 0$, where $\bar{D}_{\dot{\alpha}}$ is a super-derivative defined as,

$$\bar{D}^{\dot{\alpha}} = \frac{\partial}{\partial\bar{\theta}_{\dot{\alpha}}} - i\,(\bar{\sigma}^\mu\theta)^{\dot{\alpha}}\,\partial_\mu. \tag{3.9}$$

Furthermore, expanding a chiral superfield around its fermionic coordinates results in,

$$\Phi(x^\mu, \theta) = \phi + \theta\psi + \theta\theta F, \tag{3.10}$$

where ϕ is a scalar, ψ is a fermion, and F is called F-term and has dimension $[\text{mass}]^1$.

On the other hand, if a general superfield is hermitian, then it is a *vector* superfield. That is, it satisfies $V = V^\dagger$. Expanding a vector superfield around its fermionic coordinates results in,

$$V = \bar{\theta}\bar{\sigma^\mu}\theta A_\mu + \bar{\theta}\bar{\theta}\theta\lambda + \theta\theta\bar{\theta}\bar{\lambda} + \frac{1}{2}\theta\theta\bar{\theta}\bar{\theta}D, \tag{3.11}$$

where λ is a fermion field, and D is called the D-term, which has dimension $[mass]^2$.

It turns out that the presence of F and D terms is important to ensure the closure of the SUSY algebra. Specifically, for a given two supersymmetric transformation, δ_1, δ_2 applied on a given field X, the requirement that,

$$(\delta_1\delta_2 - \delta_2\delta_1)\,X = 0 \tag{3.12}$$

will not be satisfied without the presence of the auxiliary F and D term fields in the theory.

Moreover, the F and D terms transform as total derivatives under SUSY transformations, which implies that they are not non-physical. This property enables building SUSY-invariant Lagrangians.

More pedagogical treatment can be found in [35].

3.3 The MSSM

In terms of superfields, a general renormalisable SUSY Lagrangian takes the form,

$$\mathcal{L} = (\frac{1}{4}\left[\mathcal{W}^{a\alpha}\mathcal{W}^{a}_{\alpha}\right]_F + c.c.) + \left[\Phi^{*i}\left(e^{2g_aT^aV^a}\right)_i{}^j\,\Phi_j\right]_D + (\left[W(\Phi_i)\right]_F + c.c.)\,, \tag{3.13}$$

where Φ and V are chiral and vector superfields. $\mathcal{W}_\alpha$ is the field-strength superfield defined as,

$$\mathcal{W}_\alpha = -\frac{1}{4}D^\dagger D^\dagger D_\alpha V, \tag{3.14}$$

and $W(\Phi)$ is the superpotential.

The superpotnetial, W, contains the supersymmetric interactions of the theory. It is gauge-invariant and defined as,

$$W = L^i\Phi_i + \frac{1}{2}M^{ij}\Phi_i\Phi_j + \frac{1}{6}y^{ijk}\Phi_i\Phi_j\Phi_k. \tag{3.15}$$

where L^i is a parameter of dimension $[mass]^2$ and is present if Φ_i is a gauge singlet and if the theory is not scale-invariant. M^{ij} is a mass matrix, and y^{ijk} are Yukawa couplings. Moreover, W is strictly complex-analytic in the chiral superfields. This is to ensure constructing a supersymmetric Lagrangian.

The MSSM is minimal in the sense that it adds superpartners to the SM particles without the inclusion of other gauge and SUSY allowed terms. The superpotential reads

$$W_{MSSM} = y_u\hat{\bar{u}}\hat{Q}\hat{H}_u - y_d\hat{\bar{d}}\hat{Q}\hat{H}_d - y_e\hat{\bar{e}}\hat{L}\hat{H}_d + \mu\hat{H}_u\hat{H}_d, \tag{3.16}$$

where μ is the Higgs and Higgsino (fermion partner of the scalar Higgs) mass term. The hats denote superfields.

As mentioned previously, W, is holomorphic the the chiral superfields. Therefore, it is essential to introduce two Higgs doublets with the opposite hypercharge in order to have mass terms for up- and down-type quarks via the Higgs mechanism described in Ch. 2.4.

Notice that not all terms allowed by gauge and SUSY invariance are present in Eq. 3.16. In particular,

$$\alpha_1 Q^i L^j \bar{D}^k + \alpha_2 L^i L^j \bar{E}^k + \alpha_3 \bar{D}^i \bar{D}^j \bar{U}^k. \tag{3.17}$$

These terms correspond to lepton and baryon number violation respectively. To formally disallow such terms, a matter parity (equivalent to R-parity) is usually imposed on the low scale SUSY models. Under this discrete symmetry, ordinary matter is even, while superpartners are odd.

3.3.1 Soft SUSY-breaking

Sparticles have not been observed in particle physics experiments. Thus, SUSY must not be a symmetry of the weak scale. The issue of breaking SUSY is still the subject of research and its technicalities are irrelevant to our discussion. However, we will briefly discuss broken SUSY. First, it turns out that attempting to spontaneously break SUSY extensions of the SM will be always associated with the prediction that some sparticles will have masses smaller than their SM partners, which is ruled out. To overcome this, it is assumed that there exists a sector with suppressed couplings to SM particles, called the Hidden Sector, in which SUSY is spontaneously broken by some mechanism [36]. Then this breakdown is mediated to the "visible" sector either via gravity, or gauge interactions, or other means (e.g. anomaly mediation) as illustrated in Fig. 3.1.

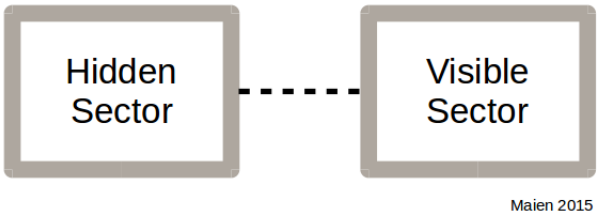

FIGURE 3.1: Spontaneous SUSY breaking takes place in a hidden sector. It is then mediated to the visible sector.

Therefore, the type of realistic SUSY models that we discuss in this thesis is that in which SUSY is explicitly broken at the low energy scale. That is, we add, by hand, terms that explicitly break SUSY. However, not all such term are allowed. Only the ones that keep the feature that quadratic divergences are cancelled since the main

motivation for low energy scale SUSY is stabilising the weak scale by protecting the Higgs squared-mass parameter from large radiative corrections (as discussed in Sec. 2.6).

The set of allowed soft SUSY-breaking masses contains:

- Gaugino masses: M_1, M_2, and M_3,
- Scalar squared-mass terms: m_i^2,
- Trilinear scalar couplings: A_u, A_d, and A_L, and finally,
- Higgs bilinear term: b.

The matter content of the MSSM is compiled in Table 3.1

	Field	Superpartner	$SU(3)_C \times SU(2)_L \times U(1)_Y$	$SL(2,\mathbf{C})$
Quark/squark doublets	$\binom{u}{d}_L$	$\binom{\tilde{u}}{\tilde{d}}_L$	$(3,2,\frac{1}{6})$	$(\frac{1}{2},0)$
and Singlets	u_R	$\tilde{u}_R$	$(3,1,\frac{2}{3})$	$(0,\frac{1}{2})$
	d_R	$\tilde{d}_R$	$(3,1,-\frac{1}{3})$	$(0,\frac{1}{2})$
Lepton/slepton doublets	$\binom{\nu}{e}_L$	$\binom{\tilde{\nu}}{\tilde{e}}_L$	$(1,2,-\frac{1}{2})$	$(\frac{1}{2},0)$
and Singlets	e_R	$\tilde{e}_R$	$(1,1,-1)$	$(0,\frac{1}{2})$
Down-type Higgs	H_d	$\tilde{H}_d$	$(1,2,\frac{1}{2})$	$(0,0)$
Up-type Higgs	H_u	$\tilde{H}_u$	$(1,2,-\frac{1}{2})$	$(0,0)$
Gauge Bosons	G	$\tilde{G}$	$(8,1,0)$	
and their superpartners	W	$\tilde{W}$	$(1,3,0)$	$(\frac{1}{2},\frac{1}{2})$
	B	$\tilde{B}$	$(1,1,0)$	

TABLE 3.1: Matter content of the MSSM (first generation) and quantum numbers.

3.3.2 Electroweak symmetry breaking

In the MSSM, the tree-level Higgs scalar potential is (at the minimum)

$$V = m_1^2 v_d^2 + m_2^2 v_u^2 - 2b v_d v_u + \frac{1}{8}\bar{g}^2 (v_d^2 - v_u^2)^2, \tag{3.18}$$

where $m_i^2 = m_{H_{d,u}}^2 + \mu^2$, and $\bar{g}^2 = (g^2 + g'^2)$.

Here, it is worth mentioning the difference between the Higgs potential in the SM (Eq. 2.40), and in the MSSM (Eq. 3.18). The former was designed and contains a free parameter λ_ϕ, whereas in the MSSM the Higgs potential is derived, and λ_ϕ is no longer a free parameter, but instead a quantity that depends on the gauge couplings, g' and g.

Applying the minimisation conditions,

$$\frac{\partial V}{\partial v_d} = \frac{\partial V}{\partial v_u} = 0, \tag{3.19}$$

to Eq. 3.18 leads to,

$$\frac{m_Z^2}{2} = \frac{(m_1^2 - \tan^2\beta m_2^2)}{\tan^2\beta - 1} \tag{3.20}$$

$$\sin 2\beta = \frac{2m_3^2}{m_1^2 + m_2^2} \tag{3.21}$$

where, $m_3 = b$ and the ratio of the two Higgs VEVs is

$$\tan\beta = \frac{v_u}{v_d}. \tag{3.22}$$

These electroweak symmetry breaking conditions will restrict the parameter space of the MSSM. Moreover, it is important to include quantum corrections to Eqs. 3.18- 3.21 in order to obtain more precise and reliable predictions. There are two types of corrections. First, there is the so-called Coleman-Weinberg correction to the potential (in the $\overline{DR}$ scheme),

$$V^{(1)} = \frac{1}{64\pi^2}\mathrm{STr}M^4\left[\log\left(\frac{M^2}{m_{\mathrm{soft}}^2}\right) - \frac{3}{2}\right], \tag{3.23}$$

where, (1) is for one-loop, and STr is the supertrace [1]. M denotes all particles in the model. Notice that the Coleman-Weinberg potential depends on the physical masses of squarks. It is proportional to logarithmic quantities that can be small.

[1] Defined as: $\mathrm{STr}(M^2) = \left(\sum_{\mathrm{scalars}} m^2\right) - \left(2\sum_{\mathrm{fermions}} m^2\right)$

On the other hand, there are radiative corrections to the up- and down-type Higgs doublets. For instance, the correction δm_{H_u} can be given as,

$$\delta m_{H_u}^2 \approx -\frac{3}{8\pi^2} y_t^2 \left(m_{\tilde{Q}_t}^2 + m_{\tilde{u}_t}^2 + A_t^2 \right) \log \left(\frac{M_X}{M_S} \right), \tag{3.24}$$

where, $m_{\tilde{Q}_t}^2, m_{\tilde{u}_t}^2$, and A_t^2 are soft SUSY-breaking terms associated with the top squarks. M_X is a high energy scale (e.g. M_{GUT}), and $M_S^2 = \frac{1}{2}(m_{\tilde{Q}_t}^2 + m_{\tilde{u}_t}^2)$ is the average top squark mass.

Here, we notice that such corrections depend on logarithms that can be large.

3.3.3 The Higgs sector

Unlike the SM where only one physical Higgs is present, the MSSM predicts the existence of five Higgs particles. They are,

$$\{h, H^0, H^{\pm}, A\}, \tag{3.25}$$

where h is a SM-like CP-even Higgs, H is a non-SM-like CP-even Higgs particle, $H^{\pm}$ are two charged Higgs particles, and A is a CP-odd Higgs particle.

One of the important features of low scale SUSY models is that, there exists a limit, called the decoupling limit, where the theory predicts a SM-like Higgs, in terms of mass and couplings, and the rest of the Higgs particles can be heavy enough to escape detection. In this limit, $m_A >> m_Z$. And,

$$m_h^2 \approx m_Z^2 \cos 2\beta^2 + \Delta m_h^2 \tag{3.26}$$

where,

$$\Delta m_h^2 = \frac{3 m_t^4}{2\pi^2 v^2} \ln \frac{m_{\tilde{t}}^2}{m_t^2} + \frac{X_t^2}{m_{\tilde{t}}^2}\left(1 - \frac{X_t^2}{12 m_{\tilde{t}}^2}\right), \tag{3.27}$$

and $m_{\tilde{t}}^2 = m_{\tilde{t_1}} m_{\tilde{t_2}}$; the mass eigenstates of the stop, and $X_t = A_t - \mu \cot \beta$ is a mixing term.

While the other Higgs particles take similar heavy masses

$$m_A \approx m_H \approx m_{H^\pm} >> m_Z. \tag{3.28}$$

3.3.4 MSSM RGEs

For large tanβ, Eq. 3.20 can be written as,

$$\frac{m_Z^2}{2} = -\mu^2 - m_{H_u}^2, \tag{3.29}$$

where the parameters in this equation are low energy scale parameters. However, it is possible to express $m_{H_u}^2$ in terms of high energy (GUT) input parameters, which are considered as the fundamental parameters of the model. For example, in the constrained MSSM, the fundamental parameters are; a universal scalar mass, m_0, a universal gaugino mass, $m_{1/2}$, and a universal trilinear coupling A_0, μ_0, and the bilinear B_0. Therefore, m_Z can be expanded in terms on high energy input parameters, obtained from the relevant RGEs as,

$$m_Z^2 = a\ \mu^2(0) + b\ m_{1/2}^2 + c\ m_0^2 + d\ A_0^2 + e\ A_0\ m_{1/2} \tag{3.30}$$

The target is, then, to calculate these coefficients by setting a value for one input parameter at the GUT scale to unity, say m_0^2, while the other parameters are set to zero. Next, we run the RGEs down to the $M_{\rm SUSY}$ scale by solving the set of coupled differential equations, thereby obtaining,

$$c = \frac{m_{H_2}^2(M_{\rm SUSY})}{(1{\rm GeV})^2}. \tag{3.31}$$

It is worth mentioning that the values of the coefficients will depend on tan β as well as the gauge and Yukawa couplings.

Fig. 3.2 shows the running of MSSM parameters from the GUT scale to the weak scale. In particular, we notice that scalar masses increase as they evolve from an input

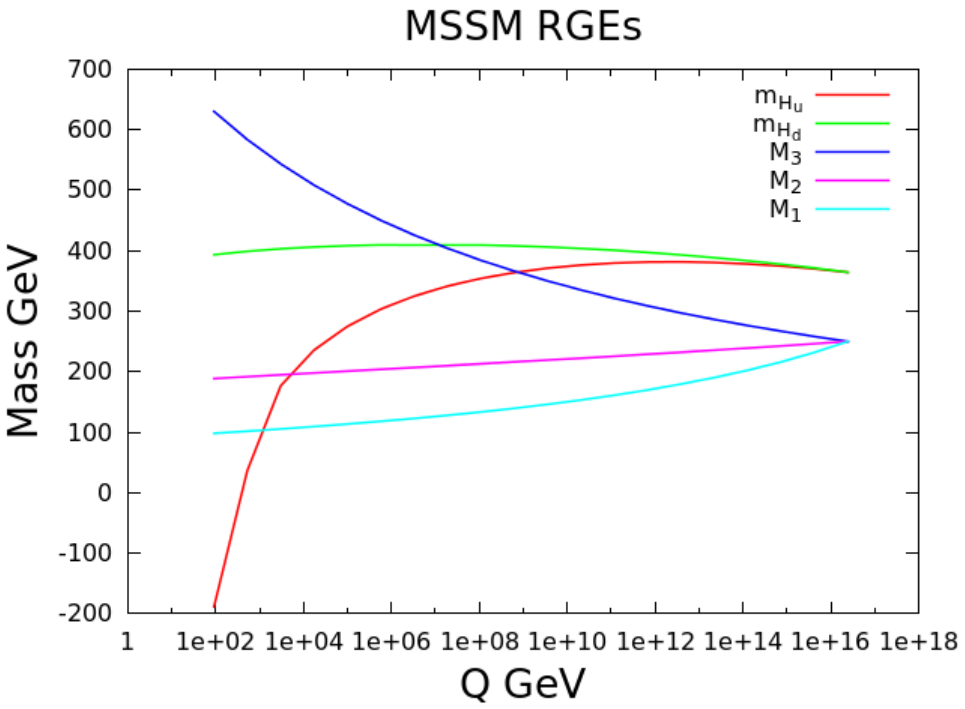

FIGURE 3.2: MSSM RG Evolution

high scale to the electroweak scale. And more importantly, the effect of the top Yukawa coupling is to decrease the Higgs mass m_{H_u} as it evolves down to lower scales. This effect can drive $m^2_{H_u}$ to a negative value near the electroweak scale. hence allowing it to obtain a non-zero VEV. This effect is called Radiative EWSB.

Using the RGEs with universal boundary conditions at the GUT scale, it is possible to write (for a fixed value of $\tan\beta = 10$),

$$\begin{aligned} -m^2_{H_u} = 2.29\ m^2_{1/2} + 0.09\ m^2_0 \\ + 0.098\ A^2_0 - 0.39\ A_0\ m_{1/2} \end{aligned} \tag{3.32}$$

We notice from Eq. 3.32 that the coefficient of the gaugino mass parameter assumes the largest value. This means that $m^2_{H_u}$ can be very sensitive to changes in $m^2_{1/2}$ and is driven more negative as $m^2_{1/2}$ increases.

On the other hand, in a non-universal case, one can expand m^2_Z in terms of the GUT scale parameters as,

$$\begin{aligned}\frac{m_Z^2}{2} =& c_0\mu_0^2 + c_1 M_3^2 + c_2 M_2^2 + c_3 M_1^2 \\ &+ c_4 m_{H_u}^2 + c_5 m_{H_d}^2 + c_6 m_q^2 + c_7 m_u^2 \\ &+ c_8 A_t M_3 + c_9 A_t M_2 + c_{10} A_t M_1 + c_{11} A_t^2 \\ &+ c_{12} M_2 M_3 + c_{13} M_1 M_3 + c_{14} M_1 M_2.\end{aligned} \tag{3.33}$$

The coefficients can be calculated using the same method previously discussed for the universal case. For instance, using one-loop RGEs a number of coefficients are shown in Table 3.2.

Parameter	Coefficient
M_3^2	3
M_2^2	- 0.11
M_1^2	0.008
$m_{H_u}^2$	- 0.65
A_t^2	0.08

TABLE 3.2: Coefficients of MSSM non-universal parameters with $\tan\beta = 2.5$ using one-loop RGEs.

We notice that the coefficient of M_3^2 is the largest, and therefore, m_Z^2 is significantly affected by changes of M_3^2 at the GUT scale. However, there could be some subtle effects that alter this behaviour to some extent if one takes into account all corrections to m_Z as discussed in [37].

Finally, in both of the previous cases, the coefficient of m_0^2 is found to be significantly small. This indicates that $m_{H_u}^2$ and m_Z^2 are insensitive to changes in m_0^2 at the GUT scale. This this sometimes called the focus point region [38].

3.4 The little hierarchy problem

In Sec. 3.3.2, we saw that the mass of the Z boson is a derived quantity (Eq. 3.20). In particular, we found that m_Z^2 is related to SUSY soft-breaking parameters, m_{H_u}, m_{H_d}, and the μ term. Furthermore, we saw in Sec. 3.3.4 that m_Z^2 can be expanded in terms

of GUT scale fundamental parameters that might be universal or otherwise. By inspecting Eq. 3.20, we can see that $m^2_{H_u}$ should be of the same order as m^2_Z for fine tuning to be absent. Theoretically this can be achieved. However, one needs to ask if there is another derived quantity that requires $m^2_{H_u}$ to be considerably larger than m^2_Z, since in such a case, fine tuning in inevitable. This is indeed the case, and the other quantity is the physical Higgs mass in Eq. 3.26. This equation shows that the MSSM predicts the Higgs mass that is always smaller than the Z mass at tree-level.

However, it is possible to rely on higher order corrections to increase the predicted Higgs mass to the desired range of values between $123 - 128$ GeV. This in turn can only take place if either the average top squark mass in Eq. 3.27 is significantly large, or if the mixing term in the same equation is close to maximum. Both cases are problematic, in terms of fine tuning. First, the more we separate the SUSY scale from the weak scale, the more fine tuning we expect in our model. Indeed, as we have seen in Eq. 3.24, the correction to $m^2_{H_u}$ is dominated by the top squarks. The larger the input value for the top squark parameters, the larger the correction to $m^2_{H_u}$, and the further it is from $\mathcal{O}(M^2_Z)$. This is the case in the MSSM since large top squarks are required in order to enhance the loop correction to the mass of the physical Higgs. This is the *little* hierarchy problem. It is a main source of fine tuning and is present in all low scale SUSY models, as far as we are aware.

3.5 Measuring the fine tuning

Given the little hierarchy problem, it is desired to ask the questions:

- Does the fine tuning depend on the boundary conditions of the model and how much?
- Which of the fundamental parameters are more relevant to fine tuning?
- What are the sources of fine tuning in a given model?
- How do different models compare in terms of fine tuning?

- What is the least fine tuned model?

All of these questions, and more, require a mean of measuring the fine tuning in a practical way.

This has been addressed in [39], where a fine tuning measure was introduced and became popular after its usage in [40].

In particular, it is a sensitivity measure that quantifies the fractional change in m_Z in response to a fractional change in a given fundamental parameter, a,

$$\Delta = \left| \frac{\partial \log m_Z}{\partial \log a} \right|. \tag{3.34}$$

Applying this formula to Eq. 3.20 leads to a fine tuning master formula for the MSSM (Ref. [41]),

$$\Delta = \left| \frac{a_i}{(\tan^2\beta - 1)m_Z^2} \left\{ \frac{\partial m_1^2}{\partial a_i} - \tan^2\beta \frac{\partial m_2^2}{\partial a_i} - \frac{\tan\beta}{\cos 2\beta} \times \right.\right.$$
$$\left.\left. \left(1 + \frac{m_Z^2}{m_1^2 + m_2^2}\right) \left[2\frac{\partial m_3^2}{\partial a_i} - \sin 2\beta \left(\frac{\partial m_1^2}{\partial a_i} + \frac{\partial m_2^2}{\partial a_i} \right) \right] \right\} \right|, \tag{3.35}$$

where $m_1^2 = m_{H_d}^2 + \mu^2$, $m_2^2 = m_{H_u}^2 + \mu^2$.

This formula can then be implemented in a spectrum generator and calculated for each point in the parameter space. It is necessary to understand the sources of fine tuning, and to quantify this fine tuning in order to compare different regions of the parameter space of a certain model or different models. Ultimately, this might help in discovering the least fine tuned supersymmetric model, and could provide guidance to SUSY searches at the LHC as it is believed that regions with high fine tuning might be less likely to be discovered.

This measure has been used extensively within the literature e.g.
[42, 43, 44, 45, 46, 47, 48, 38, 49, 50, 51, 52, 53, 54, 55, 56, 57, 58, 59, 60, 61, 62, 63].

3.5.1 Alternative fine tuning measures

Although the fine tuning measure in Eq. 3.34 is widely used, there exists a number of alternative fine tuning measures in the literature
[64, 65, 66, 67, 68, 69, 70, 71, 72, 73, 74, 75, 76, 77, 78, 77].

These measures are motivated by some issues associated with the traditional measure. For instance, the value of the fine tuning can vary depending on how one defines the measure. Some authors define it with m_Z^2 in the nominator while the parameters in the denominator correspond to are not squared. Others discriminate between the parameters such that scalar masses are squared while the other parameters are not. All of this can cause confusion when comparing the results of different papers. Therefore, some of the alternative measures try to overcome this issue by having a normalised measure that is insensitive to different definitions.

Moreover, the fine tuning associated with a point in the parameter space can be taken to be the maximum fine tuning in that point (as is done in this paper), or could be chosen to be a sum of quadrature [72, 73, 74, 75, 79].

We will use the traditional measure for the following reasons:

1. It is the most widely used tuning measure with which one can compare;
2. It is simple to understand and apply;
3. It is in better agreement with the more complicated measure [77] than other measures that use the quadrature summation.

Finally, it is important to note that, while the different definitions of the fine tuning measure can produce different values of fine tuning for a given point in a given parameter space, the overall conclusions regarding which model is less fine tuned than the other will be consistent regardless of which measure has been used.

3.6 Non-minimal supersymmetric models

There are several issues in the MSSM that motivate the departure from minimality. First, we have seen that the weak sector is fine tuned, and hence it is tempting to ask if it is possible to find a model that is significantly less fine tuned. Second, there is an issue with the μ-term (the supersymmetric Higgs/Higgsino mass term). Looking at Eq. 3.29, we see that a supersymmetric term must be of the same order as a soft-breaking term. This is a phenomenological requirement. Theoretically, however, μ could be zero, or of $\mathcal{O}(M_{\rm GUT})$, which is not viable phenomenologically. This is the μ problem in the MSSM. It also motivates departing from minimality and finding a dynamical origin of this parameter.

3.6.1 The NMSSM

In the NMSSM (see [80, 81] for a review), the μ parameter is replaced with a new SM-gauge-singlet superfield $\hat{S}$. This singlet couples to the Higgs ($\lambda S H_d H_u$). Hence, its superpotential takes the form,

$$W_{\rm NMSSM} = W_{\rm MSSM}(\mu = 0) + \lambda S H_d H_u. \tag{3.36}$$

However, this superpotential has a Pecci-Quinn symmetry where,

$$\begin{aligned} S &\rightarrow e^{i2\alpha} S, \\ (H_u, H_d) &\rightarrow e^{-i\alpha}(H_u, H_d) \\ (Q, L) &\rightarrow e^{i\alpha}(Q, L), \\ (u, d, e) &\rightarrow (u, d, e). \end{aligned} \tag{3.37}$$

Once a VEV is acquired by S near the weak scale, this symmetry is spontaneously broken, resulting in a massless axion, which has not been observed (detailed discussion and analysis can be found in [82]). In order to avoid issues with this axion, a cubic

interaction term is added to Eq. 3.36,

$$W_{\rm NMSSM} = W_{\rm MSSM}(\mu = 0) + \lambda S H_d H_u + \frac{\kappa}{3} S^3, \tag{3.38}$$

where κ is the cubic self-coupling of S. This is called the Z_3 invariant NMSSM, which is what is considered in this thesis (other possibilities include e.g. [83]). Therefore, we will refer to it simply as the NMSSM in the next Chapters.

More details about the NMSSM will be discussed in Ch. 4.

3.6.2 The E$_6$SSM

Unification of the gauge couplings at the GUT scale indicates that the SM group is embedded in a larger group at the GUT scale with one coupling constant. The E$_6$ group is such a group [84]. It is a rank-6 Lie group, and hence it contains $SO(10)$. However, $SO(10)$ is a rank-5 group. Therefore, E_6 contains,

$$E_6 \ni SO(10) \times U(1)_\psi, \tag{3.39}$$

Moreover, $SO(10)$ contains $SU(5)$, which is a rank-4 group as well as a $U(1)$ group,

$$SO(10) \ni SU(5) \times U(1)_\chi. \tag{3.40}$$

The SM group, which is a rank-4 group is contained in $SU(5)$,

$$SU(5) \ni SU(3) \otimes SU(2) \otimes U(1). \tag{3.41}$$

Furthermore, the E$_6$ group has complex representations. This is crucial for having chiral representations as is required by the SM.

A fundamental representation of E_6 that accommodates the SM particles could be the **27**-dimensional representation. In general, it decomposes under $SO(10) \times U(1)_\psi$ as ,

$$27 \to (16; 1) + (10; -2) + (1; 4), \tag{3.42}$$

Then it is possible to decompose the **16**, **10** and **1** representations under $SU(5) \times U(1)_\chi$ as,

$$\begin{aligned} 16 &\rightarrow (10;-1) + (\bar{5};3) + (1;-5), \\ 10 &\rightarrow (5;2) + (\bar{5};-2), \\ 1 &\rightarrow (1;0). \end{aligned} \tag{3.43}$$

The general form of **27** under $SU(5) \times U(1)_\chi \times U(1)_\psi$ is,

$$27 \rightarrow \underbrace{10_{-1,1} + \overline{5}_{-2,-2}}_{\substack{\text{Quarks \&} \\ \text{Leptons}}} + \underbrace{\overline{5}_{3,1} + 5_{2,-2}}_{\substack{\text{Higgs doublets \&} \\ \text{Coloured exotics}}} + \underbrace{1_{-5,1}}_{\text{Singlets}} + \underbrace{1_{0,4}}_{\text{RH Neutrinos}}, \tag{3.44}$$

where the numbers in the underscript denote the $U(1)$ charges.

Defining a linear combination of the two separate $U(1)$ charges as,

$$Q_\alpha = Q_\psi \cos\alpha - Q_\chi \sin\alpha \tag{3.45}$$

It is possible to choose an angle that renders the last term in Eq. 3.44 chargesless (see [85] and references therein). This multiplet is associated with RH neutrinos. And this defines the E_6SSM model that we will discuss in more details in Ch 5.

Chapter 4

Naturalness in scale-invariant NMSSMs with and without extra matter

4.1 Overview

The scalar particle discovered in July 2012 [25, 26] is increasingly consistent with a Standard-Model-like Higgs boson [86]. This may reinforce the hierarchy problem and the call for new physics at low scales just above the electroweak scale [87, 88]. Low scale supersymmetry (SUSY) is perhaps the most well-motivated candidate for such new physics beyond the Standard Model (SM) since it provides, for e.g., a solution to the hierarchy problem, a candidate for Dark Matter and unifies the SM group at the Grand Unification (GUT) scale. However low scale SUSY remains elusive at the LHC [89].

The naturalness problem in SM [29] is associated with the large ratio between the weak scale (M_W) and the Planck scale (M_P). If no new physics enters at the weak scale or the TeV scale, then the Higgs mass has to be fine tuned against the Planck scale, GUT scale, or any new scale represented by possible heavy masses (e.g. a heavy right-handed neutrino). This situation is theoretically unpleasant and the lightness of

the Higgs needs to be explained or maintained without huge fine tuning. Supersymmetry (SUSY) can resolve this issue by cancelling the quadratic divergence associated with fundamental scalars.

Nevertheless, the observed value of the Higgs mass ($m_h \sim 126$ GeV) already places the minimal supersymmetric extension of the standard model (the MSSM) in tension with the naturalness requirement since the tree-level Higgs mass bound $m_h \leq m_Z$ implies that very large stop masses and mixing is required in order to radiatively increase the Higgs mass to its observed value, leading to a fine tuning in the permille level (see [90] for a general discussion on Naturalness and SUSY). Moreover, the lower bound on the gluino mass at the LHC of greater than 1 TeV or so is exacerbating the situation, since the gluino mass radiatively increases the mass of the top squarks, independently of their experimental limit, especially in high scale SUSY models such as the constrained MSSM (cMSSM) or minimal supergravity (mSUGRA) where the effect of gluino radiative corrections occurs over a larger energy range (for a general discussion on the Status of SUSY after LHC8 we refer the reader to [91]).

Non-minimal SUSY models, such as the next-to-minimal standard model (NMSSM) (for a review see [81]), can accommodate a 126 GeV Higgs boson without requiring such large stop masses and mixing. This is because non-minimal models usually introduce additional contributions to the physical Higgs mass at tree level. In particular, the superpotential of the NMSSM contains an F-term interaction ($\lambda \hat{S} \hat{H}_u \hat{H}_d$) that couples the up- and down-Higgs doublets with the SM singlet. This will enhance the Higgs mass with an additional term proportional to λ at tree-level (Equation 5.1 in Sec. 4.2). Thus, the fine tuning is expected to be less severe than in the MSSM since one does not require large stop loop contributions as is the case in the MSSM [92, 93, 94]. However, there is an upper bound on λ at the low scale ($\lambda \lesssim 0.7$) [95] for it to be perturbative to the GUT scale. This indeed will limit the tree-level enhancement to the Higgs mass in the NMSSM. Moreover, the increased lower bounds on sparticles from direct searches at the LHC sets the minimum amount of fine tuning in the electroweak sector of all SUSY models, and the NMSSM is no exception.

Adding extra matter to the particle content of the NMSSM has a profound impact on the phenomenology and predictions of the model. In particular, it allows λ to be larger at the low scale [96, 97, 98], while still perturbative to the GUT scale. Indeed, this can improve the tree-level enhancement to the Higgs mass in comparison with the NMSSM without extra matter. Conventional wisdom dictates that increasing λ at the low scale, by adding extra matter, reduces the fine tuning of the model. However, surprisingly, this question has not been fully addressed in the literature in a Z_3-invariant semi-constrained SUGRA framework, as far as we know. In this Chapter, we consider two examples of the NMSSM with extra matter, and we find that, although λ is increased at the low scale, neither model leads to a reduction in fine tuning. The two models are called: the "NMSSM+", which is defined by adding extra matter filling three $(5 + \bar{5})$ of $SU(5)$ (cf. 3.44), and the "NMSSM++", where four extra $(5 + \bar{5})$ matter representations of $SU(5)$ are added to that present in the NMSSM.

Although the fine tuning in the "NMSSM+" has not been discussed before, a related model, the "Peccei-Quinn NMSSM" with additional three $(5 + \bar{5})$ states of $SU(5)$ has been considered [97], where the fine tuning due to the parameter A_λ (the trilinear soft SUSY breaking term associated with λ) was discussed. This model is characterised by removing the cubic self-coupling term of the singlet superfield $(\frac{\kappa}{3}\hat{S}^3)$ from the superpotential. On the other hand, the analysis in [99] considered a non-scale invariant version of the Peccei-Quinn NMSSM, as well as the so-called "λ-SUSY" model, where λ is not required to be perturbative to the GUT scale, but only to ~ 10 TeV to comply with electroweak precision tests. Further references will be given in Sec. 4.4.

In this Chapter, then, we study and compare the fine tuning in three Z_3-invariant semi-constrained GUT models: the NMSSM, where we update previous literature, and the NMSSM+ and NMSSM++ for the first time. We show that, surprisingly, while λ assumes larger values in the plus-type models than in the NMSSM, hence the tree-level Higgs mass is larger in such models, there is an indirect RGE effect, played by the gluino, that renders the plus-type models more fine tuned than the NMSSM. [1] As a

[1] In particular, we find that, in order to obtain the same physical gluino mass at the low scale in the three models, the GUT scale boundary condition of the gluino mass parameter $M_3(M_{\rm GUT})$ will follow a specific ordering. Namely, $M_3(M_{\rm GUT})$ is larger in the NMSSM+, and even larger in the NMSSM++, as compared to the NMSSM.

consequence of this unavoidable RGE effect (explained in Sec. 4.3), the mass of the top squarks will always be larger than in the NMSSM+, and even larger in the NMSSM++, as compared to the NMSSM. Taking into account current LHC limits and constraints on the Higgs, third generation squarks, and the gluino, the lowest fine tuning in the semi-constrained NMSSM, NMSSM+, and NMSSM++ is found to be about 100, 200 and 600, respectively, which is a new and unexpected result. While the NMSSM and the NMSSM+ are less fine tuned than the cMSSM, the NMSSM++ is fine tuned to a level comparable to that in the cMSSM. More importantly, our results show that increasing the perturbativity bound on λ by adding extra matter does not reduce the fine tuning. In fact, it can increase the fine tuning significantly.

In Sec. 4.2, we give a brief overview of the models is given. Sec. 4.3 discusses certain one-loop RGEs and features of each model. In Sec. 4.4, we discuss the fine tuning measure that is used, and the two-loop RGEs implementations. Next, we discuss the theoretical framework at the GUT scale, and the ranges of parameter space we are considering in each model in Sec. 4.5. Sec. 4.6 is where we present our main results. Finally, we conclude in Sec. 4.8.

4.2 The models

Non-minimal models are associated with adding fields not present in the SM, and/or enlarging the gauge structure. The NMSSM is a well-known example where the μ term in the MSSM is omitted, and a SM-singlet field is introduced. This field acquires VEV near the weak scale to dynamically generate a μ effective term. The NMSSM keeps all the good features of the MSSM, such as unification of gauge couplings, and radiative electroweak symmetry breaking. It is also known to have lower fine tuning than the MSSM as mentioned in Sec. 4.1. However, to avoid unwanted weak-scale Axion, one introduces a cubic term for the singlet and the superpotential is invariant under a discrete Z_3 symmetry,

$$\mathcal{W}_{\rm NMSSM} = \frac{\kappa}{3}\hat{S}^3 + \lambda\hat{S}\hat{H}_1\hat{H}_2 + \mathcal{W}_{\rm MSSM}(\mu = 0) \tag{4.1}$$

where $\hat{H}_1 = \hat{H}_d$, $\hat{H}_2 = \hat{H}_u$ are the down- and up-type Higgs superfields, $\hat{S}$ is a SM singlet superfield. κ is the cubic coupling of the singlet, and λ is the Higgs singlet-doublet coupling. $\mathcal{W}_{\rm MSSM}(\mu = 0)$ is the superpotential of the MSSM without a μ term. Note that 4.1 is invariant under a discrete Z_3 symmetry, and once the VEVs are acquired this symmetry is broken.

The Higgs and the SM singlet superfields will acquire VEVs represented classically as,

$$\langle H_1 \rangle = \begin{pmatrix} v_1 \\ 0 \end{pmatrix}, \quad \langle H_2 \rangle = \begin{pmatrix} 0 \\ v_2 \end{pmatrix}, \langle S \rangle = v_3, \tag{4.2}$$

In terms of these VEVs, the scalar Higgs potential reads,

$$\begin{aligned} V_{\rm NMSSM} =& m_1^2 v_1^2 + m_2^2 v_2^2 + \lambda^2 v_1^2 v_2^2 + 2\mu_{\rm eff} B_{\rm eff} v_1 v_2 \\ &+ \frac{\bar{g}^2}{8}(v_1^2 - v_2^2)^2 + v_3^2(m_S^2 + \frac{2}{3} k v_3 A_\kappa + \kappa^2 v_3^2). \end{aligned} \tag{4.3}$$

where, $m_j^2 = m_{H_j}^2 + \mu_{\rm eff}^2$, for $j = 1, 2$. $\mu_{\rm eff} = \lambda v_3$ and $B_{\rm eff} = \kappa v_3 + A_\lambda$ are effective terms produced as the SM singlet acquires its VEV. A_λ and A_κ are trilinear soft terms associated with the couplings λ and κ. m_S is the soft mass of the singlet. And $\bar{g}^2 = g_1^2 + g_2^2$, where g_1 and g_2 are the gauge couplings associated with $U(1)_Y$ and $SU(2)_L$, respectively.

From the minimisation conditions, $\frac{\partial V}{\partial v_i} = 0$, where the index i runs from 1 to 3, we obtain three conditions for electroweak symmetry breaking in terms of the mass of the Z boson, m_Z, and $\sin 2\beta$, where $\tan\beta = \frac{v_2}{v_1}$, and the soft mass of the SM singlet, m_S:

$$\frac{m_Z^2}{2} = \frac{m_1^2 - \tan^2\beta m_2^2}{\tan^2\beta - 1}, \tag{4.4}$$

$$\sin 2\beta = \frac{2\mu_{\rm eff} B_{\rm eff}}{m_1^2 + m_2^2 + \lambda^2 v^2}, \tag{4.5}$$

$$m_S^2 + \kappa A_\kappa v_3 + \kappa^2 v_3^2 \simeq 0 \tag{4.6}$$

where, $v^2 = v_1^2 + v_2^2 = (174 \text{ GeV})^2$ [2].

Equations 4.4- 4.5 are similar to those of the MSSM, while Equation 4.6 is absent in the MSSM since it does not contain a SM singlet superfield. In contrast to the MSSM, the μ_{eff} in the NMSSM depends on soft parameters as it includes v_3, which, in turn, can be written in terms of m_S and A_κ by using Equation 4.6.

The soft terms, $\{m_{H_j}, m_S, A_\kappa, \text{and } A_\lambda\}$, at the low scale, e.g. $M_{\text{SUSY}} \sim \mathcal{O}(1\text{TeV})$, can be expanded in terms of the fundamental parameters of the theory that are specified at the GUT scale using the Renormalisation Group Equations (RGEs) (this will be briefly discussed in Sec. 4.3). In particular, in the framework of mSUGRA/CNMSSM, all scalar masses share a common mass: m_0, all gaugions share a common mass: $m_{1/2}$, and all trilinear couplings share a common value: A_0. This is called universal boundary conditions. One can work on a framework where some or all of this universality is relaxed.

One of the remarkable features of the NMSSM is that it allows for the increase of the tree-level Higgs physical mass via an additional F-term contribution:

$$m_h^2 \leq m_Z^2 \cos^2 2\beta + \lambda^2 v^2 \sin^2 2\beta, \tag{4.7}$$

therefore, unlike the case in the MSSM, moderate values of $\tan\beta$ (<10) are preferred in conjunction with large values of $\lambda \sim 0.7$. Additionally, loop corrections to the physical Higgs mass, which are dominated by the top/stop, need not be as large as in the MSSM. This means that, in the NMSSM, the A-term can be as small as zero, and the lightest stop can be significantly smaller than in the MSSM (more discussion can be found in [98]). Moreover, it is well-known that in the NMSSM, the SM-like Higgs can be either the lightest or the next-to-lightest CP-even Higgs states.

Nevertheless, the NMSSM is also known to have its own issues, namely, the "domain wall problem" that arises as the Z_3 symmetry is spontaneously broken near the electroweak scale [100]. This problem, as well as the 0.7 bound on $\lambda(M_{\text{SUSY}})$ are the

[2] cf. 2.43, and notice that the value of v depends on the definition of the Higgs fields, specifically, whether the square-root is absorbed into the fields or not.

main motivation for studying extensions of the NMSSM where extra matter surviving to a scale of a few TeV are present. Plus-type models can overcome both issues [101] and offer a link to a more fundamental (F-Theory) framework [102].

In the notation of $SU(5)$ representations, the two models we are considering and comparing with the NMSSM can be viewed as:

$$\text{NMSSM+} \approx \text{ NMSSM } + 3(5+\bar{5}), \tag{4.8}$$

and

$$\text{NMSSM++} \approx \text{ NMSSM } + 4(5+\bar{5}). \tag{4.9}$$

From low energy standpoint, Eqs. 4.4-4.6 hold in the plus-type models to a good approximation, this is because the extra matter resides in a secluded sector that only relates to ordinary NMSSM superfields through gauge interactions, and therefore, any contributions to EWSB conditions from such sector could be suppressed [101]. This is a key feature of the models we are considering, and as a consequence, the chief effect of the presence of the extra matter is the modification of running of the gauge couplings (and gaugino mass running) at one-loop, and the running of the rest of the parameters at two-loop. Gauge coupling unification is approximately achieved at two-loop in both plus-type models (Fig. 4.1) since the extra matter form complete representations of SU(5). Furthermore, in the NMSSM+ (++), and for a mass scale of the extra matter of 3 (6) TeV, the unification scale is $M_{\rm GUT} \sim 2.5 \times 10^{16}$ GeV ($M_{\rm GUT} \sim 3.6 \times 10^{16}$ GeV), and the unified coupling is $\alpha_{\rm GUT} \sim 0.11$ ($\alpha_{\rm GUT} \sim 0.33$). This can be compared to the NMSSM, where $M_{\rm GUT} \sim 1.5 \times 10^{16}$ GeV, and $\alpha_{\rm GUT} \sim 0.04$. Moreover, the implication of such increase in $M_{\rm GUT}$, and $\alpha_{\rm GUT}$ is that the proton lifetime from dimension-6 operators ($\tau_p \propto \frac{M_{\rm GUT}^4}{\alpha_{\rm GUT}^2}$) will be roughly, $\tau_p \sim 2.5 \times 10^{34}$ years ($\tau_p \sim 1 \times 10^{34}$ years), in comparison to the NMSSM where $\tau_p \sim 2.1 \times 10^{34}$ years. These are well above the limit on $\tau_p\,(p \to e\pi) > 8.2 \times 10^{33}$ years [103].

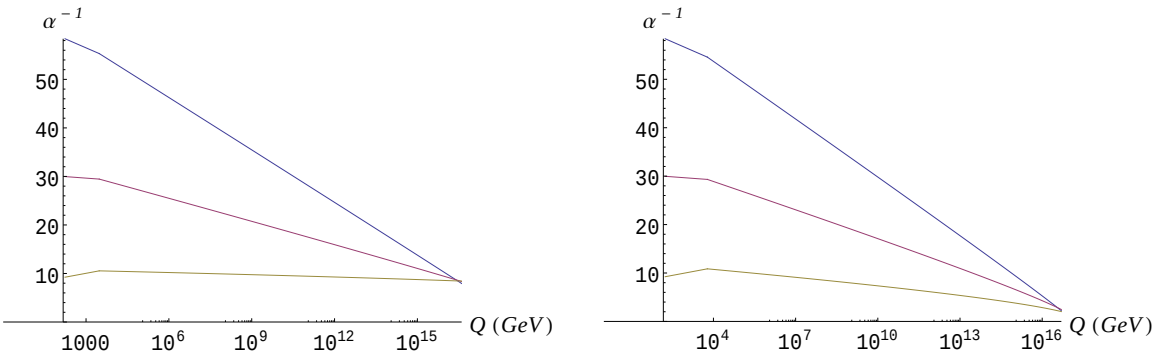

FIGURE 4.1: Gauge coupling unification to two-loop in the NMSSM+ (left) and the NMSSM++ (Right). The mass scale of the extra matter in the NMSSM+ (NMSSM++) is taken here to be 3 (6) TeV. Below that scale, the NMSSM without extra matter is assumed. At $M_t = 173.6$ GeV, we set: $g_{1,\mathrm{SM}} = 0.35940$, $g_2 = 0.64754$, $g_3 = 1.1666$, $h_t = 1.01685$, $\tan\beta = 5$, $\lambda = 0.7$, and $\kappa = 0.1$.

In Sec. 4.3 we provide a comparison of specific one-loop RGEs and approximate solutions in order to establish some crucial differences between the models that will be relevant in subsequent Sections.

4.3 One-loop renormalisation group analysis

In this Sec. we present a one-loop analysis of the three models to illustrate a few key points that will aid in anticipating and understanding the fine tuning results in Sec. 4.6. The main arguments will still be valid even though we incorporate two-loop RGEs in our analysis in Sec. 4.6.

The addition of extra matter in the plus-type models is motivated both from the high scale and the low scale model building point of view. In particular, by examining the effects on the RGEs, one can show that the perturbativity bound on λ at the SUSY scale ($\lambda_{M_{\mathrm{SUSY}}}$) increases in the plus-type models as shown in the left panel of Fig. 4.2.

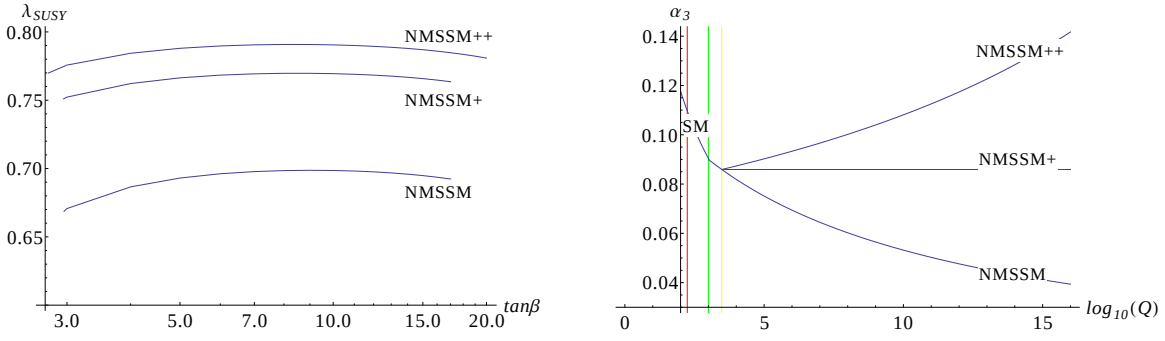

FIGURE 4.2: The left panel: $\lambda(1\text{ TeV})$ as a function of $\tan\beta$ in the three different models (for $\kappa(1\text{ TeV}) \sim 0.002$). Right panel: The one-loop running of the strong coupling $\alpha_3(\equiv \alpha_s)$, where the running from m_Z (vertical black line), passing through $m_t = 173.6$ GeV (vertical red line), to a fixed SUSY scale at 1 TeV (vertical green line) is performed using SM RGE. Next, the running from 1 TeV to the GUT scale is performed using the NMSSM RGE, and at 3 TeV (vertical yellow line) the NMSSM+ and the NMSSM++ RGEs are used to run up to the GUT scale.

The reason behind this increase can be understood by inspecting the RGEs of the gauge couplings: g_a (where $a = 1, 2$ and 3, for $U(1)_Y$, $SU(2)_L$, and $SU(3)_c$ gauge groups, respectively), the top Yukawa coupling: h_t, the doublet-singlet coupling: λ, in the three models. At one-loop, the RGEs take the following form:

$$16\pi^2\partial_t g_1^2 = \left(11, 16, \frac{53}{3}\right) g_1^4 \tag{4.10}$$

$$16\pi^2\partial_t g_2^2 = (1, 4, 5)\, g_2^4 \tag{4.11}$$

$$16\pi^2\partial_t g_3^2 = (-3, 0, 1)\, g_3^4 \tag{4.12}$$

$$16\pi^2\partial_t h_t^2 = h_t^2\left(6h_t^2 + h_b^2 + \lambda^2 - \frac{13}{9}g_1^2 - 3g_2^2 - \frac{16}{3}g_3^2\right) \tag{4.13}$$

$$16\pi^2\partial_t \lambda^2 = \lambda^2\left(3h_t^2 + 3h_b^2 + 4\lambda^2 - g_1^2 - 3g_2^2\right), \tag{4.14}$$

where, $\partial_t \equiv \frac{\partial}{\partial \ln Q^2}$, and Q is the renormalisation scale. The coefficients between parentheses in Equations 4.10-4.12 belong to the NMSSM, the NMSSM+ and the NMSSM++, respectively. And g_1 is SM normalized (as opposed to the GUT normalization that introduces a factor of $\sqrt{\frac{3}{5}}$, i.e. $g_{1,\text{SM}}^2 = \frac{3}{5}g_{1,\text{GUT}}^2$). The magnitudes and the signs of these β-function coefficients lead to larger g_3 and smaller h_t, at the

GUT scale, in the NMSSM+ compared to the NMSSM, and similarly larger values of both couplings in the NMSSM++ compared to the NMSSM+, at the GUT scale. This allows larger λ at the low scale (e.g. 1 TeV) while keeping its perturbativity to the GUT scale. The advantage of having a larger low-scale λ is that it allows for a larger tree-level Higgs mass in 5.1. Moreover, since the top/stop Yukawa coupling depends on $\sin\beta$ as follows,

$$h_t(Q) = \frac{m_t(Q)}{v \sin\beta}, \tag{4.15}$$

it is possible to achieve smaller $\tan\beta$ in the plus-type models.

Moreover, it is instructive to examine the running of $\alpha_3 = \frac{g_3^2}{4\pi}$ (which runs similar to the gluino mass parameter M_3). This is shown in the right panel of Fig. 4.2. Note that, in order to reach the same point at the low scale, say $\alpha_3(1\text{ TeV})$, in three models, the starting point at the GUT scale (i.e. the boundary condition: $\alpha_{3,\text{GUT}} \equiv \alpha_3(M_{\text{GUT}})$ is significantly different. In particular,

$$\alpha_{3,\text{GUT}}^{\text{NMSSM++}} > \alpha_{3,\text{GUT}}^{\text{NMSSM+}} > \alpha_{3,\text{GUT}}^{\text{NMSSM}}. \tag{4.16}$$

This effect will play a profound role in shaping the fine tuning (as we show in Sec. 4.6) since we expect a similar behaviour in the running of the gluino mass parameter M_3. And although we use two-loop RGEs to obtain our fine tuning results in Sec. 4.6, the argument is still valid, namely that, in order to reach the same physical gluino mass at the low scale in the three models, the GUT scale boundary condition $M_{3,\text{GUT}} \equiv M_3(M_{\text{GUT}})$ will follow the ordering:

$$M_{3,\text{GUT}}^{\text{NMSSM++}} > M_{3,\text{GUT}}^{\text{NMSSM+}} > M_{3,\text{GUT}}^{\text{NMSSM}}. \tag{4.17}$$

The physical gluino mass at the low scale can be approximately related to the input parameter $m_{1/2}$, which is a universal gaugino mass at the GUT scale, as follows: $m_{\tilde{g}} \approx f m_{1/2}$, where the coefficient f is model-dependent. We will present these values in Sec. 4.6. Next, we consider the implication of the ordering in 4.17. The gluino

affects the running of the squarks at one-loop in the following fashion,

$$\frac{\partial m^2_{\tilde{Q}_3}}{\partial t} = -\frac{3\alpha_3}{8\pi} M_3^2 + f(m^2_{\text{scalars}}, A^2, g_a^2, \dots), \tag{4.18}$$

where we are only showing the gluino mass term explicitly. It is well-known [47, 104, 105] that the gluino mass parameter, if large enough at the GUT scale, can dominate the running of the scalars. It is also well-known that coloured scalars run from the GUT scale to the low scale in such a way that the running masses increase. Any negative term in the RGE will enhance this increase in the running mass at the low scale, and indeed the gluino mass term in Equation 4.18 is negative, thus the larger the boundary condition ($M_{3,\text{GUT}}$) the larger the scalar mass will be at the low scale.

We wish to point out that, in the MSSM, obtaining a physical Higgs mass of 126 GeV requires very large top squarks or large stop mixing (large A-term), hence, it is requiring a 126 GeV Higgs that is causing the fine tuning (in addition to direct limits on sparticles). Whereas in the NMSSM, the top squarks do not need to be as large as in the MSSM, but the limits from direct searches, especially on the top squarks will play a crucial role in determining the fine tuning. However, in the plus-type models we are considering, we expect that the top squarks in the NMSSM+ will always be larger than in the NMSSM, and they will always be larger in the NMSSM++ than in the NMSSM+. This is a result of the rather larger values of the $M_3(M_{\text{GUT}})$, or $m_{1/2}$, that one has to start with at the GUT scale in order to achieve a gluino mass larger than 1.2 TeV at the low scale, as indicated in Equation 4.17. Therefore, we expect that the gluino is the main source of fine tuning in the plus-type models, and we verify that in Sec. 4.6.

Next, we present approximate solutions of the one-loop RGE of the parameter m_{H_u} in the three models. This is for $\tan\beta = 2, \kappa(M_{\text{SUSY}}) = 0.002$, and $M_{\text{SUSY}} = 1$ TeV, and we expand $m_{H_u}(M_{\text{SUSY}})$ in terms of universal GUT parameters: $m_{1/2}$, m_0 and A_0,

1. NMSSM ($\lambda(M_{\text{SUSY}}) = 0.6$):

$$-m^2_{H_u}(M_{\text{SUSY}}) \approx 3m^2_{1/2} + 0.8m_0^2 + 0.07A_0^2 - 0.09m_{1/2}A_0 \tag{4.19}$$

2. NMSSM+ ($\lambda(M_{\rm SUSY}) = 0.72$):

$$-m^2_{H_u}(M_{\rm SUSY}) \approx 2.04 m^2_{1/2} + 0.74 m^2_0 + 0.09 A^2_0 - 0.18 m_{1/2} A_0 \tag{4.20}$$

3. NMSSM++ ($\lambda(M_{\rm SUSY}) = 0.75$):

$$-m^2_{H_u}(M_{\rm SUSY}) \approx 1.78 m^2_{1/2} + 0.71 m^2_0 + 0.1 A^2_0 - 0.3 m_{1/2} A_0. \tag{4.21}$$

While it is clear from Equations 4.19- 4.21 that the sensitivity of $m^2_{H_u}(M_{\rm SUSY})$ to $m^2_{1/2}$ is reduced by adding extra matter, it is important to notice the ordering in Equation 4.17. Clearly, the more matter included, the larger the required $m_{1/2}$ in order to produce the desired physical $m_{\tilde{g}}$, hence the larger the top squarks. We quantify this to two-loop and study the associated fine tuning in the following Sec.s.

4.4 Fine tuning and two-loop implementations

4.4.1 Fine tuning

To quantify fine tuning at each point in the parameter space, one can measure the fractional sensitivity of an observable, namely the mass of the Z boson, m_Z to fractional variations in the fundamental GUT parameters,
$a = \{m_{1/2}, m_0, m_S, m_{H_u}, m_{H_d},\ A, A_\lambda, A_\kappa,\ \lambda, \kappa, h_t\}$ ([39] and [40]),

$$\Delta_a = \left| \frac{\partial \log m_Z}{\partial \log a} \right|, \tag{4.22}$$

where $\Delta^{-1} \times 100\%$ represents the percentage to which a parameter is fine tuned.

This measure is usually called the Barbieri-Giudice measure, and it has been extensively used in the literature (see for e.g. [106, 107, 108, 109, 110, 111, 112, 113], and [114] and references therein). Note that some authors prefer to use m^2_Z instead of m_Z and/or a^2 instead of a. All different choices can be related to each other by the

inclusion of an appropriate factor. This global sensitivity of Equation 4.22, alternative measures, and Bayesian approaches has been briefly discussed in [114].

Moreover, the measure (Equation 4.22) is already implemented in the Fortran code NMSPEC [115] that we use, which is part of the package NMSSMTools 4.1.2. In this package, the fine tuning is calculated in two steps: first, the tuning with respect to SUSY scale parameters

$$m_{H_{u,d}}(M_{\rm SUSY}), m_S(M_{\rm SUSY}), A_{\lambda,\kappa}(M_{\rm SUSY}), \lambda(M_{\rm SUSY}), \kappa(M_{\rm SUSY}), h_t(M_{\rm SUSY}) \quad (4.23)$$

is calculated using Equation 4.22 with the parameter a being a SUSY scale parameter in 4.23. Second, the results are linked to GUT scale parameters using the RGEs, hence determining the fine tuning with respect to the GUT scale parameters. The procedure is discussed in details in [93]. This method is equivalent to deriving a fine tuning "master formula" for the NMSSM, as in [92].

4.4.2 Two-loop implementations

We modify the tool for both the NMSSM+ and the NMSSM++ cases by adding the relevant two-loop RGEs (presented in Appendix A) to enable calculating the mass spectrum of each model and study the fine tuning.

The procedure for calculating the RGEs is to start from the two-loop RGEs of the NMSSM, and then modify them for the NMSSM+ and the NMSSM++ cases. This is since only a specific set of coefficients will be altered due the presence of extra matter. Particularly, the extra fields, which are charged under the SM gauge group, will change the coefficients of $\mathcal{O}(g_a^4)$ terms of the beta functions since they can run in the loop as depicted in Fig. 4.3

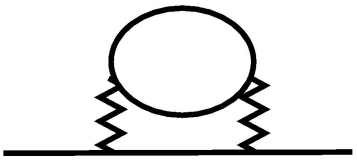

FIGURE 4.3: A schematic two-loop diagram illustrating how extra matter loops can modify $\mathcal{O}(g_a^4)$ terms of the running scalars, gauginos, trilinears, and Yukawas (see Appendix A)

The relevant terms to be modified are calculated using the results in [116], and the full set of RGEs are cross-checked using the package SARAH [117] by manually carrying out algebraic operations of adding traces, obtaining the RGEs for the trilinears

$$\partial_t A = \partial_t \left(\frac{\mathbf{a}(t)}{h(t)} \right), \tag{4.24}$$

since SARAH outputs the RGEs of $\mathbf{a}(t)$, and ensuring the consistency of the conventions. Furthermore, we take an effective theory approach whereby the extra matter are integrated out via a step-function change of the beta functions at a scale

$$Q_{\rm SUSY} = \sqrt{\frac{2m_{Q_1}^2 + m_{U_1}^2 + m_{D_1}^2}{4}}, \tag{4.25}$$

as defined in NMSSMTools to be the scale of the first and second generations squarks. $m_{Q_1}^2, m_{U_1}^2$, and $m_{D_1}^2$ are scalar squared masses of the first generation squarks. In the parameter spaces scanned in Sec. 4.6, it ranges between 1.1-4.1 TeV in the NMSSM, 1.9-6.4 TeV in the NMSSM+, and 3.5-7.5 TeV in the NMSSM++.

Moreover, for convenience, we assume a degenerate mass scale for the extra matter, and we set it to be $Q_{\rm SUSY}$. Consequently, the RGEs of the full theory, i.e. the NMSSM+(++), are used between the GUT scale and the scale $Q_{\rm SUSY}$, whereas the RGEs of the effective theory, i.e. the NMSSM, are used below that. As the RGEs descend from $Q_{\rm SUSY}$, NMSSMTools includes leading logarithmic threshold corrections to the gauge and Yukawa couplings from the relevant superpartners. However, since the mass scale of some of the squarks (and all of the extra matter) is assumed to be of

order $Q_{\rm SUSY}$, such states do not contribute to the threshold corrections, as pointed out in [81].

Nevertheless, the extra matter sector is in fact a secluded sector since no Yukawa couplings are shared with the NMSSM superfields. The extra matter will obtain fermionic and scalar masses in the secluded sector by mechanisms that are irrelevant to the weak scale (further details in [101]). As such, we have not calculated the precise mass spectrum of this secluded sector. Additionally, in our set-up, the contributions from the running masses of the extra matter to the NMSSM scalar masses can be safely ignored at one- and two-loop [3] since they are highly suppressed and only introduce a relative error smaller than 1%.

Finally, it worth mentioning that the ordering in Equation 4.17 will remain valid at the two-loop order, therefore the situation will always be such that for a given physical gluino mass, say 1.2 TeV, the NMSSM+ will require $M_3(M_{\rm GUT})$ to be larger than that in the NMSSM, and hence the top squarks in the NMSSM+ will be larger than the top squarks in the NMSSM. Similarly, the NMSSM++ will require $M_3(M_{\rm GUT})$ to be larger than that in the NMSSM+, which means the top squarks will be larger in the former than in the latter. We verify this and study the implication on the fine tuning in Sec. 4.6.

4.5 Framework and parameter space

4.5.1 Framework

We choose to work in a semi-constrained framework where the gaugino masses are universal at the GUT scale, i.e. $M_1(M_{\rm GUT}) = M_2(M_{\rm GUT}) = M_3(M_{\rm GUT}) = m_{1/2}$, where M_1, M_2 are Bino and Wino mass parameters. One the other hand, we allow m_S, m_{H_u} and m_{H_d} to differ from the rest of the scalars that have a common mass m_0 at the GUT scale. However, since we use $\mu_{\rm eff}$ as an input, NMSSMTools will output the allowed values for those parameters at the GUT scale. In addition, the trilinears A_λ

[3] In ξ, ξ', σ_1, σ_2 and σ_3 in Equation A.3 in Appendix A

and A_κ can take different values, at the GUT scale, from the universal trilinear $A_0 = A_t(M_{\rm GUT}) = A_b(M_{\rm GUT}) = A_\tau(M_{\rm GUT})$, where the indices t, b, τ denote the top, bottom, and τ squarks.

Moreover, it is crucial to note that choosing non-universal gauginos at the GUT scale, i.e. $M_1(M_{\rm GUT}) \neq M_2(M_{\rm GUT}) \neq M_3(M_{\rm GUT})$ might be desirable [4]. However, we do not make this assumption here since it has no impact on the fine tuning comparison for the three models. In particular, as we show in Sec. 4.6, $M_3(M_{\rm GUT})$ controls the fine tuning in the plus-type models, while the other two parameters (M_1 and M_2) have little or no impact. Hence, we find it simpler to assume universality in our analysis. Finally, we do not include constraints from dark matter in our analysis (although we check that regions of low fine tuning are not excluded by an upper bound of $\Omega h^2 < 0.13$ as calculated by the package micrOMEGAs [118] that is embedded in NMSSMTools), and we are not addressing the issue of the anomalous magnetic moment of the muon [5].

4.5.2 Parameter space

We have focused on the parameter space where λ, at the low scale, can be as large as possible, while $\tan\beta$ can be as small as possible in the three models, this is subject to constraints from perturbativity, successful electroweak symmetry breaking, and experimental limits, all of which are taken into account in NMSSMTools [6] (including: LEP bounds on Higgs searches and invisible Z decays [120, 121, 122], constraints on new physics from $\mathrm{Br}(b \to s\gamma) = (355 \pm 24 \pm 9) \times 10^{-6}$ [123] , $\mathrm{Br}(B_s \to \mu^+\mu^-) = (3.2^{+1.5}_{-1.2} \times 10^{-9})$ [124], and $\mathrm{Br}(B \to \tau\nu_\tau) = (1.12 \pm 0.22) \times 10^{-4}$ [125], all to within 2σ). The mass of the SM-like Higgs is required to be $m_h = 125.7 \pm 3$ GeV to account for uncertainties. If the SM-like Higgs is the second-to-lightest Higgs in the NMSSM, then NMSSMTools will ensure that the lightest Higgs satisfies LEP constraints. Furthermore, NMSSMTools ensures that the couplings and signals of the SM-like Higgs comply with LHC results as studied in [126]. Additionally, we require

[4] One possible situation where abandoning this universality is desirable is to have $M_1(M_{\rm GUT}) \neq m_{1/2}$ to satisfy dark matter constraints as discussed in [93]

[5] This means that it is possible that some points in the parameter space do not satisfy the experimental limit on $(g-2)_\mu$, which is already in tension with the SM. In the NMSSM $(g-2)_\mu$ was analysed in [119]

[6] A full list of constraints can be found in the official website of NMSSMTools:`http://www.th.u-psud.fr/NMHDECAY/nmssmtools.html`

that $m_{\tilde{t}_1} > 700$ GeV, and $m_{\tilde{g}} > 1.2$ TeV [127]. Removing the constraint on $m_{\tilde{t}_1}$ from our analysis does not negate our main finding that the NMSSM is less fine tuned than the NMSSM+, and the NMSSM+ is less fine tuned than the NMSSM++. Additionally, it is difficult to relax this constraint since this will depend on certain mass relations (e.g. between $m_{\tilde{t}_1}$ and $m_{\tilde{\chi}_1^0}$), which we are not analysing here [7]

We use the simple random sampling method provided by NMSSMTools. However, in order to test the effect of increasing λ by adding extra matter on the fine tuning, we choose a representative range of the parameters λ, $\tan\beta$, and μ that leads to an enhancement to the tree-level Higgs mass, and to a reduction of the tuning in m_Z. Our strategy is to scan small patches of the parameter space, with narrow ranges of m_0, $m_{1/2}$, and A in order to find solutions where the fine tuning is expected to be small. With this in mind, we scan up to 6×10^7 points in this region of the parameter space in each model. Next, points that violate the constraints mentioned previously are removed. Finally, we divide the data into two sets, the first set is where the lightest Higgs is SM-like, and the second set is where the second-to-lightest Higgs is SM-like. The scanned range of parameters is,

$$0 < m_0 < (2, 4, 7) \text{ TeV}$$
$$0 < m_{1/2} < (2, 4, 7) \text{ TeV}$$
$$-3.5 < A < 7 \text{ TeV}$$
$$-3.5 < A_\lambda < 3.5 \text{ TeV}$$
$$-3.5 < A_\kappa < 3.5 \text{ TeV}$$
$$100 < \mu_{\text{eff}} < 400 \text{ GeV}$$
$$0 < \tan\beta < 5$$
$$0.5 < \lambda < 1$$
$$10^{-4} < \kappa < 0.6$$

where the numbers between parentheses in the first two lines correspond to the range in the NMSSM, the NMSSM+, and the NMSSM++, respectively. In all models, the

[7] It is important to mention that, while the lightest stop plays a role in the determination of the fine tuning, the heavy stop also plays a role, as well as the trilinear coupling A_t, and the soft Higgs mass m_{H_u}. For instance, a very light $m_{\tilde{t}_1}$ can be obtained if A_t is quite large. However, this will lead to a rather large $m_{\tilde{t}_2}$, which in turn will contribute to the fine tuning via the radiative corrections to the Higgs potential.

fine tuning plots range from 0 to 2000 –we stop at $\Delta = 2000$ for convenience– using the same colour scheme. This enables direct comparison between the parameter spaces of the three models.

4.6 Results

In this Sec., we present the results for the fine tuning in the parameter spaces of the three models. For each model, we have divided the parameter space into two cases, the first (case 1) is where the SM-like Higgs is the lightest CP-even Higgs, whereas the second (case 2) is where the SM-like Higgs is the next-to-lightest CP-even Higgs. The reason for this is that the detailed phenomenology of the two cases can be different (e.g. see [128] and [98]).

4.6.1 NMSSM

As stated in Sec. 4.1, the NMSSM is well-known to be less fine tuned than the most studied supersymmetric model that is the MSSM. Given the current LHC limits on the Higgs couplings, on the mass of naturalness-related superpartners, such as the top squarks and the gluino, the results in this Sec. serve as an update to the status of the fine tuning in the NMSSM within the range of parameter space specified in Sec. 4.5.

4.6.1.1 Case 1: m_{h_1} is SM-like.

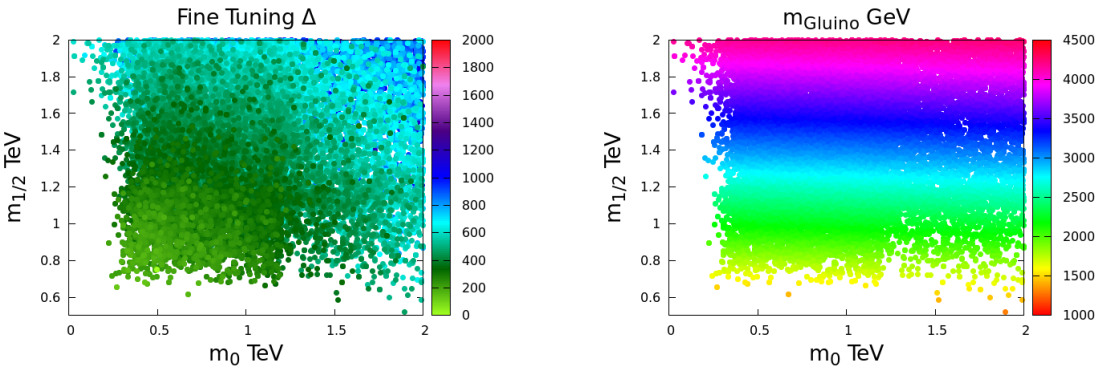

FIGURE 4.4: The left panel shows the fine tuning while the right panel shows the gluino mass, both in the $m_0 - m_{1/2}$ plane in the NMSSM when m_{h_1} is SM-like.

Fig. 4.4 (left) shows the fine tuning, $\max(\Delta_a)$ or simply Δ, represented by colours in the $m_0 - m_{1/2}$ plane, which ranges from 0 to 2 TeV. In this range of parameter space we find that $\Delta \ll 2000$. The lowest fine tuning was found to be $\Delta \sim 120$ for $m_{h_1} = 124$ GeV, $m_{\tilde{g}} = 1.4$ TeV, $m_{\tilde{t}_1} = 750$ GeV. Furthermore, the fine tuning forms contours in this plane and the band of contours associated with $120 < \Delta < 300$ corresponds to values of m_0 and $m_{1/2}$ that range from 0.3 - 1 TeV and 0.6 - 1.2 TeV, respectively. As $m_{1/2}$ becomes smaller and approaches 0.5 TeV, m_0 becomes larger and approaches 1.9 TeV, thus increasing the fine tuning up to ~ 500. On the other hand, as m_0 becomes smaller and approaches zero, $m_{1/2}$ rises to around 1.7 TeV. Consequently, the fine tuning rises above 600. Additionally, regions where m_0 and $m_{1/2}$ are both above 1.3 TeV are associated with $\Delta > 500$. In particular, at the top-right corner where both m_0 and $m_{1/2}$ are of $\mathcal{O}(2$ TeV), $\Delta \sim 1000$. It is worth-noting that this parameter space is in fact multidimensional since all fundamental parameters assume different values at each point.

A number of observables is significantly linked with fine tuning, this includes: $m_{h_1}, m_{\tilde{g}}$, and $m_{\tilde{t}_{1,2}}$. In the NMSSM, the lowest fine tuning ranges from 100 to 200 for a Higgs mass between 123 and 127 GeV.

The gluino mass (Right panel of Fig. 4.4) in this parameter space form plateaus specified by the value of the parameter $m_{1/2}$. In particular, $m_{\tilde{g}}$ ranges between ~ 1.4

TeV and 2 TeV for values of $m_{1/2}$ between 0.5 TeV and 0.8 TeV, and increases gradually with $m_{1/2}$ to reach values of order 4.5 TeV as $m_{1/2}$ reaches 2 TeV. In fact, by examining the data one finds that $m_{\tilde{g}} \sim 3m_{1/2}$ in the NMSSM. This will remain true for case 2 in 4.6.1.2.

For convenience, we define the root-mean-square (RMS) stop mass, which we will frequently use,

$$M_S = \sqrt{\frac{m_{\tilde{t}_1}^2 + m_{\tilde{t}_2}^2}{2}} \tag{4.26}$$

and we plot it in the $m_0 - m_{1/2}$ plane. Since we require the lowest mass for the lightest stop to be larger than 700 GeV, M_S can tell us if there is much separation between $m_{\tilde{t}_1}$ and $m_{\tilde{t}_2}$. Our aim is to search for points where both masses are close to 700 GeV or with the minimum separation since such points are associated with low fine tuning. From the left panel in Fig. 4.5, M_S starts at nearly 900 GeV, and increases steadily until reaching 3.4 TeV with increasing $m_{1/2}$. However, it increases very slowly in respond to an increase in m_0, particularly in this range of parameter space.

In the right panel of Fig. 4.5, the distribution of the lightest stop mass $m_{\tilde{t}_1}$ shows that it ranges from 700 GeV to ~ 2.7 TeV. Also, it grows steadily with increasing $m_{1/2}$.

Moreover, Fig. 4.6 presents the fine tuning against $m_{\tilde{g}}, M_S$ and $m_{\tilde{t}_1}$. Notice how the data points of each parameter correlate with the lowest fine tuning. In particular, $M_S, m_{\tilde{g}}$, and $m_{\tilde{t}_1}$ increase from 900 GeV to 3 TeV, 1.2 TeV to 4.3 TeV and 700 GeV to 2.5 TeV, fine tuning increases from 100 to 600, 400 and 600, respectively. Clearly, the stop plays the dominant role in determining the fine tuning. Thus, the gluino can become as large as 4.3 TeV without impacting the fine tuning as much as the top squarks.

The impact of increasing $m_{1/2}$ (and $m_{\tilde{g}}$) on the top squarks, represented by M_S, will turn to be more significant in the plus-type models. In the NMSSM, having a gluino mass of 1.2 TeV does not require $m_{1/2}$ to be larger than ~ 600 GeV -recall that $m_{1/2}$ determines, along with other parameters, the value of the top squarks via its RGE effect- and the top squarks can be as light as 700 GeV. Varying both $m_{1/2}$ and $m_{\tilde{g}}$ from 600 GeV to 2 TeV and 1.2 TeV to 4.3 TeV, corresponds to M_S in the range 900

GeV-3.4 TeV. Therefore, one can escape the LHC limit on the gluino mass without dragging the top squarks to too heavy masses.

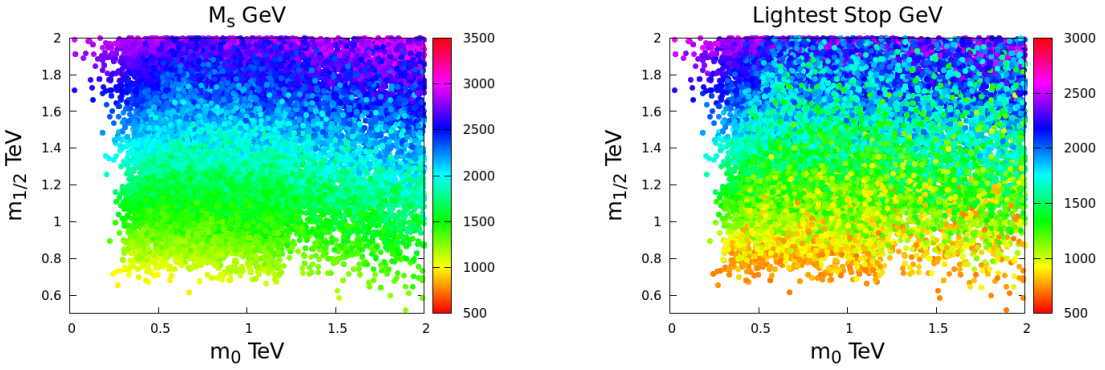

FIGURE 4.5: The left panel shows the RMS stop mass, while the right panel shows the lightest stop mass, both in the $m_0 - m_{1/2}$ plane in the NMSSM when m_{h_1} is SM-like.

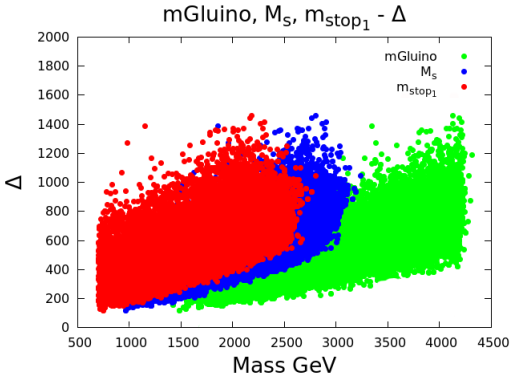

FIGURE 4.6: Fine tuning as a function of $m_{\tilde{g}}, M_S$, and m_{stop_1} in the NMSSM when m_{h_1} is SM-like.

4.6.1.2 Case 2: m_{h_2} is SM-like.

Here we present the results of fine tuning in the Higgs sector of the NMSSM where the next to lightest Higgs, m_{h_2}, is SM-like. First, we note that the fine tuning, Fig. 4.7 (left panel), is roughly similar to case 1 in 4.6.1.1. However, the lowest fine tuning here was found to be $\Delta \sim 71$ for: $m_{h_2} = 127$ GeV, $m_{\tilde{g}} = 1.34$ TeV, $m_{\tilde{t}_1} = 700$ GeV, which is slightly smaller than case 1 in 4.6.1.1 because $m_{\tilde{t}_1}$ is slightly smaller. Moreover, in this parameter space, we find valid points where $m_{1/2}$ can assume lower values than found

in the previous case, and more points occupying regions where $m_0 = 0$. Those points at $m_0 \sim 0$ are particularly associated with $A_\lambda(M_{\rm GUT}) > 1$ TeV, and $100 \leq \mu_{\rm eff} \leq 260$.

As for the gluino mass (Right panel of Fig. 4.7), it ranges from ~ 1.3 TeV to 4.4 TeV, and it correlates to $m_{1/2}$ as expected from the approximate relation $m_{\tilde{g}} \sim 3m_{1/2}$. Notice that increasing m_0 can have a small effect on raising $m_{\tilde{g}}$. This is a loop effect related to quark/squark corrections to the physical gluino mass.

The lowest fine tuning forms a plateau, of order 100, as one increases m_{h_2} from 123 GeV to 127 GeV. Next, Fig. 4.8 (left panel) shows how the parameter M_S varies in the $m_0 - m_{1/2}$ plane; it ranges from 900 GeV to 3.4 TeV, while the right panel shows that the lightest stop varies between 700 GeV and 3 TeV.

Moreover, Fig. 4.9 shows that increasing M_S, $m_{\tilde{g}}$, and $m_{\tilde{t}_1}$ from 900 GeV to 3.3 TeV, 1.2 TeV to 4.3 TeV, and 700 GeV to 2.8 TeV results in a rise in the lowest fine tuning from 71 to roughly 450 in the three cases. Therefore, it is still clear that the top squarks are in control of the fine tuning, whereas the gluino mass can assume a value as large as 4.3 TeV without worsening the situation.

While this parameter space contains the lowest fine tuned point in all our study, it is still of $\mathcal{O}(100)$, and the parameter space is not as rich as the previous one.

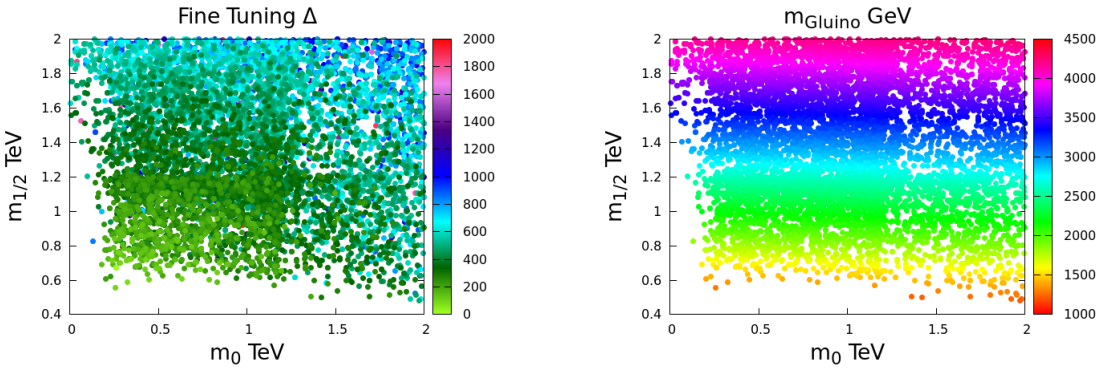

FIGURE 4.7: The left panel shows the fine tuning while the right panel shows the gluino mass, both in the $m_0 - m_{1/2}$ plane in the NMSSM when m_{h_2} is SM-like.

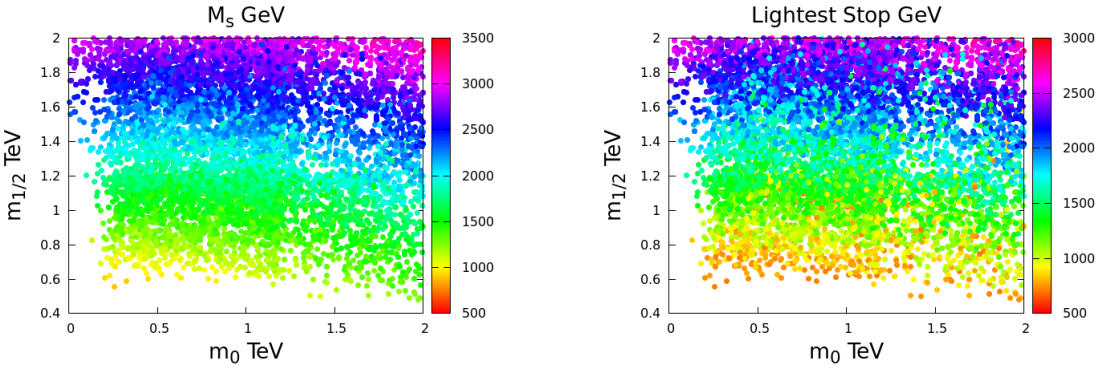

FIGURE 4.8: The left panel shows the RMS stop mass, while the right panel shows the lightest stop mass, both in the $m_0 - m_{1/2}$ plane in the NMSSM when m_{h_2} is SM-like.

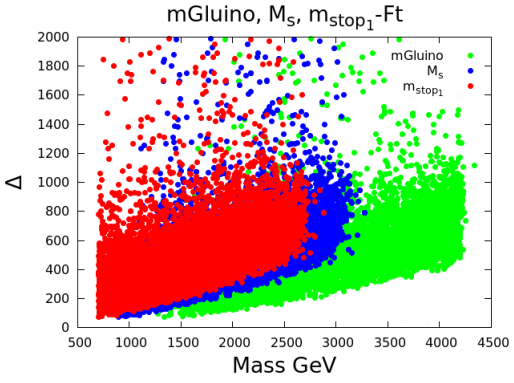

FIGURE 4.9: Fine tuning as a function of $m_{\tilde{g}}, M_S$, and m_{stop_1} in the NMSSM when m_{h_2} is SM-like.

4.6.2 NMSSM+

As discussed in Sec. 4.3, the gaugino mass parameter $m_{1/2}$ has to be larger in the NMSSM+ than in the NMSSM in order to produce the same physical gluino mass at the low scale. Moreover, the RG running of scalars depends strongly on the parameter M_3, which is equal to $m_{1/2}$ at the GUT scale. Therefore, larger $m_{1/2}$, as required by the gluino, means larger top squarks, as dictated by the RGEs. Thus, we expect the fine tuning to be larger in the NMSSM+ than in the NMSSM because the top squarks are heavier. The following results show for the first time the fine tuning in the Higgs sector of the NMSSM+ with a Z_3-invariant superpotential.

4.6.2.1 Case 1: m_{h_1} is SM-like.

The parameter space of the NMSSM+ is richer than that of the NMSSM. In particular, it is easier to obtain a Higgs mass near 126 GeV since both λ and the top squarks are larger in the NMSSM+ than in the NMSSM.

Fig. 4.10 shows the fine tuning (left panel) distribution in the $m_0 - m_{1/2}$ plane, which ranges from 0 to 4 TeV each. Only a relatively small area, located at the bottom-left corner, corresponds to fine tuning between 200 and 400. As both m_0 and $m_{1/2}$ grow larger than 2 TeV, the fine tuning steadily exceeds 400 reaching values up to 2000. The fine tuning contours show how the fine tuning is more sensitive to changes in $m_{1/2}$ than in m_0. However, as m_0 becomes larger than 3.5 TeV, the fine tuning rapidly increases. Regions where $m_0 = 0$ are not associated with low fine tuning since they correspond to large values of $m_{1/2}$. The lowest fine tuning is $\Delta \sim 205$ for: $m_{h_1} = 126$ GeV, $m_{\tilde{g}} = 1.2$ TeV, $m_{\tilde{t}_1} = 727$ GeV.

Moreover, notice how the physical gluino mass in the right panel of Fig. 4.10 is associated with larger values of $m_{1/2}$ than in the NMSSM (Fig. 4.4) as explained in Sec. 4.3. Particularly, one requires 1.3 TeV $< m_{1/2} <$ 1.5 TeV to achieve $m_{\tilde{g}} \approx 1.2$ TeV. And the approximate relation between the two parameters is: $m_{\tilde{g}} \sim 0.85 m_{1/2}$.

As a result of having a rather large $m_{1/2}$, the smallest value of the parameter M_S is now around 1.2 TeV (Fig. 4.11, left panel). One can also see that it is not possible to access smaller values of M_S because either $m_{1/2}$ or m_0 will become exceedingly large. Recall that the scalar masses are controlled by both parameters as explained in Sec. 4.3. The right panel of Fig. 4.11 presents the mass distribution of lightest stop. It can be as small as 700 GeV and as large as 4 TeV. It worth recalling that not only m_0 and $m_{1/2}$ determine $m_{\tilde{t}_1}$ and $m_{\tilde{t}_2}$, but also A_0. Large values of A_0 can lead to large splitting between the lightest and heaviest top squarks. Therefore, the data points in Fig. 4.11 (right panel) where small $m_{\tilde{t}_1}$ corresponds to large M_S (left panel), hence large $m_{\tilde{t}_2}$, are associated with large A_0.

Both $m_{\tilde{t}_1}$ and $m_{\tilde{t}_2}$ contribute to the fine tuning. Hence, it is necessary to look at the parameter M_S to understand the fine tuning results. As stated previously, the larger M_S becomes, the more the fine tuning required.

As was the case in the NMSSM, varying the Higgs mass between 123 GeV and 127 GeV has a little impact on the lowest fine tuning in the NMSSM+. However, the lowest fine tuning here forms a plateau around $\Delta \sim 200$.

Moreover, M_S, $m_{\tilde{g}}$, and $m_{\tilde{t}_1}$ (Fig. 4.12) cause the lowest fine tuning to increase from 200 to roughly 2000 as they rise from 1.2 TeV to 4.2 TeV, 1.2 TeV to 3.7 TeV, and 700 GeV to 4 TeV, respectively. The important feature that distinguishes the NMSSM+ from the NMSSM is the steady to sharp increase in the lowest fine tuning associated with increasing the gluino mass (c.f. Fig. 4.6). The lightest stop can now become more massive than the gluino and still leads to the same amount of the lowest fine tuning, in contrast to the situation in the NMSSM. Clearly, the gluino here is a major factor in determining the fine tuning since it requires a large $m_{1/2}$, which in turn affects the running of the top squarks, making them larger in comparison to the NMSSM.

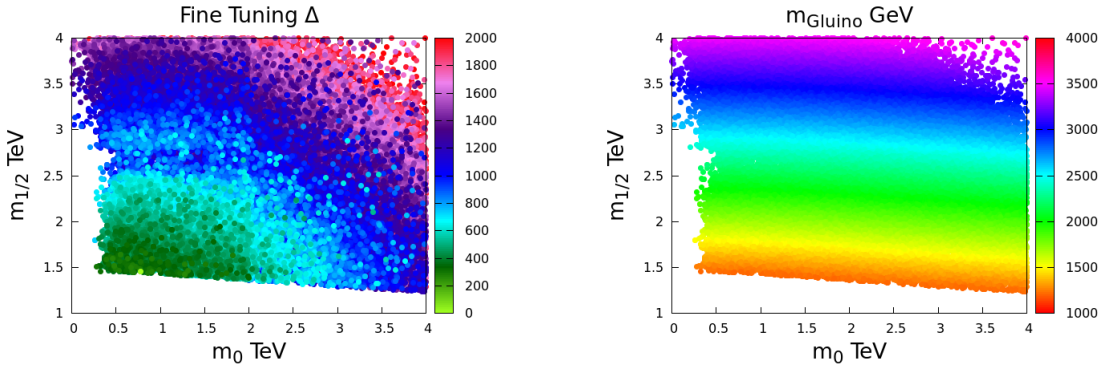

FIGURE 4.10: The left panel shows the fine tuning while the right panel shows the gluino mass, both in the $m_0 - m_{1/2}$ plane in the NMSSM+ when m_{h_1} is SM-like.

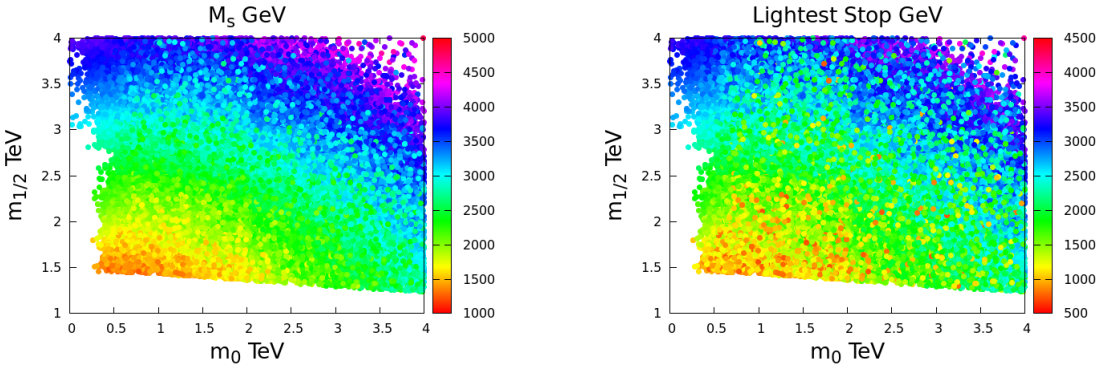

FIGURE 4.11: The left panel shows the RMS stop mass, while the right panel shows the lightest stop mass, both in the $m_0 - m_{1/2}$ plane in the NMSSM+ when m_{h_1} is SM-like.

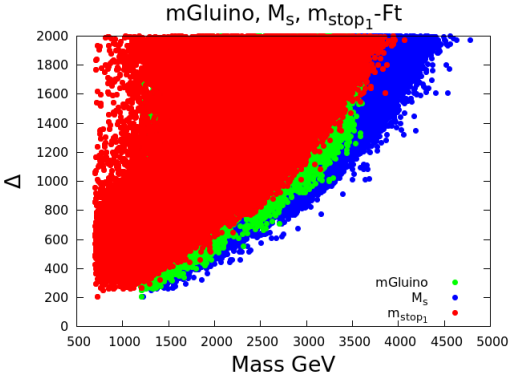

FIGURE 4.12: Fine tuning as a function of $m_{\tilde{g}}, M_S$, and m_{stop_1} in the NMSSM+ when m_{h_1} is SM-like.

4.6.2.2 Case 2: m_{h_2} is SM-like.

Here we examine the parameter space of the NMSSM+ where m_{h_2} is SM-like. Fig. 4.13 shows the fine tuning, which starts from about 188 and reaches 2000, in the $m_0 - m_{1/2}$ plane. The features of the fine tuning are similar to those found in case 1 in 4.6.2.1. However, more points can reach the $m_0 = 0$ region in this parameter space. Points close to $m_0 \sim 100$ GeV, and between 2 TeV $< m_{1/2} <$ 3 TeV are particularly associated with $A_0 > 2400$ TeV. Moreover, the lowest fine tuning that was found is $\Delta \sim 188$ for: $m_{h_2} = 126.5$ GeV, $m_{\tilde{g}} = 1.2$ TeV, $m_{\tilde{t}_1} = 793$ GeV.

The gluino mass (Fig. 4.13, right panel) also ranges from 1.2 to 3.7 TeV, and shares the same features as in case 1. Again, it correlates to $m_{1/2}$ as: $m_{\tilde{g}} = 0.85 m_{1/2}$. Next, the average stop mass, M_S, starts from 1.2 TeV and approaches 5 TeV (Fig. 4.14, left panel). On the other hand, the lightest stop mass (right panel) takes values between 700 GeV and 4.2 TeV.

Furthermore, when m_{h_2} varies between 123 GeV and 127 GeV, the fine tuning is a plateau around 200. However, Fig. 4.15 shows that the lowest fine tuning increases from ~ 200 to 2000 when M_S, $m_{\tilde{g}}$, and $m_{\tilde{t}_1}$ change from 1.2 TeV to 3.6 TeV, 1.2 TeV to 4.9 TeV, and 700 GeV to 4 TeV, respectively. Notice that the lightest stop can be as large as 4 TeV and still results in the same degree of the lowest fine tuning as that associated with a gluino mass of 3.6 TeV. Therefore, we again see, as expected, the important effect the gluino has on the lowest fine tuning in the NMSSM+. Indeed, the curves that the data points form in conjunction with the lowest fine tuning clearly show that the gluino mass is now most relevant to the fine tuning and in fact controls it, as opposed to the situation in the NMSSM in 4.6.1.

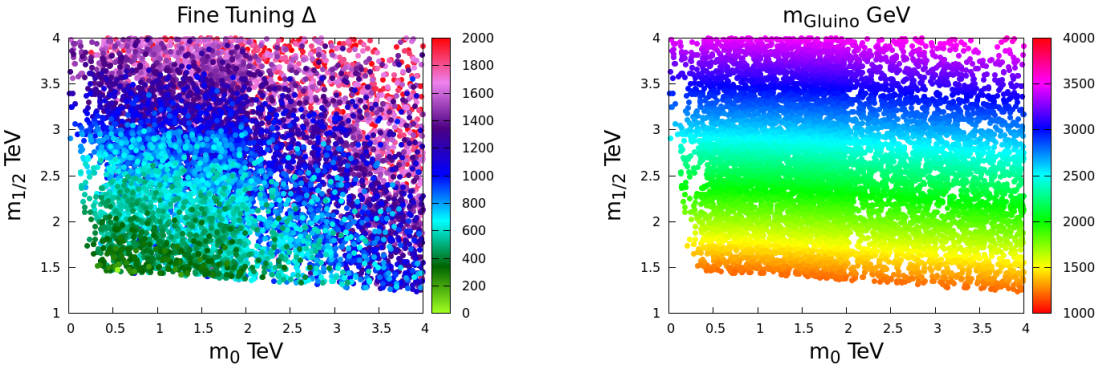

FIGURE 4.13: The left panel shows the fine tuning while the right panel shows the gluino mass, both in the $m_0 - m_{1/2}$ plane in the NMSSM+ when m_{h_2} is SM-like.

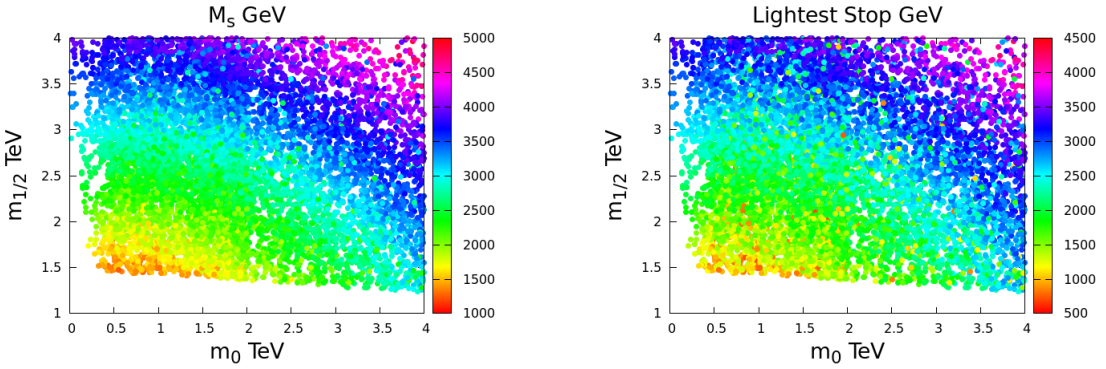

FIGURE 4.14: The left panel shows the RMS stop mass, while the right panel shows the lightest stop mass, both in the $m_0 - m_{1/2}$ plane in the NMSSM+ when m_{h_2} is SM-like.

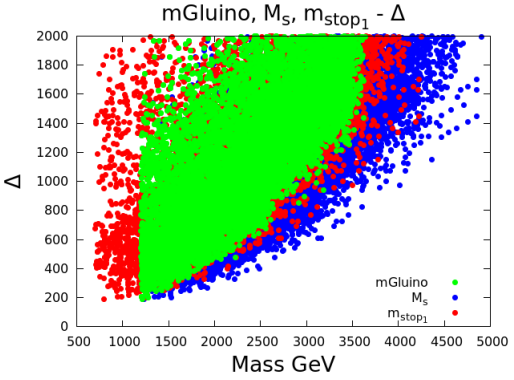

FIGURE 4.15: Fine tuning as a function of $m_{\tilde{g}}, M_S$, and m_{stop_1} in the NMSSM+ when m_{h_2} is SM-like.

4.6.3 NMSSM++

Finally, the fine tuning in the parameter space specified in Sec. 4.5 for the NMSSM++ is shown for the first time. The effect of having to start with a very large $M_3(M_{\text{GUT}}) = m_{1/2}$ as explained in Equation 4.17 is very significant here in comparison with the previous two models. Particularly, the minimum mass scale of the top squarks in the NMSSM++ will be larger than that in the NMSSM+.

4.6.3.1 Case 1: m_{h_1} is SM-like.

The parameter space of the NMSSM++ is significantly different from both the parameter spaces of the NMSSM and the NMSSM+. It is charactarized by large values of m_0 and $m_{1/2}$ in order to be compatible with our phenomenology constraints.

The fine tuning starts at a value of $\mathcal{O}(600)$, shown in Fig. 4.16, and rapidly increases as m_0 and $m_{1/2}$ increase. In this parameter space, the lowest fine tuning found is $\Delta \sim 663$ for: $m_{h_1} = 126$ GeV, $m_{\tilde{g}} = 1.2$ TeV, $m_{\tilde{t}_1} = 2.1$ TeV.

Note that a large value of $m_{1/2}$, ~ 4 TeV is needed to obtain a gluino mass of 1.2 TeV. And very roughly the correlation between $m_{1/2}$ and $m_{\tilde{g}}$ is on average: $m_{\tilde{g}} \sim 0.25 m_{1/2}$. Only when m_0 is significantly large, one can access slightly smaller values of $m_{1/2}$. Moreover, since $m_{1/2}$ is very large it controls the scalar masses as demonstrated in the left panel of Fig. 4.17 which shows that the parameter M_S is always larger than 1.8 TeV in this parameter space, and rises rapidly with $m_{1/2}$ to values close to ~ 5 TeV.

Furthermore, the mass of the lightest stop (Fig. 4.17, right panel) assumes values between 700 GeV and 4.5 TeV. However, those points with $m_{\tilde{t}_1} \sim 700$ GeV correspond to $m_{\tilde{t}_2} > 2.6$ TeV, and $m_{H_u}(M_{\rm GUT}) \sim 5$ TeV. Next, the fine tuning is almost a plateau around 600 with respect to m_{h_1}. Again, the mass of the Higgs plays no role in controlling the lowest fine tuning in the NMSSM++.

On the other hand, the lowest fine tuning sharply increases from ~ 600 to 2000 as M_S, $m_{\tilde{g}}$, and $m_{\tilde{t}_1}$ increase from 2.5 TeV to around 4.8 TeV, 1.2 TeV to 2.6 TeV, and 2.5 TeV to 4.2 TeV, respectively as Fig. 4.18 shows. Clearly, the gluino mass in the NMSSM++ strongly drives the lowest fine tuning to be larger than that in the NMSSM and the NMSSM+ because it raises M_S to quite large values. Therefore, even though the original goal of increasing λ at the low scale can be easily achieved in the NMSSM++, it comes at the expense of having very large $M_3(M_{\rm GUT}) = m_{1/2}$ in order to obtain the gluino mass around 1.2 TeV. Consequently, this will dominate the running of the top squarks, thereby making them much heavier than the current experimental limits. This effect is the reason why the NMSSM++ (similarly the NMSSM+) is more fine tuned than the NMSSM.

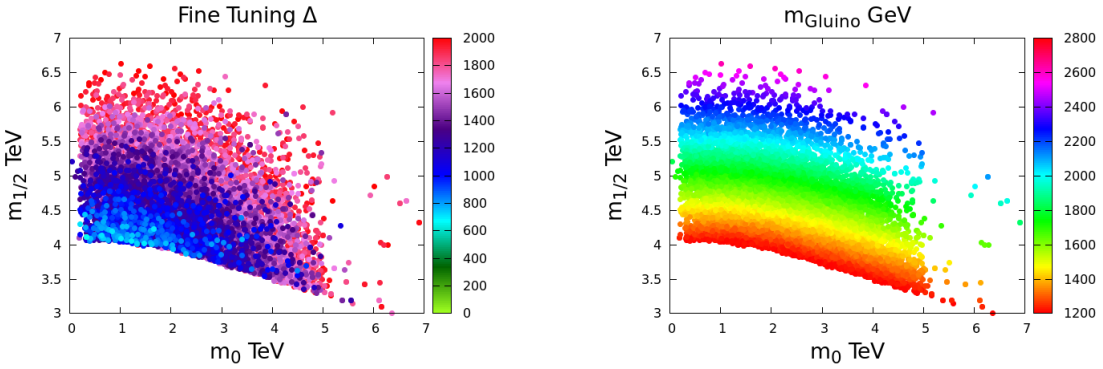

FIGURE 4.16: The left panel shows the fine tuning while the right panel shows the gluino mass, both in the $m_0 - m_{1/2}$ plane in the NMSSM++ when m_{h_1} is SM-like.

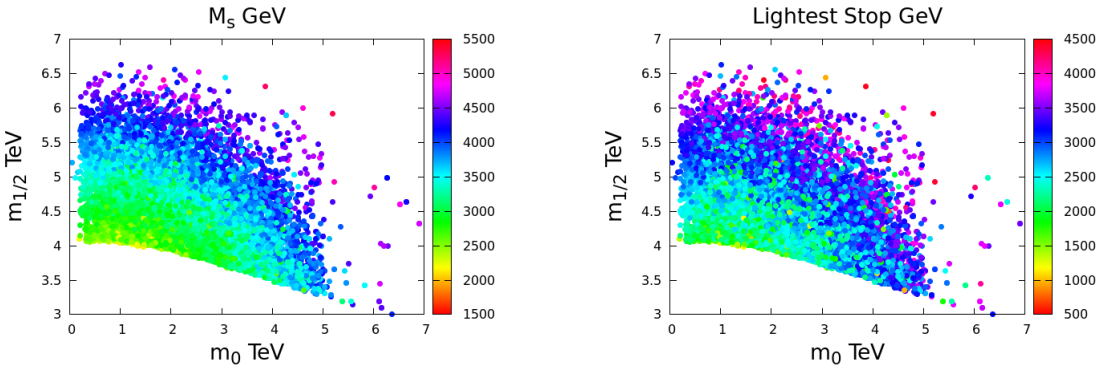

FIGURE 4.17: The left panel shows the RMS stop mass, while the right panel shows the lightest stop mass, both in the $m_0 - m_{1/2}$ plane in the NMSSM++ when m_{h_1} is SM-like.

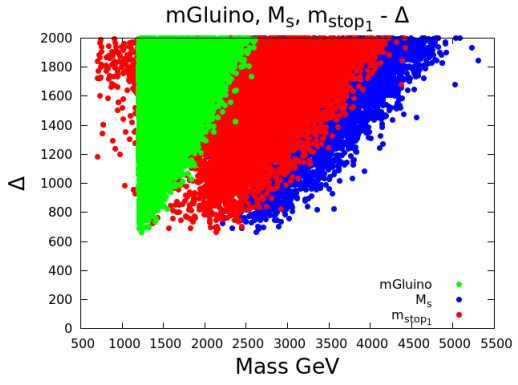

FIGURE 4.18: Fine tuning as a function of $m_{\tilde{g}}, M_S$, and m_{stop_1} in the NMSSM++ when m_{h_1} is SM-like.

4.6.3.2 Case 2: m_{h_2} is SM-like.

Here, we present the results of case 2 where m_{h_2} is SM-like in the NMSSM++. First, due to our sampling procedure, the parameter space contains fewer points satisfying the applied cuts than in the previous case. The fine tuning results in the $m_0 - m_{1/2}$ plane are presented in the left panel of Fig. 4.19. Overall, the patterns are similar to those found in the case 1 in 4.6.3.1. While the lowest fine tuning possible is still around 600, most of the points in this parameter space has fine tuning above 800. The fine tuning, again, is more sensitive to changes in $m_{1/2}$ than in m_0. The lowest fine tuning found in this parameter space is $\Delta \sim 634$ for: $m_{h_2} = 126$ GeV, $m_{\tilde{g}} = 1.2$ TeV, and $m_{\tilde{t}_1} = 2.76$ TeV.

The gluino mass distribution in Fig. 4.19 (right panel) shows that it ranges from 1.2 TeV to 2.8 TeV. Again, very roughly and on average $m_{\tilde{g}} \sim 0.25 m_{1/2}$. The reason this correlation is very rough in the NMSSM++ is that we are presenting regions where m_0 is very large. This means that the corrections to the gluino mass due from scalars is significant.

Next, the RMS stop mass,M_S, see Fig. 4.20, is quite large as it starts from 2 TeV (as opposed to 900 GeV and 1.2 TeV in the NMSSM and the NMSSM+). Thus, both top squarks are pushed to heavy values. Again, this is because $m_{1/2}$ has to be very large ~ 4 TeV in order to satisfy the gluino mass limit.

Moreover, the fine tuning does not vary significantly with m_{h_2} as it is found to be ~ 600 for $123 \leq m_{h_2} \leq 127$ GeV. On the other hand, Fig. 4.21 shows that that increasing the lightest stop from around 2 TeV to 4.5 TeV, and increasing M_S from 2.5 TeV to 5 TeV, results in a raise in the fine tuning from around 600 to 2000. More noticeably, the fine tuning increases sharply from around 600 to 2000 as $m_{\tilde{g}}$ increases from 1.2 TeV to around 2.8 TeV. This is a key feature of the NMSSM++ and the reason why it is much more fine tuned than the NMSSM, and the NMSSM+.

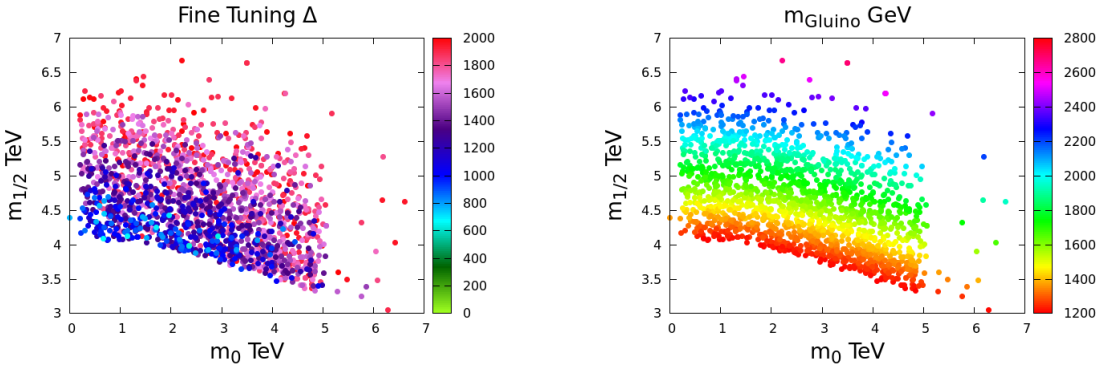

FIGURE 4.19: The left panel shows the fine tuning while the right panel shows the gluino mass, both in the $m_0 - m_{1/2}$ plane in the NMSSM++ when m_{h_2} is SM-like.

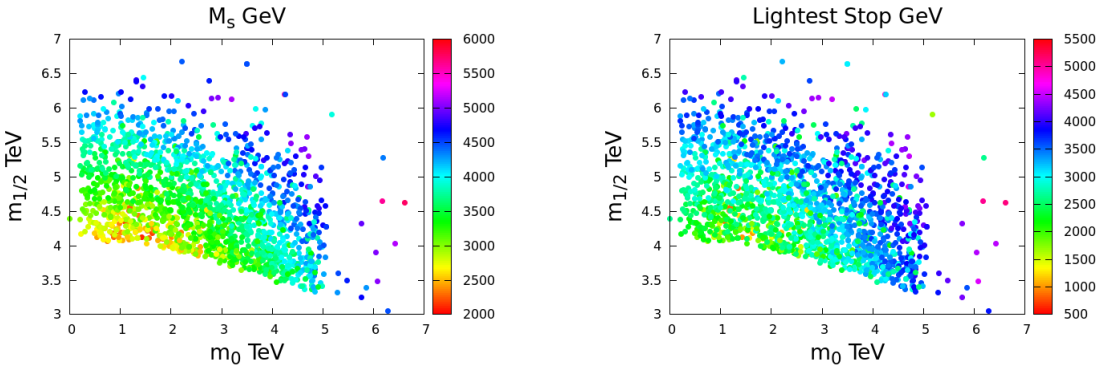

FIGURE 4.20: The left panel shows the RMS stop mass, while the right panel shows the lightest stop mass, both in the $m_0 - m_{1/2}$ plane in the NMSSM++ when m_{h_2} is SM-like.

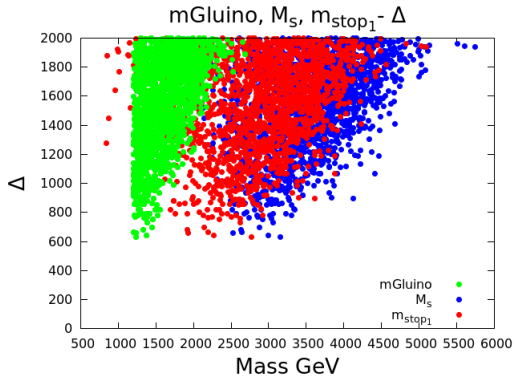

FIGURE 4.21: Fine tuning as a function of $m_{\tilde{g}}, M_S$, and m_{stop_1} in the NMSSM++ when m_{h_2} is SM-like.

4.6.4 Comparison

Here, we compare the three models to point out the main finding which is that adding extra matter to the NMSSM, hence increasing $\lambda(M_{\rm SUSY})$, does not necessarily improve the fine tuning. In fact, it makes it worse, especially in the framework we have chosen. We found that the RG running of the α_s and similarly the gluino forces one to start with a large $m_{1/2}$ ($M_3(M_{\rm GUT})$) at the GUT scale in the plus-type models in order to reach the desired gluino mass at the low scale. This, in turn, causes an increase in the mass of the top squarks at the low scales in comparison to the NMSSM as Fig. 4.22 shows. It is clear from this Fig. that, in all of the parameter spaces we studied, and for a given physical gluino mass, it is always possible to find M_S that is smaller in the NMSSM than in both the NMSSM+ and the NMSSM++, and smaller in the NMSSM+ than in the NMSSM++. This is an RGE effect that was explained in Sec. 4.3. The larger M_S is, the larger the separation between the weak and the SUSY scales, and, as a consequence, the larger the fine tuning in the plus-type models, especially the NMSSM++.

The fine tuning results in the three models can be straightforwardly compared by referring to Fig.s 4.4, 4.10, and 4.16 for case 1, and Fig.s 4.7, 4.13, and 4.19 for case 2. Moreover, the correlation between the fine tuning and both of $m_{\tilde{t}_1}$ and $m_{\tilde{g}}$ in each model is shown in Fig. 4.6, Fig. 4.12, and 4.18, for case 1. And in Fig. 4.9, Fig. 4.15, and 4.21, for case 2.

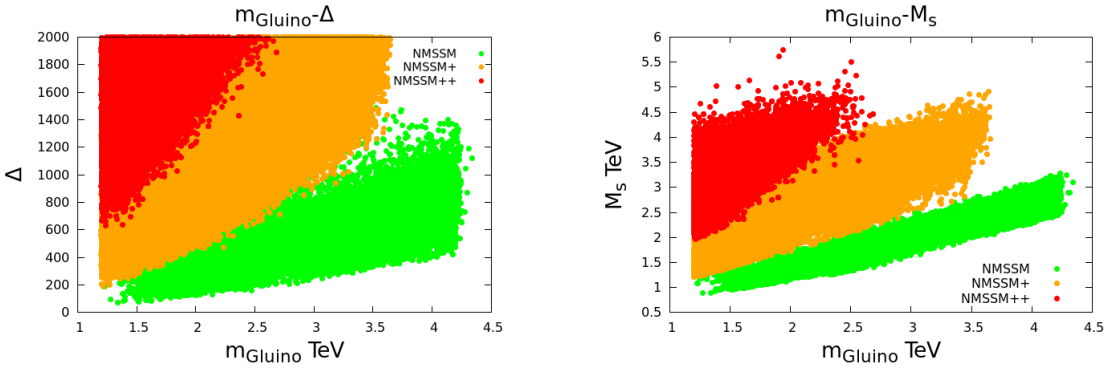

FIGURE 4.22: The left panel shows the correlation between the fine tuning and the gluino mass for the three models. The right panel shows the correlation between the RMS stop mass and the gluino mass for the three models.

4.7 Dark matter relic density constraints on the parameter space of the NMSSM+

4.7.1 Overview

In the previous Sections, we investigated the effect of adding vector-like states to the NMSSM on the fine tuning. In particular three and four (5+5*) fundamental states of SU(5) were added to the NMSSM, and the mass spectrum satisfying experimental constraints from LEP, Tevatron, B-Physics, and the LHC was generated using modified version of the publicly available package NMSSMTools4.1.2. Next, the fine tuning in the two new models, called the NMSSM+ and the NMSSM++, was compared with that in the NMSSM, and the main finding was that the running mass of the gluino from the GUT scale to the SUSY scale will drive both the light and heavy top squarks, as well as the soft-supersymmetry breaking mass of the up-type Higgs, m_{H_u}, to rather large values, thereby reintroducing the fine tuning. In fact, the fine tuning in such models was found to be significantly worse than in the standard NMSSM. However, in the previous study, the constraints on DM relic density were only partly taken into account. Namely, the region of the parameter space that is associated with lowered fine tuning is required to only contain model points that do not exceed the upper bound on DM relic density set by Planck experiment by more than 10% [129]. This means that such points may contain models that do not fully account for the current DM relic density in the Universe. In this Sec., we explore the parameter space of the NMSSM+, and apply up-to-date experimental constraints by using NMSSMTools4.4.0, which we modify to generate the mass spectrum of the NMSSM+ as explained in 4.4.2, and more importantly we impose DM constraints by Planck (+/- 10%) on the scanned parameter space of the NMSSM+. The results are them compared with the results of the NMSSM presented in [130].

4.7.2 Experimental constraints

Using a modified version of NMSSMTools4.4.0, we choose a semi-constrained framework where, at the GUT scale, Gaugino masses are universal ($m_{1/2}$), and the masses of scalars are universal (m_0), expect for m_{H_u}, m_{H_d}, and m_S. Additionally, the A-terms are universal,expect for A_λ, A_κ. We fix $\tan\beta = 3$, $\kappa = 0.4$, $A_0 = -1$ TeV, and $\mu = 250$. Next, we scan up to 10^5 points over the following range of parameters,

$$300 < m_0 < 2000 \text{ GeV}$$

$$300 < m_{1/2} < 2000 \text{ GeV}$$

$$0.45 < \lambda < 0.7$$

$$-100 < A_\lambda < 100 \text{ GeV}$$

$$-100 < A_\kappa < 100 \text{ GeV}$$

Finally, we apply the experimental constraints listed in Table 4.1.

Constraint	Details
LEP Bounds	Higgs searches and invisible Z decays [120, 121, 122]
New Physics (to within 2σ)	B $\to$ sγ, $B_s \to \mu^+ + \mu^-$, B $\to \tau\nu_\tau$ (See Sec. 4.5.2)
Higgs mass	125.7 ± 3 GeV
DM relic density	$0.107 < \Omega h^2 < 0.131$ [129]

TABLE 4.1: Phenomenological constrains.

Finally, the fine tuning results are calculated via NMSSMTools using the common fine tuning measure that was introduced in 3.5.

4.7.3 Preliminary results

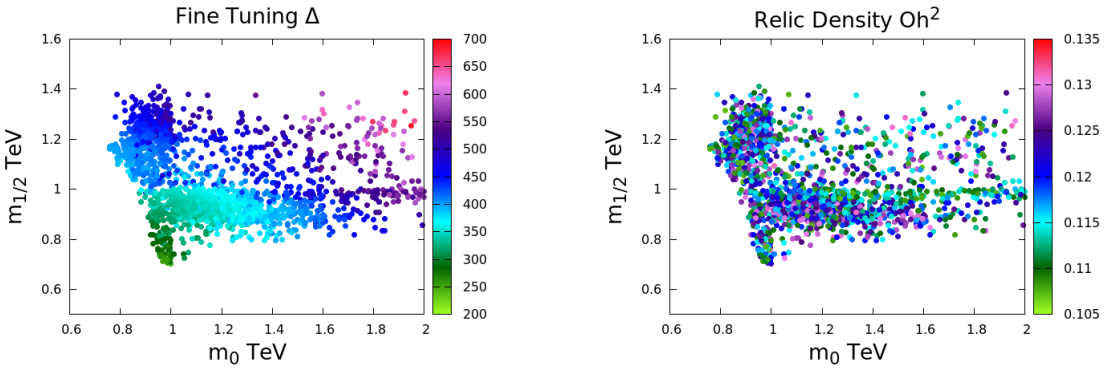

FIGURE 4.23: The left panel shows the fine tuning while the right panel shows the gluino mass, both in the $m_0 - m_{1/2}$ plane in the NMSSM+.

Preliminary results are presented in this Section. We plot the parameter space in the m_0-$m_{1/2}$ plane to show the available range of models. The reason for this choice is that the predicted masses of sparticles will depend strongly on these two parameters. In this plane, the fine tuning is shown in colours in Fig. 4.23 (left). The lowest possible fine tuning is about 250. It increases steadily as $m_{1/2}$ and m_0 are increased reaching a value of 700 in the corner where both parameters are larger than 1.2 TeV and 1.8 TeV respectively.

Next, Fig. 4.23 (right) shows the DM relic density in colours. Clearly, it is possible to account for DM relic density in the NMSSM+ since all points appearing in this figure have the parameter Ωh^2 within the experimental limit imposed by the Planck satellite.

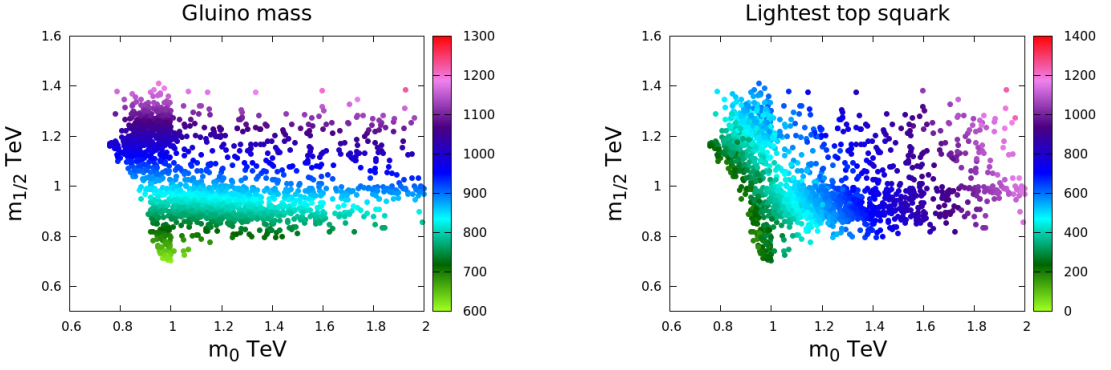

FIGURE 4.24: The left panel shows the gluino mass while the right panel shows the lightest to squark mass, both in the $m_0 - m_{1/2}$ plane in the NMSSM+.

Fig. 4.24 (left) shows the range of the gluino mass in colours. It is clear that lower fine tuning prefers regions of the parameter space where the gluino mass is smaller than 1 TeV. However, this could be in tension with the LHC limits which require that the gluino mass is larger than 1.4 TeV if the mass of the LSP is smaller than 600 GeV [8]. Next, Fig. 4.24 (right) shows the mass range of the lightest top squark in colours. Lower fine tuning lies in the region where the lightest top squark has a mass of about 200 GeV. Again, this might be in tension with LHC limits since it is required that the mass of such a sparticle is larger than 600 GeV if the LSP is lighter than 250 GeV. From those results, it is clear that the NMSSM+ could accommodate a 125.7±3 GeV SM-Higgs, satisfying a range of phenomenological constraints, as well as accounting from DM relic density. However, compared with the fine tuning results [130] the the NMSSM+ remains more fine tuned than the NMSSM.

Finally, in all of the scanned parameter space, the LSP is mostly bino with a mass range 88 GeV $< m_{\tilde{\chi}_1^0} <$ 210 GeV.

4.8 Conclusions

In this Chapter, we have considered three non-minimal Z_3-invariant supersymmetric models. Namely, the NMSSM, the NMSSM+ that adds $3(5, \overline{5})$ extra states of SU(5) to the NMSSM, and the NMSSM++ that adds $4(5, \overline{5})$ extra states of SU(5) to the NMSSM. Moreover, the extra matter in the NMSSM+ and NMSSM++ is treated as a secluded sector that only affects the mass spectrum of the ordinary sparticles through gauge interactions. We have calculated the low energy spectrum (focusing on naturalness-related sparticles and the SM-like Higgs boson) using the package NMSSMTools. We have modified NMSSMTools by implementing two-loop RGEs of the NMSSM+, and the NMSSM++. Furthermore, we have assumed that the extra matter is mass degenerate at the scale of the first and second generations of squarks. Hence, the running masses of the extra matter was ignored due to suppression by powers of gauge couplings and loop factors at one- and two-loop.

[8] These limits are available on the official website of the CMS and ATLAS experiments' summary plots:`https://twiki.cern.ch/twiki/bin/view/CMSPublic/PhysicsResults` and `https://twiki.cern.ch/twiki/bin/view/AtlasPublic/CombinedSummaryPlots`

Such extensions are known to relax the perturbativity bound on $\lambda(M_{\rm SUSY})$, which is the coupling between the SM singlet superfield and the up- and down-type Higgs doublets. As a result, it is expected that the tree-level Higgs mass in the NMSSM++ will be larger than in the NMSSM+, and larger in the NMSSM+ than in the NMSSM without extra matter. Moreover, it is usually assumed that the fine tuning reduces as the perturbativity bound on λ is increased since a large tree-level Higgs mass could imply lighter top squarks in the plus-type models than in the NMSSM. We have tested this commonly held hypothesis in the context of the three models above, and surprisingly find that this is not the case. Indeed, of all three models, we find that the NMSSM is the least fine tuned ($\Delta \sim 100$). The fine tuning in the NMSSM+ was the closest of the two plus-type models to the NMSSM with the lowest value being $\Delta \sim 200$. Finally, the NMSSM++ is the most fine tuned model where the fine tuning starts from 600. In general, the mass spectrum in the NMSSM++ was found to be heavier than in the NMSSM+, and heavier in the NMSSM+ than in the NMSSM.

The reason why the fine tuning is worse in the plus-type models than in the NMSSM is that such models with extra matter involve a larger gluino mass at high energies. In particular, we find that $M_{3,\rm GUT}$ is always larger in the NMSSM+ and very much larger in the NMSSM++, as compared to the NMSSM. This ordering results in an increased low energy stop mass spectrum, well above either the stop mass experimental limits or the stop mass limits required to obtain a sufficiently large Higgs mass. The heavy stop masses appear to be unavoidable in the NMSSM+, and especially the NMSSM++, purely as a result of the low energy experimental gluino mass limit and the RGE running behaviour, at least for the class of high energy semi-constrained SUGRA inspired models under consideration. In conclusion, it appears that increasing the perturbativity bound on λ at the low scale by adding extra matter does not reduce the fine tuning, but worsens it.

We also studied the parameter space of the NMSSM+ where DM relic density constraints are imposed. We modified NMSSMTools4.4.0, were two-loop RGEs of the NMSSM+ are implemented. The mass scale of the vector-like state is fixed at 2.5 TeV. Furthermore, we considered a parameter space with a small $\tan\beta$ (fixed at 3), μ-term

(250 GeV), and large λ in order to enhance its tree-level contribution the Higgs mass. We found that the NMSSM+ have a range of parameter space that passes the experimental constraints in Table 4.1, and can account for DM relic density. We also found that the lowest fine tuning possible sets around 250. This further confirms that the NMSSM+ is more fine tuned than the NMSSM. However, the results presented a preliminary, and more thorough investigation is needed.

In conclusion, it appears that increasing the perturbativity bound on λ at the low scale by adding extra matter does not reduce the fine tuning, but worsens it.

Chapter 5

Fine tuning in the constrained exceptional supersymmetric standard model

5.1 Overview

The Large Hadron Collider (LHC) has been accumulating data since 2009 with no observation of new physics beyond the standard model (BSM) so far, placing strong limits on new coloured states in extensions of the standard model. For example, in supersymmetric (SUSY) models there are strong experimental limits on the first and second generation squark and gluino masses [131, 132] which imply that they must be at least an order of magnitude larger than the electroweak (EW) scale. Within constrained versions of SUSY, where the masses of top squarks are linked to first and second generation squarks masses, this can considerably increase fine tuning since the EW scale is very sensitive to top squark masses, through the electroweak symmetry breaking conditions.

At the same time Atlas and CMS have recently observed a new state consistent with a Standard-Model-like Higgs boson at $m_h = 125 - 126$ GeV [25, 26], which is within the range for it to be consistent with the lightest Higgs in supersymmetric models. In the

minimal supersymmetric standard model (MSSM) this introduces further tension with naturalness since the light Higgs mass at tree-level is bounded from above by the Z boson mass (M_Z). The large radiative contributions from top squarks needed to raise it to the observed value typically imply very large fine tuning. For example the constrained MSSM (cMSSM) [133] has been shown to require fine tuning of $\mathcal{O}(1000)$ if it is to contain a 125 GeV Higgs mass [134, 135].

Here we consider fine tuning in an alternative class of constrained SUSY models which involves both an extra singlet field, denoted S, and an extra $U(1)$ gauge symmetry at low energy (TeV scale). As the singlet acquires a VEV, denoted s, it produces a μ term, denoted μ_{eff}, and it breaks the extra $U(1)$ gauge symmetry, giving rise to a massive Z' boson. Such models can increase the tree-level physical Higgs boson mass above the M_Z limit of the MSSM, due to both F-term contributions of the singlet and the D-term contributions associated with the Z', allowing lighter top squark masses and hence reducing fine tuning due to top squark loops. The exceptional supersymmetric standard model (E_6SSM) [136, 137] is an example of such a model, inspired by the E_6 group. At tree-level, the light Higgs mass is given as,

$$m_h^2 \approx \underbrace{\underbrace{\underbrace{M_Z^2 \cos^2 2\beta}_{\text{MSSM}} + \frac{\lambda^2}{2} v^2 \sin^2 2\beta}_{\text{NMSSM}} + \frac{M_Z^2}{4}(1 + \frac{1}{4}\cos 2\beta)^2}_{\text{E}_6\text{SSM}} + \Delta m_h^2, \tag{5.1}$$

where, $\tan\beta = \frac{v_2}{v_1}$ is the ratio between the two Higgs doublets' vacuum expectation values (VEVs), λ is the Yukawa coupling of the singlet field to the Higgs doublets, and Δm_h^2 represents loop corrections.

Indeed, Eq. 5.1 shows that the E_6SSM allows larger tree-level Higgs masses than the NMSSM [138, 139, 140, 141, 142, 143, 144], which in turn allows larger tree-level Higgs masses than the MSSM. This means that the E_6SSM does not rely on such a large a contribution from the radiative correction term Δm_h^2 in order to reproduce the Higgs mass. As a result the E_6SSM permits lighter top squarks than either the NMSSM or the MSSM. In addition the λ coupling in the E_6SSM can be larger at low energies,

while still remaining perturbative all the way up to the GUT scale, than is the case in the NMSSM.

One might conclude that this should lead to lower fine tuning in the E_6SSM than either the NMSSM or MSSM, since the large top squark masses are usually the main source of fine tuning in SUSY models. However, the origin of the extra term in Eq. 5.1 is due to D-terms arising from the coupling of the Higgs doublets to the extra $U(1)$ gauge symmetry, and such D-terms also contribute to the minimisation conditions of the Higgs doublets. Indeed, as we shall discuss, one of the minimisation conditions of the E_6SSM can be written in the form,

$$c\frac{M_Z^2}{2} = -\mu_{\rm eff}^2 + \frac{(m_d^2 - m_u^2\tan^2\beta)}{\tan^2\beta - 1} + d\frac{M_{Z'}^2}{2}, \tag{5.2}$$

where c, d are functions of $\tan\beta$ which are of order $\sim \mathcal{O}(1)$ (given explicitly in Eq. 5.13), m_d^2, m_u^2 are soft Higgs mass squared parameters. $\mu_{\rm eff}$ arises from the singlet VEV, and $M_{Z'}^2$ is proportional to s^2 (given explicitly in Eq. 5.15). Written in this form it is clear that the D-terms are a double edged sword since they also introduce a new source of tree-level fine tuning, due to the Z' mass squared term in Eq. 5.2, which will increase quadratically as $M_{Z'}^2$, eventually coming to dominate the fine tuning for large enough values of $M_{Z'}$. This tree-level fine tuning can be compared to that due to $\mu_{\rm eff}$ which typically requires this parameter to be not much more than 200 GeV, and similar limits also apply to $M_{Z'}$. With the current CMS experimental mass limit for the Z' in the E_6SSM of $M_{Z'} \gtrsim 2.08$ TeV [145] it is clear that there is already a significant, perhaps dominant, amount of fine tuning due to the Z' mass limit.

In this Chapter we investigate this new and important source of fine tuning, namely that due to the $M_{Z'}$ limit, and compare it to the usual other sources of fine tuning in the framework of the Constrained E_6SSM (cE_6SSM) [146, 147, 148, 149]. Although the impact of a SM-like Higgs with $m_h \sim 125$ GeV on the parameters has recently been considered in [150, 151], fine tuning was not considered. In fact the present study here is the first time that fine tuning has been considered in any supersymmetric E_6 model with a low energy Z'. To obtain the required Higgs mass in the cE_6SSM, it turns out that the SM singlet field, S, must have a VEV $s \geq 5$ TeV as pointed out in [150]. This

corresponds to a mass of the Z' boson predicted by the model of 1.9 TeV, which almost reaches the experimental bound of 2 TeV [145]. Thus, all the parameter space we study respects the experimental limit on $M_{Z'}$. Fixing $\tan\beta = 10$, and taking specific values of the mass of the Z' boson, $M_{Z'}$, ranging from 1.9 to 3.8 TeV we find that the current minimum fine tuning in the cE$_6$SSM, consistent with a Higgs mass $m_h \sim 125$ GeV, varies from $\sim 200 - 400$, and is already dominated by the $M_{Z'}$ limit. However, this is significantly lower than the fine tuning in the cMSSM of $\mathcal{O}(1000)$ arising from the heavy top squarks required to achieve the Higgs mass.

The rest of the Chapter is organised as follows: Section two provides a short overview of the E$_6$SSM. Then, the scalar Higgs potential and the electroweak symmetry breaking (EWSB) conditions are discussed in Section three. In Section four we discuss the fine tuning measure we use, and derive a fine tuning master formula for the E$_6$SSM with a brief description of our semi-numerical procedure of calculating fine tuning. Section five is where we present our results and discussion, then we conclude the study in Section six.

5.2 The E$_6$SSM

The Exceptional Supersymmetric Standard Model (E$_6$SSM) is a non-minimal supersymmetric extension of the SM, which provides a low energy alternative to the MSSM and NMSSM. It is well motivated both from more fundamental theories due to its connection to E_6 GUTs, heterotic and F- string theory [152] and at the same time as a low energy effective model, providing solutions to phenomenological problems. For instance, as mentioned in the Introduction, the E$_6$SSM allows a larger Higgs mass at tree-level than in both the MSSM and the NMSSM, thereby requiring smaller contributions from loops. In addition it also solves the μ problem associated with the MSSM by dynamically producing the μ-term at the TeV scale, without introducing the domain walls or tadpole problems that can appear in the NMSSM.

The E$_6$SSM is based on the Exceptional Lie group E_6. This contains both of $SO(10)$ and $SU(5)$ as subgroups,

$$E_6 \to SO(10) \times U(1)_\psi \tag{5.3}$$

$$SO(10) \to SU(5) \times U(1)_\chi, \tag{5.4}$$

and hence also contains the Standard Model gauge group, which is a subgroup $SU(5)$. A linear combination of the two extra $U(1)_\psi$ and $U(1)_\chi$ groups can survive to low energies, where it is spontaneously broken by a SM singlet field, S. This generates the mass of the associated Z' boson and the exotic quarks, as well as dynamically producing a μ_{eff} term. The model allows right-handed (RH) neutrinos to have Majorana masses at some scale between the GUT and low scales. This is achieved by choosing this linear combination to be,

$$U(1)_N = \frac{\sqrt{15}}{4}U(1)_\psi + \frac{1}{4}U(1)_\chi \tag{5.5}$$

such that the RH neutrinos are not charged under $U(1)_N$, hence it is possible to explain the tiny neutrino masses via seesaw mechanisms.

At low energies, the group structure of the model is that of the SM, along with the additional $U(1)_N$ symmetry,

$$E_6 \to SU(5) \times U(1)_N \tag{5.6}$$

$$SU(5) \to SU(3)_c \times SU(2)_w \times U(1)_Y \tag{5.7}$$

The matter content of the model is contained in the complete 27-dimensional representation which decomposes under $SU(5) \times U(1)_N$ to,

$$27_i \longrightarrow (10,1)_i + (5^*,2)_i + (5^*,-3)_i + (5,-2)_i + (1,5)_i + (1,0)_i \tag{5.8}$$

Ordinary Quarks and Leptons are contained in the representations: $(10, 1)$ and $(5^*, 2)$. The Higgs doublets and exotic quarks are contained in $(5^*, -3)$ and $(5, -2)$. The singlets are contained in $(1, 5)$, and finally the right handed neutrinos are included in $(1, 0)$.

Moreover, the model requires three 27 representations, hence $i = 1, 2, 3$, in order to ensure anomaly cancellation. This means that there are three copies of each field present in the model. However, only the third generation (by choice) of the two Higgs doublets, and the SM singlet acquire VEVs. The other two generations are called inert. Furthermore, in order to keep gauge coupling unification, non-Higgs fields that come from extra incomplete $27', \overline{27}'$ representations are added to the model. As a result, a μ' term, which is not necessary related to the weak scale, is present in the model.

The full superpotential consistent with the low energy gauge structure of the E_6SSM includes both E_6 invariant terms and E_6 breaking terms, full details of which are given in [136]. However as in the MSSM it is necessary to forbid proton decay and therefore a generalisation of R-parity should be imposed, and additionally because the E_6SSM includes three generations of every chiral superfield, there needs to be a suppression of new terms which can induce flavour changing neutral currents. To achieve this we impose either a Z_2^L symmetry[1] (Model I) or a Z_2^B symmetry[2] (Model II) along with an approximate Z_2^H symmetry, under which all fields are odd except for the third generation Higgs superfields, which may arise from a family symmetry[153, 154].

The Z_2^H invariant superpotential then reads,

$$\begin{aligned} W_{\rm E_6SSM} \approx\ & \lambda_i \hat{S}(\hat{H}_i^d \hat{H}_i^u) + \kappa_i \hat{S}(\hat{D}_i \hat{\overline{D}}_i) + f_{\alpha\beta} \hat{S}_\alpha (\hat{H}_d \hat{H}_\beta^u) + \tilde{f}_{\alpha\beta} \hat{S}_\alpha (\hat{H}_\beta^d \hat{H}_u) \\ & + \frac{1}{2} M_{ij} \hat{N}_i^c \hat{N}_j^c + \mu'(\hat{H}' \hat{\overline{H}'}) + h_{4j}^E (\hat{H}_d \hat{H}') \hat{e}_j^c + h_{4j}^N (\hat{H}_u \hat{H}') \hat{N}_j^c \\ & + W_{\rm MSSM}(\mu = 0), \end{aligned} \tag{5.9}$$

[1] All superfields except the leptons and survival Higgs are even.

[2] All the exotic quark, lepton and survival Higgs superfields are odd while all the other superfields remain even.

where the indices $\alpha, \beta = 1, 2$ and $i = 1, 2, 3$ denote the generations. S is the SM singlet field, H_u, and H_d are the Higgs doublet fields corresponding to the up and down types. Exotic quarks and the additional non-Higgs fields are denoted by D and H' respectively.

Finally to ensure that only third generation Higgs like fields get VEVs a certain hierarchy between the Yukawa couplings must exist. Defining $\lambda \equiv \lambda_3$, we impose $\kappa_i, \lambda_i \gg f_{\alpha\beta}$, $\tilde{f}_{\alpha\beta}$, h^E_{4j}, h^N_{4j}. Moreover, we do not impose any unification of the Yukawa couplings at the GUT scale.

5.3 The Higgs potential and the EWSB conditions

The scalar Higgs potential is,

$$\begin{aligned} V(H_d, H_u, S) = {} & \lambda^2 |S|^2 (|H_d|^2 + |H_u|^2) + \lambda^2 |H_d.Hu|^2 \\ & + \frac{g_2^2}{8}(H_d^\dagger \sigma_a H_d + H_u^\dagger \sigma_a H_u)(H_d^\dagger \sigma_a H_d + H_u^\dagger \sigma_a H_u) \\ & + \frac{g'^2}{8}(|H_d|^2 - |H_u|^2)^2 + \frac{g'^2_1}{2}(Q_1 |H_d|^2 + Q_2 |H_u|^2 + Q_s |S|^2)^2 \\ & + m_s^2 |S|^2 + m_d^2 |H_d|^2 + m_u^2 |H_u|^2 \\ & + [\lambda A_\lambda S H_d.H_u + c.c.] + \Delta_{\text{Loops}} \end{aligned} \tag{5.10}$$

where, g_2, $g'(= \sqrt{3/5} g_1)$, and g'_1 are the gauge couplings of $SU(2)_L, U(1)_Y$ (GUT normalized), and the additional $U(1)_N$, respectively. $Q_1 = -3/\sqrt{40}, Q_2 = -2/\sqrt{40}$, and $Q_s = 5/\sqrt{40}$ are effective $U(1)_N$ charges of H_u, H_d and S, respectively. m_s is the mass of the singlet field, and $m_{u,d} \equiv m_{H_{u,d}}$.

The Higgs field and the SM singlet acquire VEVs at the physical minimum of this potential,

$$\langle H_d \rangle = \frac{1}{\sqrt{2}} \begin{pmatrix} v_1 \\ 0 \end{pmatrix}, \quad \langle H_u \rangle = \frac{1}{\sqrt{2}} \begin{pmatrix} 0 \\ v_2 \end{pmatrix}, \langle S \rangle = \frac{s}{\sqrt{2}}, \tag{5.11}$$

It is reasonable exploit the fact that $s \gg v$, which will help in simplifying our master formula for fine tuning as will be seen in Section 4. Then, from the minimisation conditions,

$$\frac{\partial V_{E_6SSM}}{\partial v_1} = \frac{\partial V_{E_6SSM}}{\partial v_2} = \frac{\partial V_{E_6SSM}}{\partial s} = 0, \tag{5.12}$$

the Electroweak Symmetry Breaking (EWSB) conditions are,

$$\frac{M_Z^2}{2} = -\frac{1}{2}\lambda^2 s^2 + \frac{(m_d^2 - m_u^2 \tan^2\beta)}{\tan^2\beta - 1} + \frac{g_1'^2}{2}\left(Q_1 v_1^2 + Q_2 v_2^2 + Q_s s^2\right)\frac{(Q_1 - Q_2\tan^2\beta)}{\tan^2\beta - 1} \tag{5.13}$$

$$\sin 2\beta \approx \frac{\sqrt{2}\lambda A_\lambda s}{m_d^2 + m_u^2 + \lambda^2 s^2 + \frac{g_1'^2}{2} Q_s s^2 (Q_1 + Q_2)}, \tag{5.14}$$

$$m_s^2 \approx -\frac{1}{2} g_1'^2 Q_s^2 s^2 = -\frac{1}{2} M_{Z'}^2, \tag{5.15}$$

where $M_Z^2 = \frac{1}{4}(g'^2 + g_2^2)(v_2^2 + v_1^2)$ and $M_{Z'}^2 \approx g_1'^2 Q_s^2 s^2$.

Eq. 5.13 can be written in the form,

$$c\frac{m_Z^2}{2} = -\mu_{\text{eff}}^2 + \frac{(m_d^2 - m_u^2\tan^2\beta)}{\tan^2\beta - 1} + d\frac{M_{Z'}^2}{2}, \tag{5.16}$$

where c, d are functions of $\tan\beta$ which are of order $\sim \mathcal{O}(1)$ and we have written $\mu_{\text{eff}} = \frac{\lambda s}{\sqrt{2}}$. Written in this form it is clear that fine tuning will increase as $M_{Z'}$ increases. Another source of fine tuning is the large $|\mu_{\text{eff}}|$ term as mentioned in the introduction since satisfying Eq. 5.16 will require this term to compensate for any increase in either the second term (term 2: $\sim m_u^2, m_d^2$) or the last term (term 3: $\sim M_{Z'}^2$).

The increasing experimental limits on $M_{Z'}(\sim s)$ results in constraining the parameter space of the E$_6$SSM such that only relatively large values of m_0 and $m_{1/2}$ result in successful solutions to the EWSB conditions (Fig. 5.1- 5.11).

Moreover, imposing universal boundary conditions, which is what characterises the cE$_6$SSM, means that all low energy SUSY parameters can be expanded in terms of a few GUT-scale universal and fundamental input parameters, namely,

$$m_0, \quad m_{1/2}, \quad A, \quad \lambda_i(0), \quad \kappa_i(0), \quad h_{t,b,\tau}(0) \tag{5.17}$$

where, $m_0, m_{1/2}$ and A are a universal scalar mass, a universal gaugino mass, and a universal trilinear coupling, respectively, and (0) means taking the parameter at the GUT scale (in the Results section, we refer to $\lambda_3(0)$ and $\kappa_{1,2,3}(0)$ as λ_0 and κ_0, respectively).

This is accomplished by using the one-loop RGEs of the scalar masses, so that one can express $m^2_{H_u}$ at the SUSY scale, M_S, as,

$$m^2_{H_u}(M_S) = z_1 m_0^2 + z_2 m_{1/2}^2 + z_3 A^2 + z_4 m_{1/2} A. \tag{5.18}$$

Then, it is possible to write,

$$\frac{m_Z^2}{2} \approx \sum_{i=1}^{n} F_i z_i a_i^2 \tag{5.19}$$

where, a denotes the fundamental parameters, z is the coefficient corresponding to each parameter, and is calculated numerically using E$_6$SSM RGEs (cf. Sec. 3.3.4). The values of these coefficients depend on the input values of λ_0, κ_0, and the other gauge and Yukawa couplings. F is some factor, possibly, involving $\tan\beta$.

Whence, one can calculate (analytically or numerically) the sensitivity of m_Z to each fundamental parameter, and this leads us to fine tuning.

5.4 Fine tuning and the master formula

To study the degree of fine tuning, a quantitative measure needs to be applied. Here we use the conventional fine tuning measure presented in Sec. 3.5,

$$\Delta_a = \left| \frac{\partial \ln m_Z}{\partial \ln a} \right|, \tag{5.20}$$

where m_Z is the mass of the Z boson[3] and a is one of the fundamental parameter in the set $\{m_0, m_{1/2}, A, \lambda(0), \kappa(0)\}$.

For example, $\Delta_a = 10$ and 200 correspond to a 10% and 0.5% tuning in the parameter a, respectively. Moreover, for a given point in the parameter space, fine tuning is the maximum value of fine tuning in the set $\{\Delta_a\}$, and is denoted Δ_{max} (or simply Δ).

5.4.1 Master Formula

We now proceed to apply it in a quantitative analysis of fine tuning. To do so we first derive and present the master formula which gives the explicit expression from which the fine tuning is calculated. Using Equations 5.13, 5.14, 5.15 and 5.20, we derive this master formula for fine tuning in the E$_6$SSM[4],

$$\begin{aligned}
\Delta_a \approx & c^{-1} \times \frac{a}{m_Z^2(\tan^2\beta - 1)} \Bigg\{ \frac{(1-\tan^2\beta)}{2} \frac{\partial(\lambda^2 s^2)}{\partial a} + \frac{\partial m_d^2}{\partial a} - \tan^2\beta \frac{\partial m_u^2}{\partial a} \\
& + \frac{g_1'^2}{2}(Q_1 - \tan^2\beta Q_2) \left(Q_s \frac{\partial s^2}{\partial a} + \frac{4m_Z^2}{\bar{g}^2} \frac{\partial}{\partial a}(Q_1 \cos^2\beta + Q_2 \sin^2\beta) \right) \\
& - \frac{\tan\beta}{\cos 2\beta} \left[1 + \frac{m_Z^2}{m_d^2 + m_u^2 + \lambda^2 s^2 + \frac{g_1'^2}{2} Q_s s^2 (Q_1 + Q_2)} \right] \times \\
& \times \left[\sqrt{2} \frac{\partial(\lambda A_\lambda s)}{\partial a} - \sin 2\beta \frac{\partial}{\partial a}(m_d^2 + m_u^2 + \lambda^2 s^2 + \frac{g_1'^2}{2} Q_s (Q_1 + Q_2) s^2) \right] \Bigg\},
\end{aligned} \tag{5.21}$$

where

$$c = \left[1 - \frac{4}{(\tan^2\beta - 1)} \frac{g_1'^2}{\bar{g}^2} (Q_1 - \tan^2\beta Q_2) \times (Q_1 \cos^2\beta + Q_2 \sin^2\beta) \right], \tag{5.22}$$

and $\bar{g}^2 = (g'^2 + g_2^2)$. For $\tan\beta = 10$; $c^{-1} \simeq 0.88$.

[3] Note that some authors choose m_Z^2 instead of m_Z. Both measures can be easily linked since $\frac{1}{2}\Delta_a(m_Z^2) = \Delta_a(m_Z)$. Our choice was made to enable straightforward comparisons with the results in [135].

[4] Note we have left two terms in the second line of Eq. 5.21 written in terms of derivatives of $\cos^2\beta$ and $\sin^2\beta$ with respect to a. Substituting for soft masses here would unnecessarily clutter the expression and we note that these terms are numerically negligible since their contribution to fine tuning is very small ($< \mathcal{O}(1)$). This is due to the fact that they will be multiplied by an overall factor of order $\mathcal{O}(< 10^{-12})$.

The aim is to expand the low energy parameters, including s, in terms of the GUT-scale universal input parameters using the E_6SSM RGEs as mentioned in the previous section. Next, the formula is implemented into a private cE_6SSM spectrum generator (described in [148, 149]) and fine tuning at each point in the scanned parameter space is calculated. In order to ensure accuracy of the results, the derivatives in the master formula for $a = \lambda(0)$ and $a = \kappa(0)$ are calculated numerically. And in order to calculate,

$$\frac{\partial}{\partial a} s^2, \tag{5.23}$$

we use

$$s^2 = -\frac{2}{g_1'^2 Q_s^2} m_s^2, \tag{5.24}$$

where, as usual, m_s^2 is expanded in terms of the GUT parameters.

Finally, throughout our study, we fix $\tan\beta = 10$ since larger and smaller values restrict the availability of $m_h \sim 125$ GeV, and the parameter space [150].

5.5 Results and discussion

The scans are taken for fixed $s = 5 - 10$ TeV corresponding to $M_{Z'} = 1.9 - 3.8$ TeV. We scan over

$$-3 \lesssim \lambda_3(0) \lesssim 0 \quad \text{and} \quad 0 \lesssim \kappa_1(0) = \kappa_2(0) = \kappa_3(0) \lesssim 3 \tag{5.25}$$

while fixing $\lambda_{1,2}(0) = 0.1$ and $\tan\beta = 10$. The sign of $\lambda \equiv \lambda_3(0)$ is a free parameter in our convention since we are setting s and $m_{1/2} > 0$. However as with previous studies [150] we found that most of the parameter space is covered with $\lambda < 0$, while $\lambda > 0$ covers a much smaller region of the parameter space. Therefore we focused on $\lambda < 0$ in our study. The other GUT parameters: $m_0, m_{1/2}$ and A_0 are obtained as an output so that the EWSB conditions are satisfied to one-loop order. Then we plot both m_h and Δ_{max} in the $m_0 - m_{1/2}$ plane. The key at the top-left of all plots corresponding to m_h shows the central value in a bin of width ± 0.5 GeV, while that corresponding to Δ shows the central value in a bin of width ± 50.

Moreover, we select a benchmark point corresponding to each value of s. These points possess the smallest fine tuning in the $m_0 - m_{1/2}$ plane consistent with a Higgs mass within the $124 < m_h < 127$ GeV range, and $m_{\tilde{g}} \geq 850$ GeV [5]. They are denoted as a black dot in Figures 5.1- 5.12. These points and the relevant physical masses are summarised in Table B.1 in Appendix B.

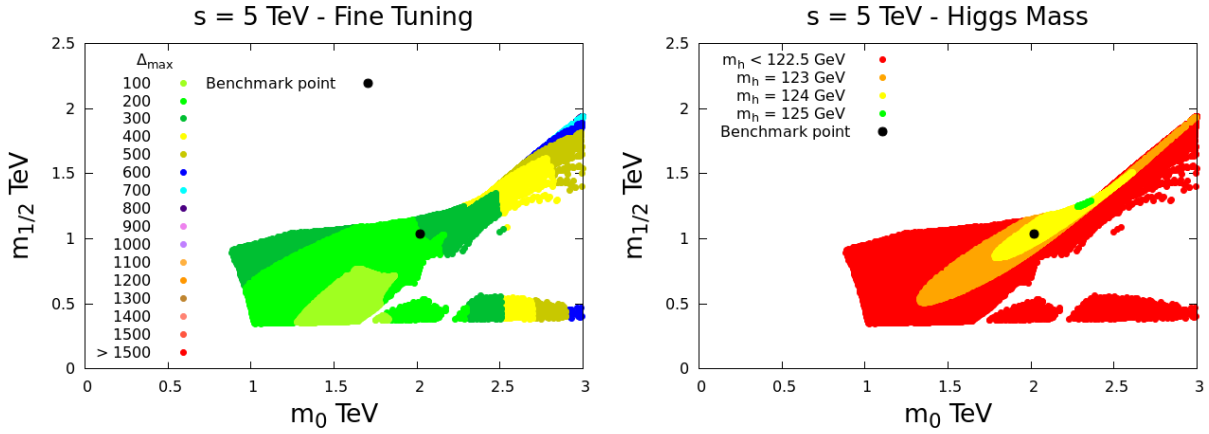

FIGURE 5.1: Δ_{max} (left) and m_h (right) in the $m_0 - m_{1/2}$ plane for $\tan\beta = 10$ and $s = 5$ TeV corresponding to $M_{Z'} = 1.9$ TeV. We also fixed $\lambda_{1,2}(0) = 0.1$ while scanning over $-3 \leq \lambda_3(0) \leq 0$ and $0 \leq \kappa_{1,2,3}(0) \leq 3$. The benchmark point corresponds to $m_0 = 2020, m_{1/2} = 1033$ GeV.

In the left panel of Fig. 5.1 the results for $s = 5$ TeV, corresponding to $M_{Z'} = 1.9$ TeV, are shown with fine tuning contours, ranging from 100 to above 800 for the highest m_0. For each value of m_0 and $m_{1/2}$, the parameters λ, κ, and A take different values. Since the Higgs mass strongly depends both on top squark corrections and λ, it will also take different values denoted by the Higgs mass contours displayed in the right panel of Fig. 5.1. Since both fine tuning and the Higgs mass vary over the $m_0 - m_{1/2}$ plane the mass of the Higgs discovered at the LHC plays a crucial rule in fixing the level of tuning, though this dependence is significantly more complicated than in the MSSM. Thus, although for $s = 5$ TeV the tuning can in principle be as low as 100, in order to obtain $m_h \sim 124$ GeV the fine tuning must be more than twice as large as this. A benchmark representing points with the lowest tuning compatible with data shown as

[5] The constraint on $m_{\tilde{g}}$ applied here is based on earlier LHC results than the constraint applied in the previous Chapter. This is because this study was published before the one in the previous Chapter.

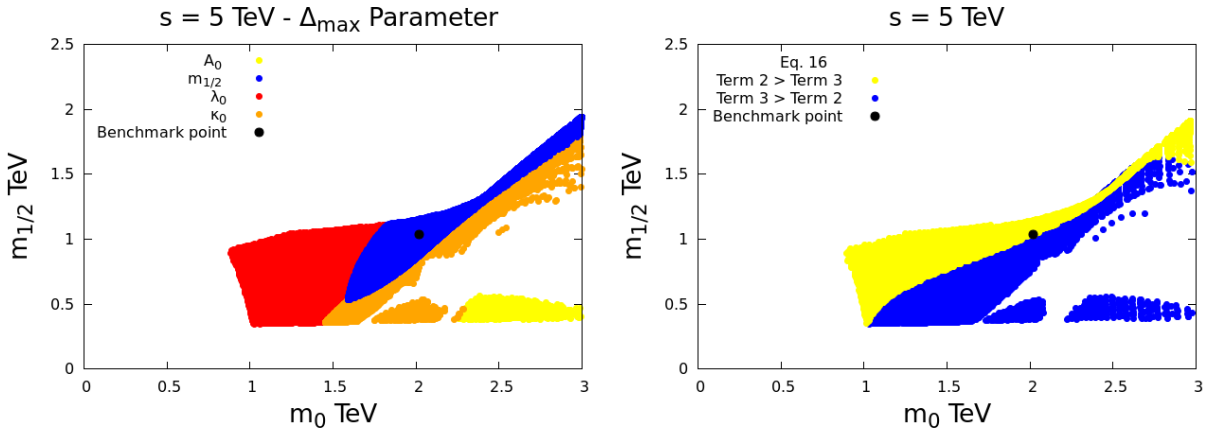

FIGURE 5.2: The left panel highlights the parameter responsible for the largest amount of fine tuning, Δ_{max}, in the $m_0 - m_{1/2}$ plane for $\tan\beta = 10$ and $s = 5$ TeV corresponding to $M_{Z'} = 1.9$ TeV. On the right a coarse scan shows which terms Eq. 5.16 give the largest contribution, with regions where the largest contribution comes from term 2, which is proportional to $m_d^2 - m_u^2 \tan^2\beta$, are shown in yellow and while regions where the dominant contribution is from term 3, proportional to $M_{Z'}^2$ are shown in blue.

black dot in Fig. 5.1 having $\Delta_{BM} = 251$ with $m_h \approx 124$ GeV. Note that $m_h \sim 125$ GeV is almost impossible to achieve for $s = 5$ TeV (represented by the very small green region in the right panel). In addition, the value $M_{Z'} = 1.9$ TeV slightly violates the CMS limit $M_{Z'} \gtrsim 2.08$ TeV [145], although this limit does not take into account the presence of lighter singlet states which increase the Z' width and reduce the leptonic branching ratio, weakening this limit as discussed in [146].

One also needs to take into account LHC constraints from squark and gluino searches which rule out $m_{1/2} \lesssim 1$ TeV corresponding to a gluino mass $m_{\tilde{g}} \lesssim 850$ GeV [150].

In Appendix B we provide a set on benchmark points corresponding to $m_{1/2} \sim 1$ TeV and these benchmark points are denoted by small black dots on the Figures. We emphasise that the cE$_6$SSM has not been studied by any of the LHC experiments, and that the gluino mass limits in the E$_6$SSM may differ from those of the MSSM as discussed recently [155]. Therefore, in choosing our minimum tuning benchmarks, the limits we assumed are quite conservative. From the results in [150], we find that in the cE$_6$SSM the gluino mass is approximately given by $m_{\tilde{g}} \sim 0.85 m_{1/2}$ and the first and second generation squark masses are given by $m_{\tilde{q}} \sim (1.3 - 1.8)m_0$, depending on $m_{1/2}$. In the future (for example when the full 8 TeV data set is analysed) the allowed values

of m_0 and $m_{1/2}$ are expected to increase according to these approximate relations. Therefore, we show in Appendix B.1 (Table B.2) the minimum allowed fine tuning associated with gluino mass in the $1 \leq m_{\tilde{g}} \leq 1.5$ TeV range, and the usual range for the singlet VEV $s = 5 - 10$ TeV. Clearly, the fine tuning in the cE$_6$SSM is not as large as that in the CMSSM, where increasing $m_{\tilde{g}}$ to 1.5 TeV leads to minimum fine tuning > 1000 as found in [135], while it varies between $\sim 600 - 800$ in the cE$_6$SSM.

At first sight, the distribution of fine tuning in the $m_0 - m_{1/2}$ plane could seem counter intuitive since one might expect the region of smaller values of m_0 and $m_{1/2}$ to possess lower fine tuning. However, the variation of Δ_{max} can be understood by studying which parameter contributes the maximum fine tuning at each point in the parameter space. We show this in Fig. 5.2 (left panel) where it is clear that the region of small m_0 and $m_{1/2}$ is dominated by large fine tuning in the parameter λ_0, resulting from a large $|\mu_{\rm eff}|$ term in this region.

In addition, κ_0 can contribute to Δ_{max} since A_λ and m_s are strongly dependent on this parameter. The physical origin of the fine tuning in κ_0 is due to the loops of exotic D-particles which serve to radiatively drive the singlet mass squared negative which triggers electroweak symmetry breaking. Finally, m_0 can be the source of fine tuning for very large values of m_0 which is the region extending beyond what we show in the plots.

The relative fine tuning in the input parameters $\{m_0, m_{1/2}, A, \lambda(0), \kappa(0)\}$ does not directly tell us any information about the relative importance of the second and third terms on the right-hand side of Eq. 5.16, both of which can independently be large and hence lead to a large $|\mu_{\rm eff}|$ which is manifested as large fine tuning in λ_0. It is therefore instructive to directly compare the magnitudes of the second and third terms of Eq. 5.16, where the former is proportional to m_u^2 and m_d^2, hence sfermions, and the latter is proportional to $M_{Z'}^2$. In Fig. 5.2 (right panel) we scan the parameter space for $s = 5$ TeV, and for each point we show which of the two terms is larger. The larger of the two would be responsible for the fine tuning at the corresponding point. It is clear, then, that $M_{Z'}$ (blue region) not only controls the minimum fine tuning allowed, but also is the dominating source of fine tuning over large regions of the parameter space.

This is true for all the other values of s. However, some substantial contribution to fine tuning comes from sfermions as seen in the yellow region.

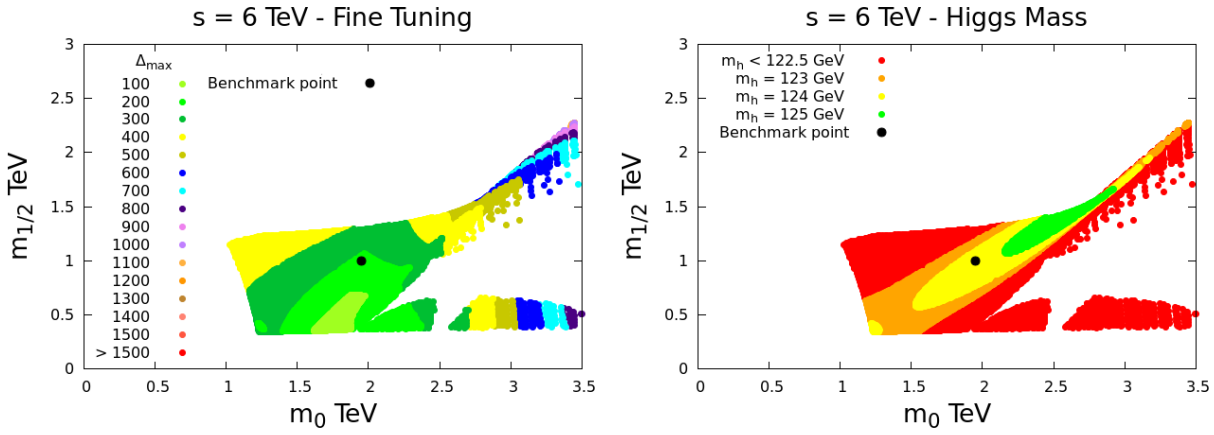

FIGURE 5.3: Δ_{max} (left) and m_h (right) in the $m_0 - m_{1/2}$ plane for $\tan\beta = 10$ and $s = 6$ TeV corresponding to $M_{Z'} = 2.3$ TeV. The benchmark point corresponds to $m_0 = 1951, m_{1/2} = 1003$ GeV.

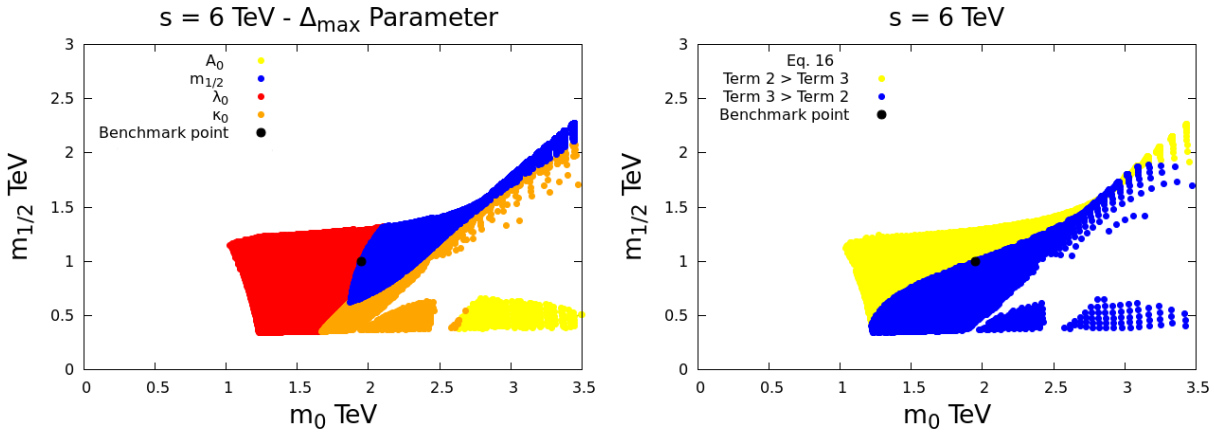

FIGURE 5.4: The left panel highlights the parameter responsible for the largest amount of fine tuning, Δ_{max}, in the $m_0 - m_{1/2}$ plane for $\tan\beta = 10$ and $s = 6$ TeV corresponding to $M_{Z'} = 2.3$ TeV. On the right a coarse scan shows which terms Eq. 5.16 give the largest contribution, with regions where the largest contribution comes from term 2, which is proportional to $m_d^2 - m_u^2 \tan^2\beta$, are shown in yellow and while regions where the dominant contribution is from term 3, proportional to $M_{Z'}^2$ are shown in blue.

As we increase s to 6 TeV (shown in Fig. 5.3), we simultaneously satisfy the CMS mass limit on the Z' mass, with $M_{Z'} = 2.3$ TeV, and we obtain more points with the heavier Higgs mass $m_h = 125$ GeV. Interestingly, the benchmark point in this case has a fine tuning $\Delta_{BM} = 233$ for $m_h \approx 124$ GeV which is slightly smaller than for the previous

case with $s = 5$ TeV. Additionally, in the left panel in Fig. 5.3 a tiny region of $\Delta_{max} = 200$ appears as a small circle inside the $\Delta_{max} = 300$ band. While it is still λ_0 that is responsible for Δ_{max} in that area as seen in the left panel in Fig. 5.4, this region is associated with a slightly smaller $|\mu_{\rm eff}|$ ($|\lambda_0|$) and larger κ_0 than in the adjacent regions, an effect which was not present in the results of $s = 5$ TeV.

Moreover, Fig. 5.4 shows that the origin of fine tuning depends on the point in the $m_0 - m_{1/2}$ plane consistent with the Higgs mass and the LHC limits of squark and gluino masses, estimated above as $m_{\tilde{g}} \sim 0.85 m_{1/2}$ and $m_{\tilde{q}} \sim (1.3 - 1.8) m_0$. For example if the squark and gluino masses are increased then it is possible that fine tuning is dominated by fine tuning in $m_{1/2}$ or in λ_0 via large $|\mu_{\rm eff}|$ which could be due to heavy top squarks rather than large $M_{Z'}$ according to the right panel in Fig. 5.4.

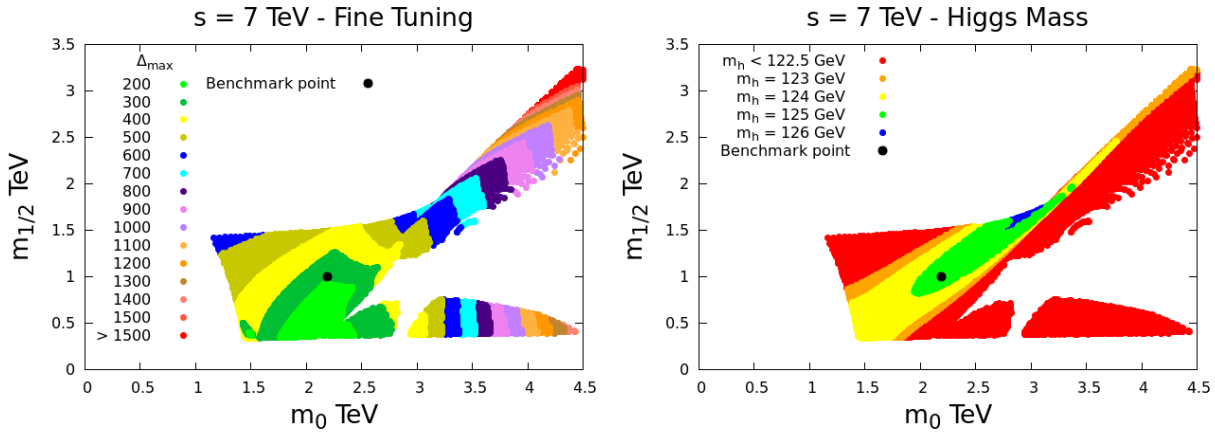

FIGURE 5.5: Δ_{max} (left) and m_h (right) in the $m_0 - m_{1/2}$ plane for $\tan\beta = 10$ and $s = 7$ TeV corresponding to $M_{Z'} = 2.6$ TeV. The benchmark point corresponds to $m_0 = 2186, m_{1/2} = 1004$ GeV.

For $s = 7$ TeV, corresponding to $M_{Z'} = 2.6$ TeV, the region with $m_h \sim 125$ GeV expands in comparison to $s = 5$ and 6 TeV, as can be seen by comparing the right panel in Fig. 5.5, to the previous plots. In addition a very small region with $m_h \sim 126$ GeV appears for the first time. In the left panel of Fig. 5.5, fine tuning starts from 200, and reaches 600 outside the middle region. In addition, the tiny circle of points with smaller fine tuning than its surroundings in the small $m_0 - m_{1/2}$ region, which appeared previously in the results for $s = 6$ TeV, now grows a little.

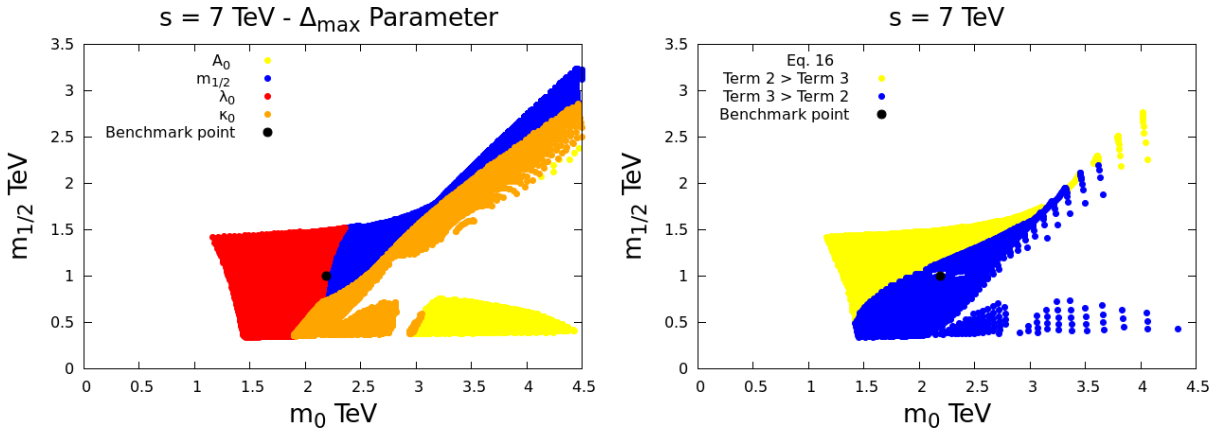

FIGURE 5.6: The left panel highlights the parameter responsible for the largest amount of fine tuning, Δ_{max}, in the $m_0 - m_{1/2}$ plane for $\tan\beta = 10$ and $s = 7$ TeV corresponding to $M_{Z'} = 2.6$ TeV. On the right a coarse scan shows which terms Eq. 5.16 give the largest contribution, with regions where the largest contribution comes from term 2, which is proportional to $m_d^2 - m_u^2 \tan^2\beta$, are shown in yellow and while regions where the dominant contribution is from term 3, proportional to $M_{Z'}^2$ are shown in blue.

The chosen benchmark point has $\Delta_{BM} = 270$ for $m_h \approx 125$ GeV. Notice how increasing s, hence $M_{Z'}$, affects the lowest fine tuning possible in the parameter space, confirming that it is the $M_{Z'}$ term in Eq. 5.16 dominating fine tuning and defining its lowest value as can be seen in the right panel of Fig. 5.6. As before, this conclusion depends on the particular point in the $m_0 - m_{1/2}$ plane.

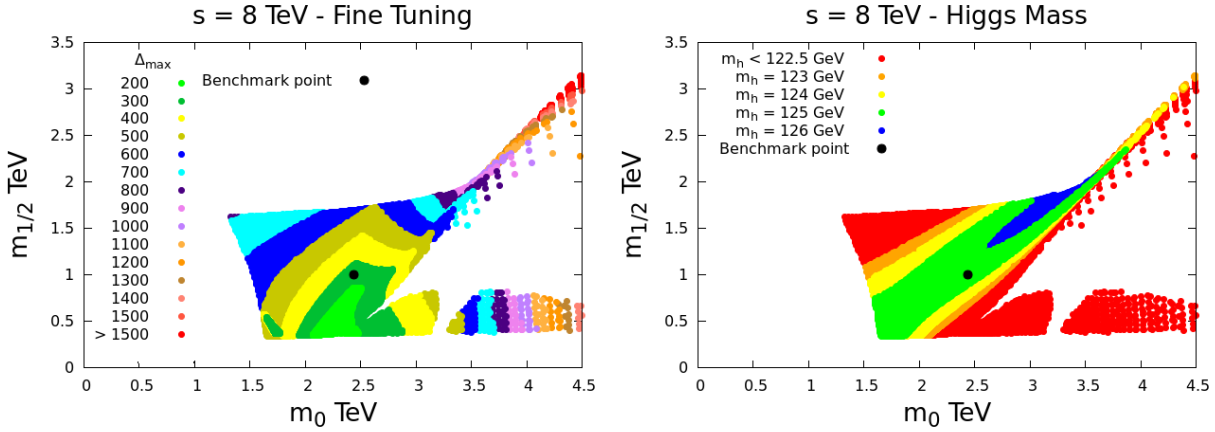

FIGURE 5.7: Δ_{max} (left) and m_h (right) in the $m_0 - m_{1/2}$ plane for $\tan\beta = 10$ and $s = 8$ TeV corresponding to $M_{Z'} = 3.0$ TeV. The benchmark point corresponds to $m_0 = 2441, m_{1/2} = 1002$ GeV.

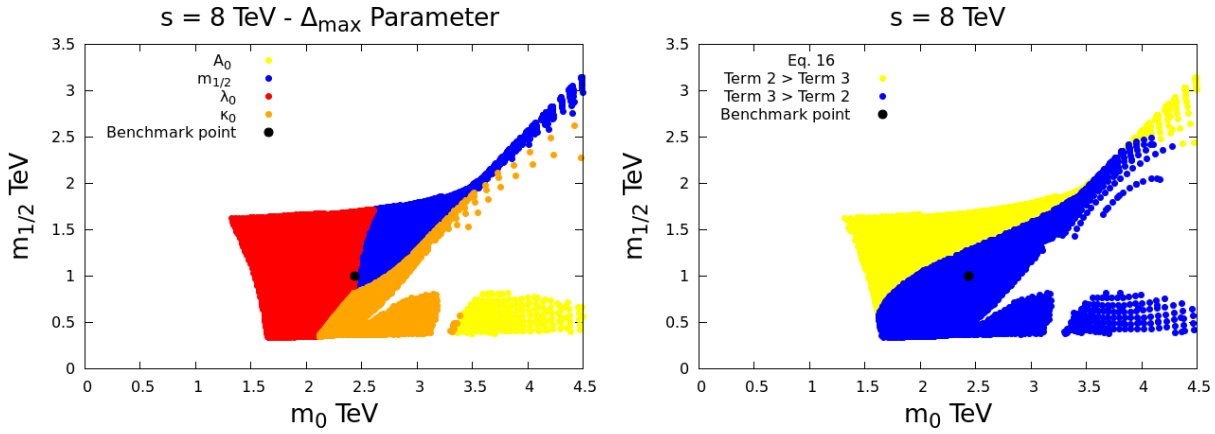

FIGURE 5.8: The left panel highlights the parameter responsible for the largest amount of fine tuning, Δ_{max}, in the $m_0 - m_{1/2}$ plane for $\tan\beta = 10$ and $s = 8$ TeV corresponding to $M_{Z'} = 3.0$ TeV. On the right a coarse scan shows which terms Eq. 5.16 give the largest contribution, with regions where the largest contribution comes from term 2, which is proportional to $m_d^2 - m_u^2 \tan^2\beta$, are shown in yellow and while regions where the dominant contribution is from term 3, proportional to $M_{Z'}^2$ are shown in blue.

For $s = 8$ TeV the Higgs mass $m_h \sim 125$ GeV dominates over most of the $m_0 - m_{1/2}$ plane as shown in the right panel of Fig. 5.7. Also the $m_h \sim 126$ GeV region has become larger. However, fine tuning starts from 300, and the portion of the parameter space with $\Delta_{max} \geq 500$ is now more apparent than in the $s = 7$ TeV case. The Benchmark point has $\Delta_{BM} = 302$ for $m_h \approx 125$ GeV. The dominance of the $M_{Z'}$ term in Eq. 5.16 for fine tuning can be seen in the right panel of Fig. 5.8, with this conclusion dependent on the particular point in the $m_0 - m_{1/2}$ plane.

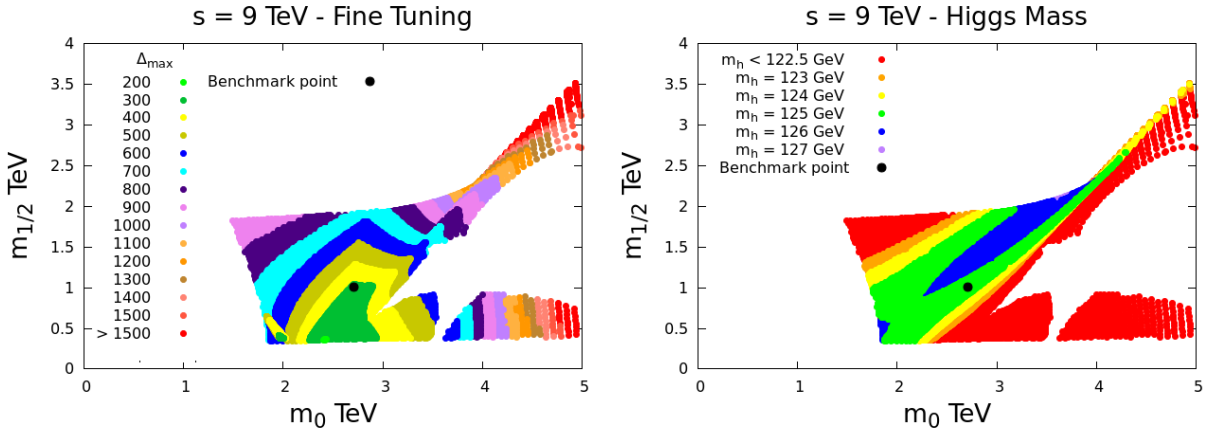

FIGURE 5.9: Δ_{max} (left) and m_h (right) in the $m_0 - m_{1/2}$ plane for $\tan\beta = 10$ and $s = 9$ TeV corresponding to $M_{Z'} = 3.4$ TeV. The benchmark point corresponds to $m_0 = 2709, m_{1/2} = 1001$ GeV.

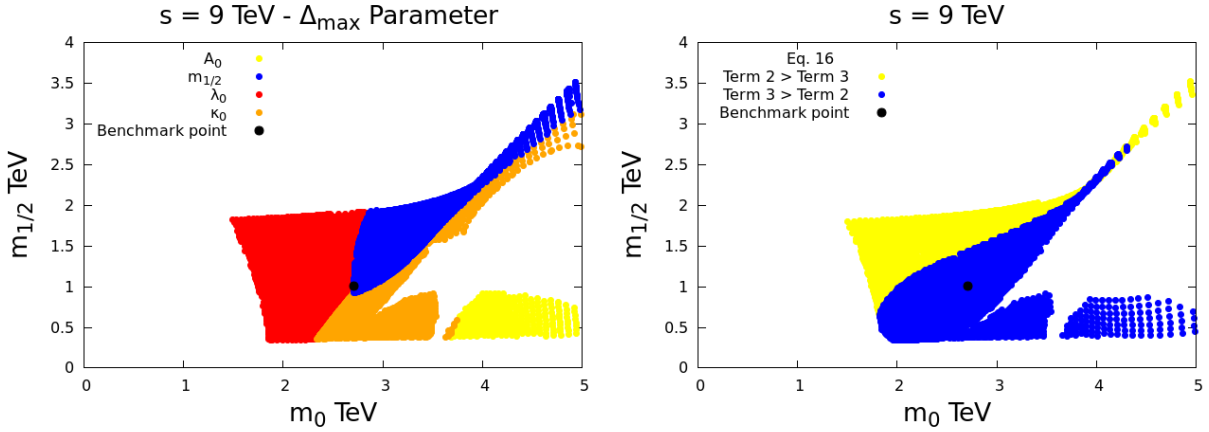

FIGURE 5.10: The left panel highlights the parameter responsible for the largest amount of fine tuning, Δ_{max}, in the $m_0 - m_{1/2}$ plane for $\tan\beta = 10$ and $s = 9$ TeV corresponding to $M_{Z'} = 3.4$ TeV. On the right a coarse scan shows which terms Eq. 5.16 give the largest contribution, with regions where the largest contribution comes from term 2, which is proportional to $m_d^2 - m_u^2 \tan^2\beta$, are shown in yellow and while regions where the dominant contribution is from term 3, proportional to $M_{Z'}^2$ are shown in blue.

As we reach $s = 9$ TeV, corresponding to $M_{Z'} = 3.4$ TeV, which is shown in Fig. 5.9, we see that the region where $m_h \sim 125$ GeV starts to shrink and is replaced by $m_h \sim 126$ GeV. If the Higgs mass is indeed $m_h \sim 126$ GeV then there is a preference for $s = 9$ TeV, especially for smaller values of m_0 and $m_{1/2}$. This illustrates the importance of an accurate determination in the Higgs mass for selecting the most

appropriate value of s. Fine tuning starts from 200, although a very small region, and quickly increases to 500 such that a significant portion of the parameter has $\Delta_{max} \gtrsim 500$. The benchmark point has $\Delta_{BM} = 330$ for $m_h \approx 125$ GeV. The dominance of the $M_{Z'}$ term in Eq. 5.16 for fine tuning can be seen in the right panel of Fig. 5.10, as usual dependent on the particular point in the $m_0 - m_{1/2}$ plane.

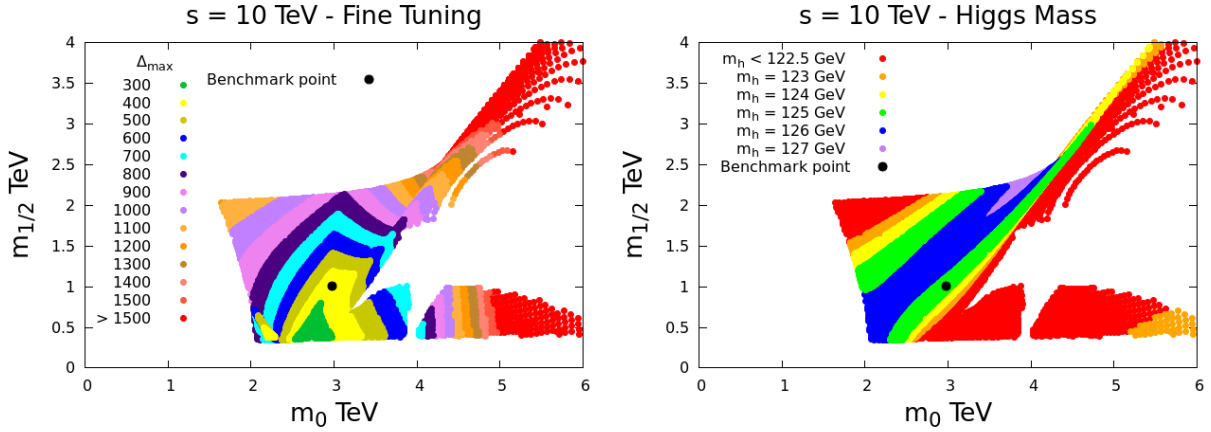

FIGURE 5.11: Δ_{max} (left) and m_h (right) in the $m_0 - m_{1/2}$ plane for $\tan\beta = 10$ and $s = 10$ TeV corresponding to $M_{Z'} = 3.8$ TeV. The benchmark point corresponds to $m_0 = 2975, m_{1/2} = 1005$ GeV.

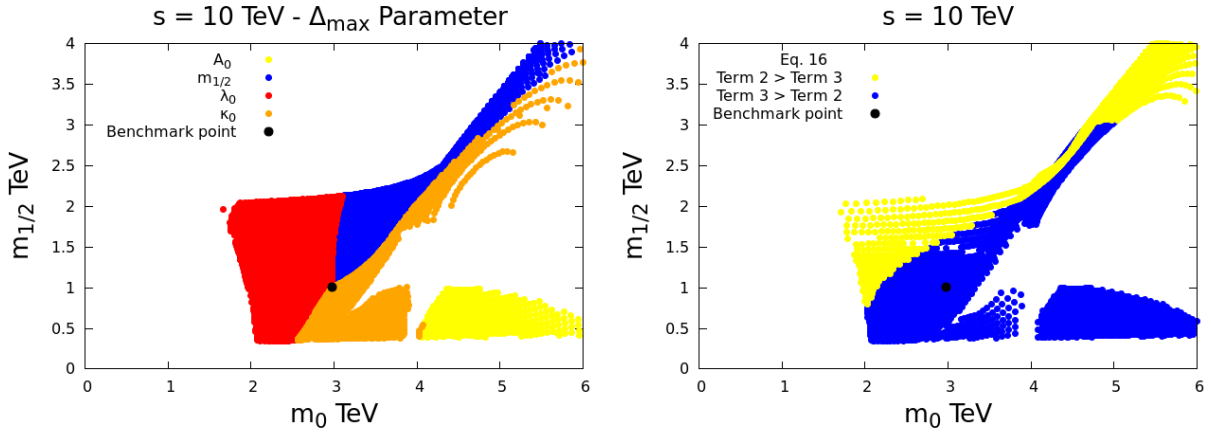

FIGURE 5.12: The left panel highlights the parameter responsible for the largest amount of fine tuning, Δ_{max}, in the $m_0 - m_{1/2}$ plane for $\tan\beta = 10$ and $s = 10$ TeV corresponding to $M_{Z'} = 3.8$ TeV. On the right a coarse scan shows which terms Eq. 5.16 give the largest contribution, with regions where the largest contribution comes from term 2, which is proportional to $m_d^2 - m_u^2 \tan^2\beta$, are shown in yellow and while regions where the dominant contribution is from term 3, proportional to $M_{Z'}^2$ are shown in blue.

Finally, for $s = 10$ TeV, corresponding to $M_{Z'} = 3.4$ TeV, in the left panel of Fig. 5.11 the fine tuning starts from 300, and the parameter space is severely restricted in terms of fine tuning as it is mostly covered by points with $\Delta_{max} > 500$. In addition, the region of $m_h \sim 125$ GeV has shrunk and now occupies a smaller portion than the $m_h \sim 126$ GeV region. In addition a small region with $m_h \sim 127$ GeV now exists prominently for the first time (only a miniscule region existed for $s = 9$ TeV). Moreover, as seen before, the left panel in Fig. 5.11 contains short lines of points in the small $m_0 - m_{1/2}$ region with smaller fine tuning than their surrounding points for the same reason as before, namely that $|\mu_{\rm eff}|$ can be somewhat smaller.

The benchmark point has fine tuning $\Delta_{BM} = 359$ and $m_h \approx 125$ GeV. The dominance of the $M_{Z'}$ term in Eq. 5.16 for fine tuning can be seen in the right panel of Fig. 5.12, with the familiar dependence on the particular point in the $m_0 - m_{1/2}$ plane.

5.6 More on the fine tuning of the E_6SSM

In the previous Sections, we have investigated the fine tuning in the cE_6SSM for the range of parameters detailed in Sec. 5.5 and a fixed value of $\tan\beta = 10$.

In this Section, we study two additional cases. The first is cE_6SSM with $\tan\beta \neq 10$, and the second is a variant of the E_6SSM where g' does not unify with the other couplings at the GUT scale.

5.6.1 Small and large $\tan\beta$

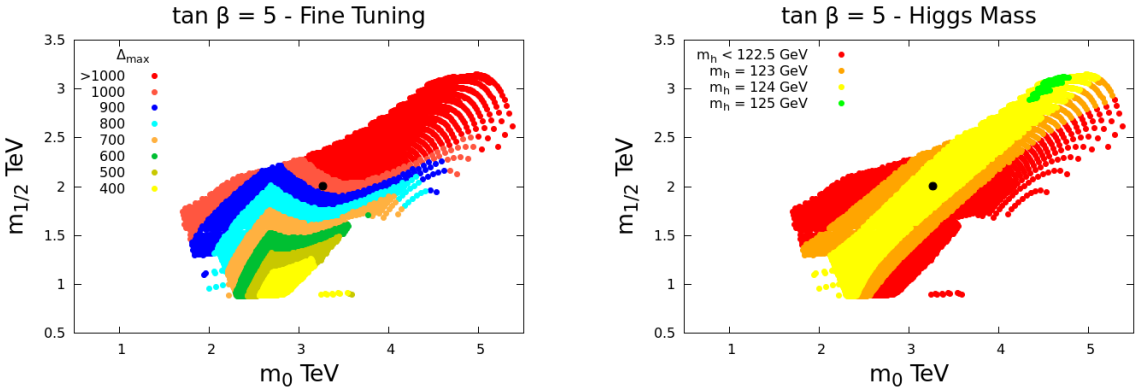

FIGURE 5.13: In the left panel, the fine tuning in the parameter space is shown in the $m_0 - m_{1/2}$ plane, while the the right panel shows the values of m_h. All with a fixed value of $M_{Z'} \approx 3.8$ TeV, and $\tan\beta = 5$.

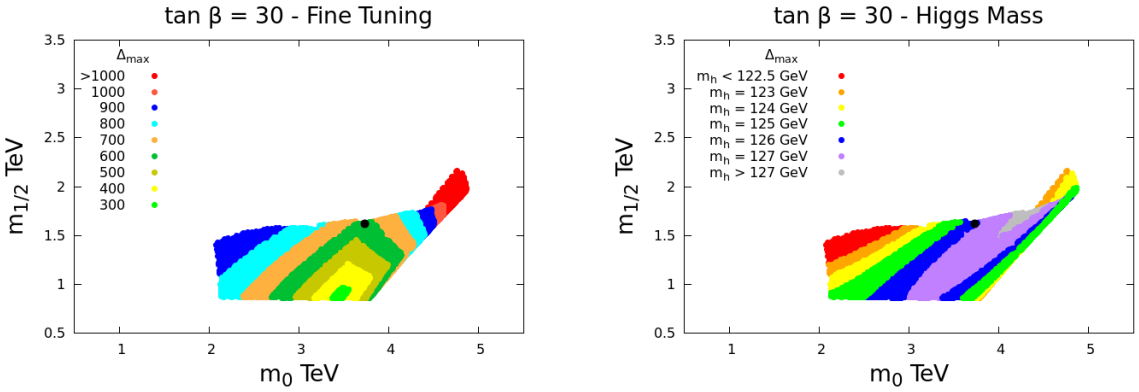

FIGURE 5.14: In the left panel, the fine tuning in the parameter space is shown in the $m_0 - m_{1/2}$ plane, while the the right panel shows the values of m_h. All with a fixed value of $M_{Z'} \approx 3.8$ TeV, and $\tan\beta = 30$.

Scanning over values of $\lambda_3(\text{GUT}) \sim \{-3, 0\}$, $\kappa_{1,2,3}(\text{GUT}) \sim \{0, 3\}$, taking specific values of $\tan\beta = 5$ and 30, while fixing $s = 10$ TeV (i.e. $M_{Z'} \approx 3.8$ TeV). The cuts we applied are rather conservative (see [114]) as we require a gluino mass $m_{\tilde{g}} > 1.4$ TeV. The Higgs mass is required to be within the range $124 < m_h < 127$ GeV.

From the right panel in Fig. 5.13, one can see that small values of $\tan\beta$ can hardly produce the desired Higgs mass. From our results we notice that the gluino mass can be large (> 1.5 TeV) in that region, however, fine tuning becomes larger as we

approach lower values of $\tan\beta$ (c.f. Fig. 5.14). The benchmark point (appears as a black dot in the Figures) for the $\tan\beta = 5$ case corresponds to a Higgs mass of 124 GeV, $m_{\tilde{g}} \sim 1.7$ TeV, and fine tuning $\Delta \sim 1000$, which is $\sim 0.1\%$ tuning.

One the other hand, in regions where $\tan\beta$ is large, as in Fig. 5.14, it is easy to find the desired Higgs mass and fine tuning is slightly lowered. However, as one approaches larger and larger values it becomes somewhat difficult to find a gluino mass larger than 1.5 TeV. Therefore, moderate values of $\tan\beta$ are favored in this model from phenomenological and naturalness standpoints. The benchmark point for $\tan\beta = 30$ corresponds to $m_h \sim 126.4$ GeV, $m_{\tilde{g}} \sim 1.4$ TeV, and fine tuning in the $\sim 0.2\%$ level ($\Delta \sim 600$), which is slightly better than the previous case.

5.6.2 lowered g'

Finally we also considered the possibility of lowering the predicted value of $M_{Z'}$ by reducing g'_1 away from the value predicted by gauge coupling unification. In order to significantly reduce, or eliminate, tree-level fine tuning associated with m_Z, both the first and third terms of Eq. 5.13 should be of $\mathcal{O}(M_W)$. This could be achieved by requiring both λ and g' to be of $\mathcal{O}(10^{-2})$.

At the GUT scale, one allows g' to break the unification of gauge couplings. For example, setting,

$$g'(\mathrm{GUT}) = \frac{g_1(\mathrm{GUT})}{100}, \tag{5.26}$$

which would result in $g'(M_{\mathrm{SUSY}}) \sim 0.011$, while $g_1(M_{\mathrm{SUSY}}) \sim 0.47$.

Moreover, for different values of g' one needs to estimate new lower bounds on $M_{Z'}$ and the corresponding increase in s. This has been carried out in [156] Without g'_1 unifying with the other gauge couplings at the GUT scale, Eq. 5.1 becomes ([136]),

$$m_h^2 \approx m_Z^2 \cos^2 2\beta + \frac{\lambda^2}{2} v^2 \sin^2 2\beta + g'^2 v^2 (Q_1 \cos^2\beta + Q_2 \sin^2\beta)^2 + \Delta m_h^2. \tag{5.27}$$

Therefore, it is clear that reducing g' and λ to order $\mathcal{O}(10^{-2})$ affects the prediction for m_h as shown in Fig. 5.6.2.

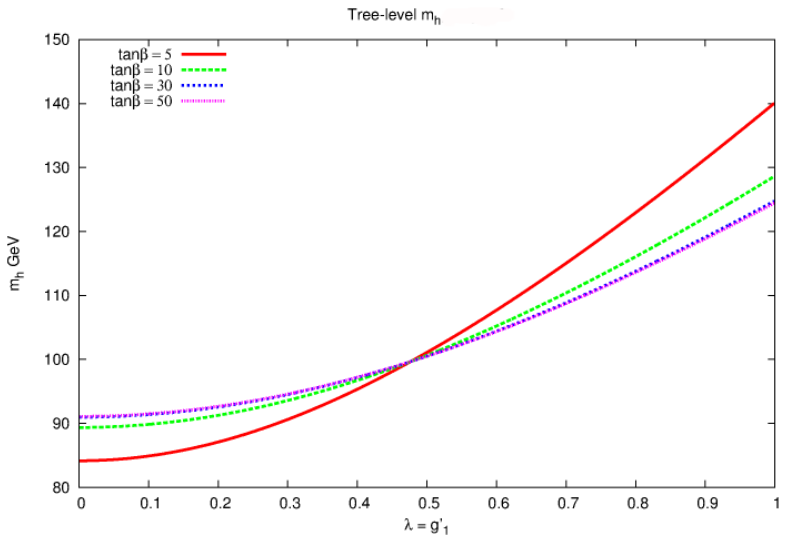

FIGURE 5.15: As both g' and λ decreases to $\mathcal{O}(10^{-2})$, the tree-level prediction of m_h decreases, since the additional contributions coming from the NMSSM-like term and the E_6SSM term are lost.

However, loop corrections can still make it possible to obtain the desired value of m_h. In order to investigate this case more systematically, we take a case where $s = 100$ TeV, $g' = 0.01$ at the GUT scale, and $\tan\beta = 30$. We modify the private code described in Sec. 5.4.1, and scan ranges and constraints on the benchmark point are chosen to be similar to those discussed in Sec. 5.5.

Fig. 5.16 shows the fine tuning and m_h in the usual m_0-$m_{1/2}$ plane in the parameter space of E_6SSM with $g' = 0.01g$ at the GUT scale, and $s = 100$ TeV.

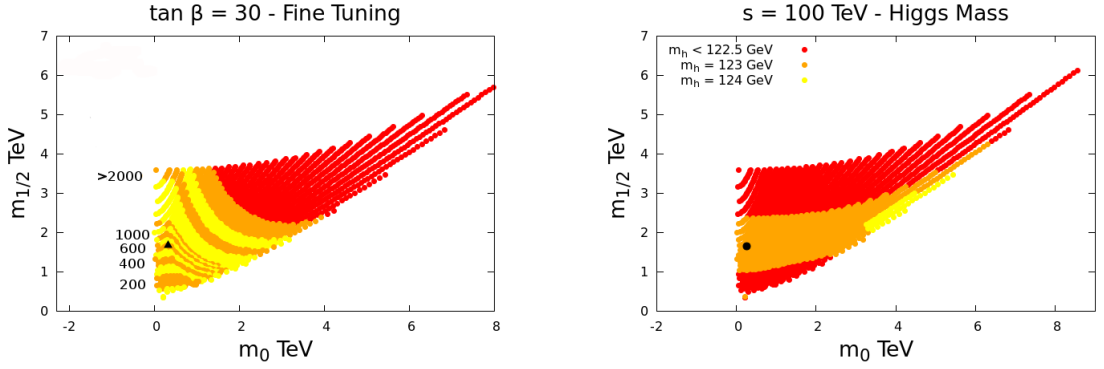

FIGURE 5.16: Left panel shows the fine tuning while the right panel shows the gluino mass, both in the $m_0 - m_{1/2}$ plane.

As can be seen in the left panel in Fig. 5.16, the fine tuning varies between $\Delta = 200$ and $\Delta = 2000$ as $m_{1/2}$ varies between ~ 500 GeV and 4 TeV. The benchmark point (black triangle), is where the fine tuning is lowest while satisfying the conditions that, 123 GeV $\leq m_h \leq$ 128 GeV, $m_{\tilde{g}} > 1$ TeV. The fine tuning was found to be $\Delta \sim 600$. The corresponding parameters and physical masses associated with this point are,

$$g' = 0.014 \ \lambda_W = -0.023 \ \kappa_W = 0.14$$

$$A_0 = 442 \text{ GeV}$$

$$m_{\tilde{g}} = 1.4 \text{ TeV} \quad m_{\tilde{t}_1} = 1.5 \text{ TeV}$$

$$m_{\tilde{\chi}_1^0} = 270 \text{ GeV} \quad m_{\tilde{\chi}_1^\pm} = 480 \text{ GeV}$$

$$M_{Z'} = 900 \text{ GeV}$$

Clearly, the E$_6$SSM with a lowered g' does not improve the fine tuning of the model as expected.

5.7 Conclusion

Supersymmetric unified models in which the singlet VEV is responsible simultaneously both for μ_{eff} and for the Z' mass, as in the E_6 class of models for example, have relatively large fine tuning which is typically dominated by the experimental mass limit on the Z'. To illustrate this, we have investigated the degree of fine tuning throughout the parameter space of the cE$_6$SSM. In fact this is the first time that fine tuning has been studied in any E_6 model containing a TeV scale Z'.

To quantify fine tuning we have derived a fine tuning master formula for the E$_6$SSM and implemented it in a spectrum generator for the constrained version of the model. Using this we scanned the parameter space of the cE$_6$SSM. The results are presented in the $m_0 - m_{1/2}$ plane for fixed $\tan\beta = 10$ and various s values corresponding to $M_{Z'} \sim 2 - 4$ TeV. This value of $\tan\beta = 10$ is the optimum choice for achieving a large enough Higgs mass in the cE$_6$SSM and so we have exclusively focussed on it here. We selected benchmark points corresponding to each value of s which possess the smallest fine tuning while allowing a Higgs mass within the $124 < m_h < 127$ GeV range, and $m_{\tilde{g}} \geq 850$ GeV. They are the black dot points in Figures 5.1- 5.12. These benchmark

points and the relevant physical masses are summarised in Table B.1 for a gluino mass of about 900 GeV. Table B.2 shows how the minimum fine tuning changes as the gluino mass limit increases up to 1.5 TeV. As remarked earlier, the fine tuning in the cE$_6$SSM is always significantly smaller than that in the cMSSM, for all gluino masses.

It is clear that the Z' mass (determined by the s VEV value) has a significant effect on the naturalness of the cE$_6$SSM model, with higher values leading to increased fine tuning. Therefore future improved direct mass limits on the Z' mass from the LHC will imply higher fine tuning. We have also seen an indirect relation between the Higgs boson mass and the Z' mass. For example if the Higgs mass turns out to be $m_h \gtrsim 127$ GeV then we are driven to $s \gtrsim 10$ TeV corresponding to $M_{Z'} \gtrsim 3.8$ TeV requiring higher fine tuning. Conversely if the Higgs mass turns out to be $m_h \lesssim 124$ GeV then $s \gtrsim 5$ TeV corresponding to $M_{Z'} \gtrsim 1.9$ TeV allowing lower fine tuning.

Given present limits, the results in Figures 5.1- 5.12 and Table B.1 show that the present lowest value of fine tuning in the cE$_6$SSM, consistent with a Higgs mass $m_h \sim 125$ GeV, varies from $\Delta \sim 200 - 400$ where the allowed lowest fine tuning values, taking into account the relevant experimental bounds, are dominated by $M_{Z'}$ rather than the other sources of fine tuning. This is presently significantly lower than the fine tuning in the cMSSM of $\Delta \sim 1000$ arising from the heavy top squarks required to achieve the Higgs mass.

In the future, the LHC lower limits on gluino and squark masses will improve, along with the Z' mass limit (or else a discovery will be made) and the Higgs boson mass will be more accurately specified. It is not completely clear where the dominant source of fine tuning in the cE$_6$SSM will originate from in future. However the results in this Chapter allow this question to be addressed. The future Z' mass limit will determine the minimum s value permitted, while the Higgs mass and gluino and squark mass limits will determine the allowed regions of the $m_0 - m_{1/2}$ plane, from which the fine tuning may be read off from the contour plots we provide.

We have also investigated regions of the parameter space of the cE$_6$SSM where $\tan\beta$ is as low as 5 and as high as 30. We find that, in general, fine tuning in the Electroweak sector lies in the percent level between $0.2\% - 0.1\%$. Small $\tan\beta$ regions are

characterized by smaller prediction for the Higgs mass, and gluino masses that are larger than experimental limits. The fine tuning is more severe in this region of the parameter space. On the other hand, large $\tan\beta$ regions are associated with Higgs masses around the experimentally observed value, and gluino masses that tend to be smaller than 1.5 TeV. However, the fine tuning is slightly less than that in the very low $\tan\beta$ regime. We can conclude that moderate values of $\tan\beta$ are favoured by naturalness in the cE$_6$SSM.

Finally, we studied a variant of the E$_6$SSM where g' is 100 times smaller than g_1 at the GUT scale. While this might reduce the tree-level fine tuning on m_Z from the term proportional $M_{Z'}$, it reintroduces fine tuning by requiring the top squarks to be large in order to obtain a ~ 126 Higgs mass. The fine tuning in this case is at least $\Delta \geq 600$.

Chapter 6

Conclusions

In Ch. 4, three non-minimal Z_3-invariant supersymmetric models has been considered. In particular, the NMSSM, and two variants that add three and four $(5, \overline{5})$ extra states of SU(5) to the matter content of the NMSSM, and they are called the NMSSM+ and the NMSSM++, respectively. This extra matter is treated as a secluded sector that affects the ordinary NMSSM matter via gauge interactions. The low energy spectrum has been calculated using the package NMSSMTools. For the cases of the NMSSM+, and the NMSSM++, two loop RGEs were implemented in a modified versions of NMSSMTools. Additionally, the running masses of the extra matter was ignored due to suppression by powers of gauge couplings and loop factors at one- and two-loop. The mass scale of the extra matter was assumed to be degenerate at the scale of first generation squarks.

The perturbativity bound on $\lambda(M_{\rm SUSY})$ can be relaxed in the NMSSM+ and the NMSSM++ due to the presence of the extra matter. Therefore, it is expected that the tree-level Higgs mass in the NMSSM++ will be larger than in the NMSSM+, and larger in the NMSSM+ than in the NMSSM without extra matter. Moreover, a common assumption is that the fine tuning reduces as the perturbativity bound on λ is increased since a large tree-level Higgs mass could imply lighter top squarks in the plus-type models than in the NMSSM.

We have investigated this hypothesis in the context of the three models above, and surprisingly have found that this is not the case. It was found that the NMSSM is the least fine tuned ($\Delta \sim 100$) mdoel. The fine tuning in the NMSSM+ was found to be the closest to the NMSSM with the lowest value being $\Delta \sim 200$. Finally, the NMSSM++ was the most fine tuned model where the fine tuning starts from 600. The mass spectrum in the NMSSM++ was found to be heavier than in the NMSSM+, and heavier in the NMSSM+ than in the NMSSM.

The reason why the fine tuning was found to be worse in the plus-type models than in the NMSSM is that such models with extra matter involve a larger gluino mass at high energies. In particular, we have found that M_3(GUT) is always larger in the NMSSM+ and very much larger in the NMSSM++, as compared to the NMSSM. This ordering results in an increased low energy stop mass spectrum, well above either the stop mass experimental limits or the stop mass limits required to obtain a sufficiently large Higgs mass. The heavy stop masses appear to be unavoidable in the NMSSM+, and especially the NMSSM++, as a result of the low energy experimental gluino mass limit and the RGE running behaviour, at least for the class of high energy semi-constrained SUGRA inspired models we have considered. Therefore, it appears that increasing the perturbativity bound on λ at the low scale by adding extra matter does not reduce the fine tuning.

We have also studied the parameter space of the NMSSM+ where DM relic density constraints were imposed. We have modified NMSSMTools4.4.0, where two-loop RGEs of the NMSSM+ were implemented. The mass scale of the vector-like state is fixed at 2.5 TeV. Furthermore, we have considered a parameter space with a small $\tan\beta$ (fixed at 3), μ-term (250 GeV), and large λ in order to enhance its tree-level contribution the Higgs mass. We have found that the NMSSM+ have a range of parameter space that passes the experimental constraints in Table 4.1, and can account for DM relic density. We have also found that the lowest fine tuning possible sets around 250. This further confirms that the NMSSM+ is more fine tuned than the NMSSM. However, the results presented are preliminary, and more thorough investigation is needed.

In Ch. 5, it has been shown that supersymmetric unified models in which the singlet VEV is responsible simultaneously both for $\mu_{\rm eff}$ and for the Z' mass, as in the E_6 class of models for example, have relatively large fine tuning which is typically dominated by the experimental mass limit on the Z'. In particular, we have investigated the degree of fine tuning throughout the parameter space of the cE$_6$SSM.

To quantify fine tuning we have derived a fine tuning master formula for the E$_6$SSM and implemented it in a spectrum generator for the constrained version of the model. Using this we scanned the parameter space of the cE$_6$SSM. The results are presented in the $m_0 - m_{1/2}$ plane for fixed $\tan\beta = 10$ and various s values corresponding to $M_{Z'} \sim 2 - 4$ TeV. This value of $\tan\beta = 10$ is the optimum choice for achieving a large enough Higgs mass in the cE$_6$SSM and so we have exclusively focussed on it here. We selected benchmark points corresponding to each value of s which possess the smallest fine tuning while allowing a Higgs mass within the $124 < m_h < 127$ GeV range, and $m_{\tilde{g}} \geq 850$ GeV. They are the black dot points in Figures 5.1- 5.12. These benchmark points and the relevant physical masses are summarised in Table B.1 for a gluino mass of about 900 GeV. Table B.2 shows how the minimum fine tuning changes as the gluino mass limit increases up to 1.5 TeV. As remarked earlier, the fine tuning in the cE$_6$SSM is always significantly smaller than that in the cMSSM, for all gluino masses.

The Z' mass (determined by the s VEV value) had a significant effect on the naturalness of the cE$_6$SSM model, with higher values leading to increased fine tuning. Therefore future improved direct mass limits on the Z' mass from the LHC will imply higher fine tuning. We have also seen an indirect relation between the Higgs boson mass and the Z' mass. For example if the Higgs mass turns out to be $m_h \gtrsim 127$ GeV then we are driven to $s \gtrsim 10$ TeV corresponding to $M_{Z'} \gtrsim 3.8$ TeV requiring higher fine tuning. Conversely if the Higgs mass turns out to be $m_h \lesssim 124$ GeV then $s \gtrsim 5$ TeV corresponding to $M_{Z'} \gtrsim 1.9$ TeV allowing lower fine tuning.

Given present limits, the results in Figures 5.1- 5.12 and Table B.1 show that the present lowest value of fine tuning in the cE$_6$SSM, consistent with a Higgs mass $m_h \sim 125$ GeV, varies from $\Delta \sim 200 - 400$ where the allowed lowest fine tuning values, taking into account the relevant experimental bounds, are dominated by $M_{Z'}$ rather

than the other sources of fine tuning. This is presently significantly lower than the fine tuning in the cMSSM of $\Delta \sim 1000$ arising from the heavy top squarks required to achieve the Higgs mass.

Future LHC lower limits on gluino and squark masses will improve, along with the Z' mass limit (or else a discovery will be made) and the Higgs boson mass will be more accurately specified. It is not completely clear where the dominant source of fine tuning in the cE$_6$SSM will originate from in future. However the results in this Chapter allow this question to be addressed. The future Z' mass limit will determine the minimum s value permitted, while the Higgs mass and gluino and squark mass limits will determine the allowed regions of the $m_0 - m_{1/2}$ plane, from which the fine tuning may be read off from the contour plots we provide.

We have also investigated regions of the parameter space of the cE$_6$SSM where $\tan\beta$ is as low as 5 and as high as 30. We find that, in general, fine tuning in the Electroweak sector lies in the percent level between $0.2\% - 0.1\%$. Small $\tan\beta$ regions are characterized by smaller prediction for the Higgs mass, and gluino masses that are larger than experimental limits. The fine tuning is more severe in this region of the parameter space. On the other hand, large $\tan\beta$ regions are associated with Higgs masses around the experimentally observed value, and gluino masses that tend to be smaller than 1.5 TeV. However, the fine tuning is slightly less than that in the very low $\tan\beta$ regime. We can conclude that moderate values of $\tan\beta$ are favoured by naturalness in the cE$_6$SSM.

We have studied a variant of the E$_6$SSM where g' is 100 times smaller than g_1 at the GUT scale. While this might reduce the tree-level fine tuning on M_Z from the term proportional $M_{Z'}$, it reintroduces fine tuning by requiring the top squarks to be large in order to obtain a ~ 126 Higgs mass. The fine tuning in this case is at least $\Delta \geq 600$.

In the future, it is interesting to consider the NMSSM with non-minimal Gauge mediation. In this scenario we allow the singlet superfield to couple the messenger superfields, and to vector-like superfields that survive to the energy scale of the first generation of sfermions. Such vector-like states originate from a (5+5*) fundamental representation of an SU(5) group at the messenger scale. One issue with gauge

mediation in the NMSSM is that the scalar component of the singlet superfield does not acquire a vacuum expectation value at the desired low energy scale due to insufficient RG running from the messenger energy scale to the weak scale (i.e. the running squared-mass parameter of the singlet does not become negative at the required energy scale). The addition of the previously mentioned vector-like states could allow this to happen. Our aim is to investigate this idea and analyse the parameter space taking into account the latest experimental constraints. We aim to see how this will affect the naturalness of the model.

Appendix A

Two-loop renormalisation group equations

In this Appendix we present the two-loop RGEs (in the $\overline{\text{DR}}$ scheme) used to obtain the mass spectrum and fine tuning results. We follow the same notation in [81], and use SM normalisation of the $U(1)_Y$ gauge coupling, g_1 in the three models. Also, $t \equiv \ln Q^2$. Finally, the RGE coefficients that are different in the three models are placed as follows:

$$\{\text{NMSSM}, \text{NMSSM+}, \text{NMSSM++}\}$$

in the same RGE equation. For example, the coefficients between braces in:

$$16\pi^2 \frac{dg_1^2}{dt} = \underline{\{11, 16, \frac{53}{3}\}} g_1^4$$

belong to the NMSSM, NMSSM+, and NMSSM++, respectively.

Two-loop RGEs of gauge and Yukawa couplings in the NMSSM, NMSSM+ and NMSSM++ are,

$$\begin{aligned}
16\pi^2\frac{dg_1^2}{dt} &= \{11,16,\frac{53}{3}\}g_1^4+\frac{g_1^4}{16\pi^2}\bigg(\{\frac{199}{9},26,\frac{737}{27}\}g_1^2+\{9,18,21\}g_2^2\\
&+ \{\frac{88}{3},40,\frac{392}{9}\}g_3^2-\frac{26}{3}h_t^2-\frac{14}{3}h_b^2-6h_\tau^2-2\lambda^2\bigg)\,,\\
16\pi^2\frac{dg_2^2}{dt} &= \{1,4,5\}g_2^4+\frac{g_2^4}{16\pi^2}\bigg(\{3,6,7\}g_1^2+\{25,46,53\}g_2^2+24g_3^2\\
&- 6h_t^2-6h_b^2-2h_\tau^2-2\lambda^2\bigg)\,,\\
16\pi^2\frac{dg_3^2}{dt} &= \{-3,0,1\}g_3^4+\frac{g_3^4}{16\pi^2}\bigg(\{\frac{11}{3},5,\frac{49}{9}\}g_1^2+9g_2^2+\{14,48,\frac{178}{3}\}g_3^2-4h_t^2-4h_b^2\bigg)\,,
\end{aligned}$$

$$\begin{aligned}
16\pi^2\frac{dh_t^2}{dt} &= h_t^2\bigg(6h_t^2+h_b^2+\lambda^2-\frac{13}{9}g_1^2-3g_2^2-\frac{16}{3}g_3^2\bigg)\\
&+ \frac{h_t^2}{16\pi^2}\bigg(-22h_t^4-5h_b^4-3\lambda^4-5h_t^2h_b^2-3h_t^2\lambda^2-h_b^2h_\tau^2-4h_b^2\lambda^2\\
&- h_\tau^2\lambda^2-2\lambda^2\kappa^2+2g_1^2h_t^2+\frac{2}{3}g_1^2h_b^2+6g_2^2h_t^2+16g_3^2h_t^2\\
&+ \{2743,3913,4303\}\frac{g_1^4}{162}+\{15,33,39\}\frac{g_2^4}{2}+\{-16,128,176\}\frac{g_3^4}{9}\\
&+ \frac{5}{3}g_1^2g_2^2+\frac{136}{27}g_1^2g_3^2+8g_2^2g_3^2\bigg)\,,
\end{aligned}$$

$$
\begin{aligned}
16\pi^2\frac{dh_b^2}{dt} &= h_b^2\Big(6h_b^2+h_t^2+h_\tau^2+\lambda^2-\frac{7}{9}g_1^2-3g_2^2-\frac{16}{3}g_3^2\Big)\\
&+ \frac{h_b^2}{16\pi^2}\Big(-22h_b^4-5h_t^4-3h_\tau^4-3\lambda^4-5h_b^2h_t^2-3h_b^2h_\tau^2-3h_b^2\lambda^2\\
&- 4h_t^2\lambda^2-2\lambda^2\kappa^2+\frac{2}{3}g_1^2h_b^2+\frac{4}{3}g_1^2h_t^2+2g_1^2h_\tau^2+6g_2^2h_b^2+16g_3^2h_b^2\\
&+ \{1435,2065,2275\}\frac{g_1^4}{162}+\{15,33,39\}\frac{g_2^4}{2}+\{-16,128,176\}\frac{g_3^4}{9}\\
&+ \frac{5}{3}g_1^2g_2^2+\frac{40}{27}g_1^2g_3^2+8g_2^2g_3^2\Big)\,,\\
16\pi^2\frac{dh_\tau^2}{dt} &= h_\tau^2\Big(4h_\tau^2+3h_b^2+\lambda^2-3g_1^2-3g_2^2\Big)\\
&+ \frac{h_\tau^2}{16\pi^2}\Big(-10h_\tau^4-9h_b^4-3\lambda^4-9h_\tau^2h_b^2-3h_\tau^2\lambda^2-3h_t^2h_b^2-3h_t^2\lambda^2\\
&- 2\lambda^2\kappa^2+2g_1^2h_\tau^2-\frac{2}{3}g_1^2h_b^2+6g_2^2h_\tau^2+16g_3^2h_b^2\\
&+ \{75,105,115\}\frac{g_1^4}{2}+\{15,33,39\}\frac{g_2^4}{2}+3g_1^2g_2^2\Big)\,,\\
16\pi^2\frac{d\lambda^2}{dt} &= \lambda^2\Big(3h_t^2+3h_b^2+h_\tau^2+4\lambda^2+2\kappa^2-g_1^2-3g_2^2\Big)\\
&+ \frac{\lambda^2}{16\pi^2}\Big(-10\lambda^4-9h_t^4-9h_b^4-3h_\tau^4-8\kappa^4-9\lambda^2h_t^2-9\lambda^2h_b^2\\
&- 3\lambda^2h_\tau^2-12\lambda^2\kappa^2-6h_t^2h_b^2+2g_1^2\lambda^2+\frac{4}{3}g_1^2h_t^2-\frac{2}{3}g_1^2h_b^2+2g_1^2h_\tau^2\\
&+ 6g_2^2\lambda^2+16g_3^2h_t^2+16g_3^2h_b^2+\{23,33,\frac{109}{3}\}\frac{g_1^4}{2}+\{15,33,\frac{117}{3}\}\frac{g_2^4}{2}+3g_1^2g_2^2\Big)\,,\\
16\pi^2\frac{d\kappa^2}{dt} &= \kappa^2\Big(6\lambda^2+6\kappa^2\Big)+\frac{\kappa^2}{16\pi^2}\Big(-24\kappa^4-12\lambda^4-24\kappa^2\lambda^2\\
&- 18h_t^2\lambda^2-18h_b^2\lambda^2-6h_\tau^2\lambda^2+6g_1^2\lambda^2+18g_2^2\lambda^2\Big)\,.
\end{aligned}
$$

Two-loop RGEs for the gauginos in the NMSSM, NMSSM+, and NMSSM++ are,

$$\begin{aligned}
16\pi^2\frac{dM_1}{dt} &= \{11,16,\frac{53}{3}\}g_1^2M_1 + \frac{g_1^2}{16\pi^2}\bigg(\frac{398}{9},52,\frac{1474}{27}\}g_1^2M_1 + \{9,18,21\}g_2^2\big(M_1+M_2\big)\\
&+ \{\frac{88}{3},40,\frac{392}{9}\}g_3^2\big(M_1+M_3\big)\\
&+ \frac{26}{3}h_t^2\big(A_t-M_1\big) + \frac{14}{3}h_b^2\big(A_b-M_1\big) + 6h_\tau^2\big(A_\tau-M_1\big) + 2\lambda^2\big(A_\lambda-M_1\big)\bigg)\,,\\
16\pi^2\frac{dM_2}{dt} &= \{1,4,5\}g_2^2M_2 + \frac{g_2^2}{16\pi^2}\bigg(\{3,6,7\}g_1^2\big(M_1+M_2\big) + \{50,92,106\}g_2^2M_2\\
&+ 24g_3^2\big(M_2+M_3\big) + 6h_t^2\big(A_t-M_2\big) + 6h_b^2\big(A_b-M_2\big)\\
&+ 2h_\tau^2\big(A_\tau-M_2\big) + 2\lambda^2\big(A_\lambda-M_2\big)\bigg)\,,\\
16\pi^2\frac{dM_3}{dt} &= \{-3,0,1\}g_3^2M_3 + \frac{g_3^2}{16\pi^2}\bigg(\{\frac{11}{3},5,\frac{49}{9}\}g_1^2\big(M_1+M_3\big) + 9g_2^2\big(M_2+M_3\big)\\
&+ \{28,96,\frac{356}{3}\}g_3^2M_3 + 4h_t^2\big(A_t-M_3\big) + 4h_b^2\big(A_b-M_3\big)\bigg)\,.
\end{aligned}$$

Two-loop RGEs of the trilinear couplings in the NMSSM, NMSSM+, and NMSSM++ are,

$$\begin{aligned}
16\pi^2\frac{dA_t}{dt} &= 6h_t^2A_t + h_b^2A_b + \lambda^2A_\lambda + \frac{13}{9}g_1^2M_1 + 3g_2^2M_2 + \frac{16}{3}g_3^2M_3\\
&+ \frac{1}{16\pi^2}\bigg(-44h_t^4A_t - 10h_b^4A_b - 6\lambda^4A_\lambda - 5h_t^2h_b^2\big(A_t+A_b\big)\\
&- 3h_t^2\lambda^2\big(A_t+A_\lambda\big) - h_b^2h_\tau^2\big(A_b+A_\tau\big) - 4h_b^2\lambda^2\big(A_b+A_\lambda\big)\\
&- h_\tau^2\lambda^2\big(A_\tau+A_\lambda\big) - 2\lambda^2\kappa^2\big(A_\lambda+A_\kappa\big) + 2g_1^2h_t^2\big(A_t-M_1\big)\\
&+ \frac{2}{3}g_1^2h_b^2\big(A_b-M_1\big) + 6g_2^2h_t^2\big(A_t-M_2\big) + 16g_3^2h_t^2\big(A_t-M_3\big)\\
&- \{2743,3919,4303\}\frac{g_1^4M_1}{81} - \{15,33,39\}g_2^4M_2 + \{32,-256,-352\}\frac{g_3^4M_3}{9}\\
&- \frac{5}{3}g_1^2g_2^2\big(M_1+M_2\big) - \frac{136}{27}g_1^2g_3^2\big(M_1+M_3\big) - 8g_2^2g_3^2\big(M_2+M_3\big)\bigg)\,,
\end{aligned}$$

$$
\begin{aligned}
16\pi^2\frac{dA_b}{dt} &= 6h_b^2A_b + h_t^2A_t + h_\tau^2A_\tau + \lambda^2A_\lambda + \frac{7}{9}g_1^2M_1 + 3g_2^2M_2 + \frac{16}{3}g_3^2M_3 \\
&+ \frac{1}{16\pi^2}\Big(- 44h_b^4A_b - 10h_t^4A_t - 6h_\tau^4A_\tau - 6\lambda^4A_\lambda - 5h_b^2h_t^2\big(A_b + A_t\big) \\
&- 3h_b^2h_\tau^2\big(A_b + A_\tau\big) - 3h_b^2\lambda^2\big(A_b + A_\lambda\big) - 4h_t^2\lambda^2\big(A_t + A_\lambda\big) \\
&- 2\lambda^2\kappa^2\big(A_\lambda + A_\kappa\big) + \frac{2}{3}g_1^2h_b^2\big(A_b - M_1\big) + \frac{4}{3}g_1^2h_t^2\big(A_t - M_1\big) \\
&+ 2g_1^2h_\tau^2\big(A_\tau - M_1\big) + 6g_2^2h_b^2\big(A_b - M_2\big) + 16g_3^2h_b^2\big(A_b - M_3\big) \\
&- \{1435, 2065, 2275\}\frac{g_1^4M_1}{81} - \{15, 33, 39\}g_2^4M_2 + \{32, -256, -352\}\frac{g_3^4M_3}{9} \\
&- \frac{5}{3}g_1^2g_2^2\big(M_1 + M_2\big) - \frac{40}{27}g_1^2g_3^2\big(M_1 + M_3\big) - 8g_2^2g_3^2\big(M_2 + M_3\big)\Big)\,, \\
16\pi^2\frac{dA_\tau}{dt} &= 4h_\tau^2A_\tau + 3h_b^2A_b + \lambda^2A_\lambda + 3g_1^2M_1 + 3g_2^2M_2 + \frac{1}{16\pi^2}\Big(\\
&- 20h_\tau^4A_\tau - 18h_b^4A_b - 6\lambda^4A_\lambda - 9h_\tau^2h_b^2\big(A_\tau + A_b\big) - 3h_\tau^2\lambda^2\big(A_\tau + A_\lambda\big) \\
&- 3h_t^2h_b^2\big(A_t + A_b\big) - 3h_t^2\lambda^2\big(A_t + A_\lambda\big) - 2\lambda^2\kappa^2\big(A_\lambda + A_\kappa\big) \\
&+ 2g_1^2h_\tau^2\big(A_\tau - M_1\big) - \frac{2}{3}g_1^2h_b^2\big(A_b - M_1\big) + 6g_2^2h_\tau^2\big(A_\tau - M_2\big) \\
&+ 16g_3^2h_b^2\big(A_b - M_3\big) - \{75, 105, 115\}g_1^4M_1 \\
&- \{15, 33, 39\}g_2^4M_2 - 3g_1^2g_2^2\big(M_1 + M_2\big)\Big)\,,
\end{aligned}
\tag{A.1}
$$

$$
\begin{aligned}
16\pi^2\frac{dA_\lambda}{dt} &= 4\lambda^2A_\lambda + 3h_t^2A_t + 3h_b^2A_b + h_\tau^2A_\tau + 2\kappa^2A_\kappa + g_1^2M_1 + 3g_2^2M_2 \\
&+ \frac{1}{16\pi^2}\Big(- 20\lambda^4A_\lambda - 18h_t^4A_t - 18h_b^4A_b - 6h_\tau^4A_\tau - 16\kappa^4A_\kappa \\
&- 9\lambda^2h_t^2\big(A_\lambda + A_t\big) - 9\lambda^2h_b^2\big(A_\lambda + A_b\big) - 3\lambda^2h_\tau^2\big(A_\lambda + A_\tau\big) \\
&- 12\lambda^2\kappa^2\big(A_\lambda + A_\kappa\big) - 6h_t^2h_b^2\big(A_t + A_b\big) + 2g_1^2\lambda^2(A_\lambda - M_1) \\
&+ \frac{4}{3}g_1^2h_t^2\big(A_t - M_1\big) - \frac{2}{3}g_1^2h_b^2\big(A_b - M_1\big) + 2g_1^2h_\tau^2\big(A_\tau - M_1\big) \\
&+ 6g_2^2\lambda^2\big(A_\lambda - M_2\big) + 16g_3^2h_t^2\big(A_t - M_3\big) + 16g_3^2h_b^2\big(A_b - M_3\big) \\
&- \{23, 33, \frac{109}{3}\}g_1^4M_1 - \{15, 33, 39\}g_2^4M_2 - 3g_1^2g_2^2\big(M_1 + M_2\big)\Big)\,, \\
16\pi^2\frac{dA_\kappa}{dt} &= 6\kappa^2A_\kappa + 6\lambda^2A_\lambda + \frac{1}{16\pi^2}\Big(- 48\kappa^4A_\kappa - 24\lambda^4A_\lambda \\
&- 24\kappa^2\lambda^2\big(A_\kappa + A_\lambda\big) - 18h_t^2\lambda^2\big(A_t + A_\lambda\big) - 18h_b^2\lambda^2\big(A_b + A_\lambda\big) \\
&- 6h_\tau^2\lambda^2\big(A_\tau + A_\lambda\big) + 6g_1^2\lambda^2\big(A_\lambda - M_1\big) + 18g_2^2\lambda^2\big(A_\lambda - M_2\big)\Big)\,.
\end{aligned}
\tag{A.2}
$$

Again, we follow the notation in [81] defining:

$$
\begin{aligned}
M_t^2 &= m_{Q_3}^2 + m_{U_3}^2 + m_{H_u}^2 + A_t^2 \,, \\
M_b^2 &= m_{Q_3}^2 + m_{D_3}^2 + m_{H_d}^2 + A_b^2 \,, \\
M_\tau^2 &= m_{L_3}^2 + m_{E_3}^2 + m_{H_d}^2 + A_\tau^2 \,, \\
M_\lambda^2 &= m_{H_u}^2 + m_{H_d}^2 + m_S^2 + A_\lambda^2 \,, \\
M_\kappa^2 &= 3m_S^2 + A_\kappa^2 \,, \\
\xi &= \mathrm{Tr}\big[\mathbf{m}_Q^2 - 2\mathbf{m}_U^2 + \mathbf{m}_D^2 - \mathbf{m}_L^2 + \mathbf{m}_E^2 + \{\mathbf{m}_{\bar{D}x}^2 - \mathbf{m}_{Dx}^2 + \mathbf{m}_{H_{ux}}^2 - \mathbf{m}_{H_{dx}}^2\}\big] + m_{H_u}^2 - m_{H_d}^2 \,, \\
\xi' &= h_t^2\big(-m_{Q_3}^2 + 4m_{U_3}^2 - 3m_{H_u}^2\big) + h_b^2\big(-m_{Q_3}^2 - 2m_{D_3}^2 + 3m_{H_d}^2\big) \\
&+ h_\tau^2\big(m_{L_3}^2 - 2m_{E_3}^2 + m_{H_d}^2\big) + \lambda^2\big(m_{H_d}^2 - m_{H_u}^2\big) \\
&+ g_1^2\Big(\mathrm{Tr}\Big[\frac{1}{18}\mathbf{m}_Q^2 - \frac{16}{9}\mathbf{m}_U^2 + \frac{2}{9}(\mathbf{m}_D^2 + \{\mathbf{m}_{\bar{D}x}^2 - \mathbf{m}_{Dx}^2\}) - \frac{1}{2}(\mathbf{m}_L^2 + \{+\mathbf{m}_{H_{ux}}^2 - \mathbf{m}_{H_{dx}}^2\}) + 2\mathbf{m}_E^2\Big] \\
&+ \frac{1}{2}\big(m_{H_u}^2 - m_{H_d}^2\big)\Big) \\
&+ \frac{3}{2}g_2^2\Big(\mathrm{Tr}\big[\mathbf{m}_Q^2 - \mathbf{m}_L^2 + \{\mathbf{m}_{H_{ux}}^2 - \mathbf{m}_{H_{dx}}^2\}\big] + m_{H_u}^2 - m_{H_d}^2\Big) \\
&+ \frac{8}{3}g_3^2\mathrm{Tr}\big[\mathbf{m}_Q^2 - 2\mathbf{m}_U^2 + \mathbf{m}_D^2\{+\mathbf{m}_{\bar{D}x}^2 - \mathbf{m}_{Dx}^2\}\big] \,, \\
\sigma_1 &= g_1^2\Big(\mathrm{Tr}\Big[\frac{1}{3}\mathbf{m}_Q^2 + \frac{8}{3}\mathbf{m}_U^2 + \frac{2}{3}(\mathbf{m}_D^2 + \{\mathbf{m}_{Dx}^2 + \mathbf{m}_{\bar{D}x}^2\}) \\
&+ \mathbf{m}_L^2 + 2\mathbf{m}_E^2 + \{\mathbf{m}_{H_{ux}}^2 + \mathbf{m}_{H_{dx}}^2\}\Big] + m_{H_u}^2 + m_{H_d}^2\Big) \,, \\
\sigma_2 &= g_2^2\Big(\mathrm{Tr}\big[3\mathbf{m}_Q^2 + \mathbf{m}_L^2 + \{\mathbf{m}_{H_{ux}}^2 + \mathbf{m}_{H_{dx}}^2\}\big] + m_{H_u}^2 + m_{H_d}^2\Big) \,, \\
\sigma_3 &= g_3^2\mathrm{Tr}\big[2\mathbf{m}_Q^2 + \mathbf{m}_U^2 + \mathbf{m}_D^2 + \{\mathbf{m}_{Dx}^2 + \mathbf{m}_{\bar{D}x}^2\}\big] \,.
\end{aligned}
\tag{A.3}
$$

where $\{\mathbf{m}_{\bar{D}x}^2, \mathbf{m}_{Dx}^2, \mathbf{m}_{H_{ux}}^2, \mathbf{m}_{H_{dx}}^2\}$ are diagonal 3×3 matrices in the NMSSM+, and diagonal 4×4 matrices in the NMSSM++.

The two-loop RGEs of the scalars in the NMSSM, NMSSM+, and NMSSM++ are,

$$
\begin{aligned}
16\pi^2\frac{dm^2_{Q_a}}{dt} &= \delta_{a3}h_t^2M_t^2+\delta_{a3}h_b^2M_b^2-\frac{1}{9}g_1^2M_1^2-3g_2^2M_2^2-\frac{16}{3}g_3^2M_3^2+\frac{1}{6}g_1^2\xi \\
&+ \frac{1}{16\pi^2}\Big(-10\delta_{a3}h_t^4\big(M_t^2+A_t^2\big)-10\delta_{a3}h_b^4\big(M_b^2+A_b^2\big) \\
&- \delta_{a3}h_t^2\lambda^2\big(M_t^2+M_\lambda^2+2A_tA_\lambda\big)-\delta_{a3}h_b^2h_\tau^2\big(M_b^2+M_\tau^2+2A_bA_\tau\big) \\
&- \delta_{a3}h_b^2\lambda^2\big(M_b^2+M_\lambda^2+2A_bA_\lambda\big)+\frac{4}{3}\delta_{a3}g_1^2h_t^2\big(M_t^2-2M_1(A_t-M_1)\big) \\
&+ \frac{2}{3}\delta_{a3}g_1^2h_b^2\big(M_b^2-2M_1(A_b-M_1)\big) \\
&+ \{199,289,319\}\frac{g_1^4M_1^2}{54}+\{33,87,105\}\frac{g_2^4M_2^2}{2}+\{-64,80,128\}\frac{g_3^4M_3^2}{3} \\
&+ \frac{1}{3}g_1^2g_2^2(M_1^2+M_2^2+M_1M_2)+\frac{16}{27}g_1^2g_3^2(M_1^2+M_3^2+M_1M_3) \\
&+ 16g_2^2g_3^2(M_2^2+M_3^2+M_2M_3)+\frac{1}{3}g_1^2\xi'+\frac{1}{18}g_1^2\sigma_1+\frac{3}{2}g_2^2\sigma_2+\frac{8}{3}g_3^2\sigma_3\Big)\,,
\end{aligned}
$$

$$
\begin{aligned}
16\pi^2\frac{dm_{U_a}^2}{dt} &= 2\delta_{a3}h_t^2M_t^2 - \frac{16}{9}g_1^2M_1^2 - \frac{16}{3}g_3^2M_3^2 - \frac{2}{3}g_1^2\xi \\
&+ \frac{1}{16\pi^2}\Big(- 16\delta_{a3}h_t^4\big(M_t^2+A_t^2\big) - 2\delta_{a3}h_t^2h_b^2\big(M_t^2+M_b^2+2A_tA_b\big) \\
&- 2\delta_{a3}h_t^2\lambda^2\big(M_t^2+M_\lambda^2+2A_tA_\lambda\big) - \frac{2}{3}\delta_{a3}g_1^2h_t^2\big(M_t^2-2M_1(A_t-M_1)\big) \\
&+ 6\delta_{a3}g_2^2h_t^2\big(M_t^2-2M_2(A_t-M_2)\big) \\
&+ \{1712,2432,2672\}\frac{g_1^4M_1^2}{27} + \{-64,80,128\}\frac{g_3^4M_3^2}{3} \\
&+ \frac{256}{27}g_1^2g_3^2(M_1^2+M_3^2+M_1M_3) - \frac{4}{3}g_1^2\xi' + \frac{8}{9}g_1^2\sigma_1 + \frac{8}{3}g_3^2\sigma_3\Big)\,, \\
16\pi^2\frac{dm_{D_a}^2}{dt} &= 2\delta_{a3}h_b^2M_b^2 - \frac{4}{9}g_1^2M_1^2 - \frac{16}{3}g_3^2M_3^2 + \frac{1}{3}g_1^2\xi \\
&+ \frac{1}{16\pi^2}\Big(- 16\delta_{a3}h_b^4\big(M_b^2+A_b^2\big) - 2\delta_{a3}h_b^2h_t^2\big(M_b^2+M_t^2+2A_bA_t\big) \\
&- 2\delta_{a3}h_b^2h_\tau^2\big(M_b^2+M_\tau^2+2A_bA_\tau\big) - 2\delta_{a3}h_b^2\lambda^2\big(M_b^2+M_\lambda^2+2A_bA_\lambda\big) \\
&+ \frac{2}{3}\delta_{a3}g_1^2h_b^2\big(M_b^2-2M_1(A_b-M_1)\big) + 6\delta_{a3}g_2^2h_b^2\big(M_b^2-2M_2(A_b-M_2)\big) \\
&+ \{404,584,644\}\frac{g_1^4M_1^2}{27} + \{-64,80,128\}\frac{g_3^4M_3^2}{3} \\
&+ \frac{64}{27}g_1^2g_3^2(M_1^2+M_3^2+M_1M_3) \\
&+ \frac{2}{3}g_1^2\xi' + \frac{2}{9}g_1^2\sigma_1 + \frac{8}{3}g_3^2\sigma_3\Big)\,, \\
16\pi^2\frac{dm_{L_a}^2}{dt} &= \delta_{a3}h_\tau^2M_\tau^2 - g_1^2M_1^2 - 3g_2^2M_2^2 - \frac{1}{2}g_1^2\xi + \frac{1}{16\pi^2}\Big(- 6\delta_{a3}h_\tau^4\big(M_\tau^2+A_\tau^2\big) \\
&- 3\delta_{a3}h_\tau^2h_b^2\big(M_\tau^2+M_b^2+2A_\tau A_b\big) - \delta_{a3}h_\tau^2\lambda^2\big(M_\tau^2+M_\lambda^2+2A_\tau A_\lambda\big) \\
&+ 2\delta_{a3}g_1^2h_\tau^2\big(M_\tau^2-2M_1(A_\tau-M_1)\big) + \{69,99,109\}\frac{g_1^4M_1^2}{2} + \{33,87,105\}\frac{g_2^4M_2^2}{2} \\
&+ 3g_1^2g_2^2(M_1^2+M_2^2+M_1M_2) - g_1^2\xi' + \frac{1}{2}g_1^2\sigma_1 + \frac{3}{2}g_2^2\sigma_2\Big)\,,
\end{aligned}
$$

$$
\begin{aligned}
16\pi^2\frac{dm_{E_a}^2}{dt} &= 2\delta_{a3}h_\tau^2M_\tau^2 - 4g_1^2M_1^2 + g_1^2\xi + \frac{1}{16\pi^2}\Big(- 8\delta_{a3}h_\tau^4\big(M_\tau^2+A_\tau^2\big) \\
&- 6\delta_{a3}h_\tau^2h_b^2\big(M_\tau^2+M_b^2+2A_\tau A_b\big) - 2\delta_{a3}h_\tau^2\lambda^2\big(M_\tau^2+M_\lambda^2+2A_\tau A_\lambda\big) \\
&- 2\delta_{a3}g_1^2h_\tau^2\big(M_\tau^2-2M_1(A_\tau-M_1)\big) + 6\delta_{a3}g_2^2h_\tau^2\big(M_\tau^2-2M_2(A_\tau-M_2)\big) \\
&+ \{156,216,236\}g_1^4M_1^2 + 2g_1^2\xi' + 2g_1^2\sigma_1\Big)\,. \qquad \text{(A.4)}
\end{aligned}
$$

The Two-loop RGEs of the Higgs doublets and singlet in the NMSSM, NMSSM+, and NMSSM++ are,

$$
\begin{aligned}
16\pi^2\frac{dm^2_{H_u}}{dt} &= 3h_t^2M_t^2+\lambda^2M_\lambda^2-g_1^2M_1^2-3g_2^2M_2^2+\frac{1}{2}g_1^2\xi \\
&+ \frac{1}{16\pi^2}\Big(-18h_t^4\big(M_t^2+A_t^2\big)-6\lambda^4\big(M_\lambda^2+A_\lambda^2\big) \\
&- 3h_t^2h_b^2\big(M_t^2+M_b^2+2A_tA_b\big)-3h_b^2\lambda^2\big(M_b^2+M_\lambda^2+2A_bA_\lambda\big) \\
&- h_\tau^2\lambda^2\big(M_\tau^2+M_\lambda^2+2A_\tau A_\lambda\big)-2\lambda^2\kappa^2\big(M_\lambda^2+M_\kappa^2+2A_\lambda A_\kappa\big) \\
&+ \frac{4}{3}g_1^2h_t^2\big(M_t^2-2M_1(A_t-M_1)\big)+16g_3^2h_t^2\big(M_t^2-2M_3(A_t-M_3)\big) \\
&+ \{69,99,109\}\frac{g_1^4M_1^2}{2}+\{33,87,105\}\frac{g_2^4M_2^2}{2} \\
&+ 3g_1^2g_2^2(M_1^2+M_2^2+M_1M_2) \\
&+ g_1^2\xi'+\frac{1}{2}g_1^2\sigma_1+\frac{3}{2}g_2^2\sigma_2\Big)\,, \\
16\pi^2\frac{dm^2_{H_d}}{dt} &= 3h_b^2M_b^2+h_\tau^2M_\tau^2+\lambda^2M_\lambda^2-g_1^2M_1^2-3g_2^2M_2^2-\frac{1}{2}g_1^2\xi \\
&+ \frac{1}{16\pi^2}\Big(-18h_b^4\big(M_b^2+A_b^2\big)-6h_\tau^4\big(M_\tau^2+A_\tau^2\big) \\
&- 6\lambda^4\big(M_\lambda^2+A_\lambda^2\big)-3h_b^2h_t^2\big(M_b^2+M_t^2+2A_bA_t\big) \\
&- 3h_t^2\lambda^2\big(M_t^2+M_\lambda^2+2A_tA_\lambda\big)-2\lambda^2\kappa^2\big(M_\lambda^2+M_\kappa^2+2A_\lambda A_\kappa\big) \\
&- \frac{2}{3}g_1^2h_b^2\big(M_b^2-2M_1(A_b-M_1)\big)+2g_1^2h_\tau^2\big(M_\tau^2-2M_1(A_\tau-M_1)\big) \\
&+ 16g_3^2h_b^2\big(M_b^2-2M_3(A_b-M_3)\big) \\
&+ \{69,99,109\}\frac{g_1^4M_1^2}{2}+\{33,87,105\}\frac{g_2^4M_2^2}{2} \\
&+ 3g_1^2g_2^2(M_1^2+M_2^2+M_1M_2)-g_1^2\xi'+\frac{1}{2}g_1^2\sigma_1+\frac{3}{2}g_2^2\sigma_2\Big)\,, \\
16\pi^2\frac{dm^2_{S}}{dt} &= 2\lambda^2M_\lambda^2+2\kappa^2M_\kappa^2+\frac{1}{16\pi^2}\Big(-8\lambda^4\big(M_\lambda^2+A_\lambda^2\big)-16\kappa^4\big(M_\kappa^2+A_\kappa^2\big) \\
&- 6\lambda^2h_t^2\big(M_\lambda^2+M_t^2+2A_\lambda A_t\big)-6\lambda^2h_b^2\big(M_\lambda^2+M_b^2+2A_\lambda A_b\big) \\
&- 2\lambda^2h_\tau^2\big(M_\lambda^2+M_\tau^2+2A_\lambda A_\tau\big)-8\lambda^2\kappa^2\big(M_\lambda^2+M_\kappa^2+2A_\lambda A_\kappa\big) \\
&+ 2g_1^2\lambda^2\big(M_\lambda^2-2M_1(A_\lambda-M_1)\big)+6g_2^2\lambda^2\big(M_\lambda^2-2M_2(A_\lambda-M_2)\big)\Big) \qquad \text{(A.5)}
\end{aligned}
$$

Finally, for completeness we add the one-loop RGEs of the extra matter, in the NMSSM+ and the NMSSM++

$$\begin{aligned}
16\pi^2 \frac{dm^2_{H^i_{ux}}}{dt} &= -g_1^2 M_1^2 - 3g_2^2 M_2^2 + \frac{1}{2} g_1^2 \xi \,, \\
16\pi^2 \frac{dm^2_{H^i_{dx}}}{dt} &= -g_1^2 M_1^2 - 3g_2^2 M_2^2 - \frac{1}{2} g_1^2 \xi \,, \\
16\pi^2 \frac{dm^2_{Dx^i}}{dt} &= -\frac{4}{9} g_1^2 M_1^2 - \frac{16}{3} g_3^2 M_3^2 - \frac{1}{3} g_1^2 \xi \,, \\
16\pi^2 \frac{dm^2_{\bar{D}x^i}}{dt} &= -\frac{4}{9} g_1^2 M_1^2 - \frac{16}{3} g_3^2 M_3^2 + \frac{1}{3} g_1^2 \xi \,.
\end{aligned} \tag{A.6}$$

Appendix B

cE$_6$SSM Benchmark points

Table B.1 lists the details on the masses and parameters associated with each benchmark (BM) point that was chosen. We can see that m_0 increases significantly as s ($M_{Z'}$) becomes larger, while $m_{1/2}$ is roughly constant. Upon choosing a BM point, we imposed the limit $m_{1/2} > 1$ TeV to have gluino mass $m_{\tilde{g}} > 850$ GeV. The gluino masses for our benchmark points are about 900 GeV or close to it, hence if the experimental limits on $m_{\tilde{g}}$ are to be increased for constrained models, then fine tuning will increase as well. The lightest stop, $\tilde{t}_1$, masses range from 1.7 TeV to 2.4 TeV for the range of s we studied, and thereby is above the experimental limits.

	BM1	BM2	BM3	BM4	BM5	BM6
s [TeV]	5	6	7	8	9	10
$\tan\beta$	10	10	10	10	10	10
$\lambda_3(M_X)$	-0.2284	-0.2646	-0.25	-0.2376	-0.2260	-0.2171
$\lambda_{1,2}(M_X)$	0.1	0.1	0.1	0.1	0.1	0.1
$\kappa_{1,2,3}(M_X)$	0.1760	0.1923	0.2111	0.2288	0.2452	0.2601
$m_{1/2}$ [GeV]	1033	1003	1004	1002	1001	1005
m_0 [GeV]	2020	1951	2186	2441	2709	2975
A_0 [GeV]	-83	500	661	781	846	888
$m_{\tilde{D}_1}(1,2,3)$ [GeV]	2252	2234	2659	3149	3680	4222
$m_{\tilde{D}_2}(1,2,3)$ [GeV]	3186	3501	3991	4499	5017	5540
$\mu_D(1,2,3)$ [GeV]	1782	2238	2752	3279	3812	4347
$\lvert m_{\chi_6^0}\rvert$ [GeV]	1973	2349	2727	3105	3483	3861
$m_{h_3} \simeq M_{Z'}$ [GeV]	1889	2267	2645	3023	3401	3779
$\lvert m_{\chi_5^0}\rvert$ [GeV]	1809	2189	2566	2944	3322	3699
$m_s(1,2)$ [GeV]	2448	2548	2897	3263	3639	4014
$m_{H_2}(1,2)$ [GeV]	1970	1847	2023	2218	2426.5	2633
$m_{H_1}(1,2)$ [GeV]	1887	1685	1824	1986	2167	2343
$\mu_{\tilde{H}}(1,2)$ [GeV]	492	569	642	711	777	841
$m_{\tilde{u}_1}(1,2)$ [GeV]	2505	2461	2687	2934	3199	3468
$m_{\tilde{u}_1} \simeq m_{\tilde{d}_1}(1,2)$ [GeV]	2553	2507	2729	2973	3235	3501
$m_{\tilde{d}_2}(1,2)$ [GeV]	2571	2558	2810	3082	3372	3665
$m_{\tilde{e}_1}(1,2,3)$ [GeV]	2136	2107	2366	2641	2935	3224
$m_{\tilde{e}_2}(1,2,3)$ [GeV]	2267	2271	2550	2848	3159	3468
$m_{\tilde{\tau}_1}$ [GeV]	2119	2090	2347	2623	2912	3200
$m_{\tilde{\tau}_2}$ [GeV]	2259	2263	2541	2838	3148	3457
$m_{\tilde{b}_1}$ [GeV]	2202	2151	2340	2549	2777	3009
$m_{\tilde{b}_2}$ [GeV]	2552	2539	2789	3059	3347	3639
$m_{\tilde{t}_1}$ [GeV]	1741	1681	1839	2016	2212	2411
$m_{\tilde{t}_2}$ [GeV]	2215	2166	2354	2561	2787	3018
$\lvert m_{\chi_{3,4}^0}\rvert \simeq \lvert m_{\chi_2^\pm}\rvert$ [GeV]	887	1174	1258	1329	1386	1443
$m_{h_2} \simeq m_A \simeq m_{H^\pm}$ [GeV]	1890	2268	2646	3025	3403	3782
m_h [GeV]	124	124	125	125	125	125
$m_{\tilde{g}}$ [GeV]	901	879	887	892	898	906
$\lvert m_{\chi_1^\pm}\rvert \simeq \lvert m_{\chi_2^0}\rvert$ [GeV]	285	279	279	279	279	280
$\lvert m_{\chi_1^0}\rvert$ [GeV]	162	157	158	158	158	158
Δ_{max}	251	233	270	302	330	359

TABLE B.1: Parameters and masses for the benchmarks with lowest fine tuning and Higgs masses in the range of $m_h = 124 - 125$ GeV in the cE$_6$SSM.

B.1 Fine tuning and $m_{\tilde{g}}$

As the lower limits on the gluino mass are expected to rise, Table B.2 shows the minimum amount of the fine tuning corresponding to different values of gluino mass within $m_{\tilde{g}} = 1 - 1.5$ TeV, and for $s = 5 - 10$ TeV. The corresponding Higgs mass is shown in parenthesis next to each value of fine tuning.

s [TeV]	5	6	7	8	9	10
$m_{\tilde{g}}$ [TeV]	Δ (m_h [GeV])					
1	293 (124)	297 (124)	324 (125)	367 (125)	405 (126)	443 (126)
1.1	388 (125)	348 (124)	358 (124)	408 (125)	454 (126)	497 (126)
1.2	474 (124)	440 (125)	400 (124)	448 (125)	500 (126)	550 (126)
1.3	-	556 (125)	462 (124)	484 (124)	547 (126)	600 (126)
1.4	-	658 (125)	617 (126)	525 (124)	587 (125)	650 (126)
1.5	-	-	767 (125)	635 (125)	628 (125)	699 (126)

TABLE B.2: For different values of the singlet VEV ($s = 5 - 10$ TeV) corresponding to $M_{Z'} \sim 2 - 3.8$ TeV, the effect of rising the lower limit on the gluino mass between $m_{\tilde{g}} = 1 - 1.5$ TeV on fine tuning is shown. Next to every fine tuning value, the corresponding Higgs mass (in GeV) is shown between parentheses. The dash means there's no $m_h \sim 124 - 127$ GeV found in the scanned parameter space.

Bibliography

[1] Steven Weinberg. The Quantum theory of fields. Vol. 1: Foundations. 1995.

[2] S.F. Novaes. Standard model: An Introduction. 1999.

[3] Michael E. Peskin and Daniel V. Schroeder. An Introduction to quantum field theory. 1995.

[4] P.D.B. Collins, Alan D. Martin, and E.J. Squires. PARTICLE PHYSICS AND COSMOLOGY. 1989.

[5] C.P. Burgess and G.D. Moore. The standard model: A primer. 2007.

[6] Murray Gell-Mann. A Schematic Model of Baryons and Mesons. *Phys.Lett.*, 8:214–215, 1964.

[7] G. Zweig. An SU(3) model for strong interaction symmetry and its breaking. Version 1. 1964.

[8] G. Zweig. An SU(3) model for strong interaction symmetry and its breaking. Version 2. pages 22–101, 1964.

[9] J.D. Bjorken and S.L. Glashow. Elementary Particles and SU(4). *Phys.Lett.*, 11:255–257, 1964.

[10] Haim Harari. A New Quark Model for Hadrons. *Phys.Lett.*, B57:265, 1975.

[11] K.A. Olive et al. Review of Particle Physics. *Chin.Phys.*, C38:090001, 2014.

[12] Martin L. Perl, G.S. Abrams, A. Boyarski, Martin Breidenbach, D. Briggs, et al. Evidence for Anomalous Lepton Production in e+ - e- Annihilation. *Phys.Rev.Lett.*, 35:1489–1492, 1975.

[13] S. Tomonaga. On a relativistically invariant formulation of the quantum theory of wave fields. *Prog.Theor.Phys.*, 1:27–42, 1946.

[14] R.P. Feynman. Relativistic cutoff for quantum electrodynamics. *Phys.Rev.*, 74:1430–1438, 1948.

[15] Julian S. Schwinger. Quantum electrodynamics. I A covariant formulation. *Phys.Rev.*, 74:1439, 1948.

[16] F.J. Dyson. The Radiation theories of Tomonaga, Schwinger, and Feynman. *Phys.Rev.*, 75:486–502, 1949.

[17] H. Fritzsch, Murray Gell-Mann, and H. Leutwyler. Advantages of the Color Octet Gluon Picture. *Phys.Lett.*, B47:365–368, 1973.

[18] A. Pich. Quantum chromodynamics. 1995.

[19] J. Goldstone. Field Theories with Superconductor Solutions. *Nuovo Cim.*, 19:154–164, 1961.

[20] F. Englert and R. Brout. Broken Symmetry and the Mass of Gauge Vector Mesons. *Physical Review Letters*, 13:321–323, August 1964.

[21] P. W. Higgs. Broken Symmetries and the Masses of Gauge Bosons. *Physical Review Letters*, 13:508–509, October 1964.

[22] G. S. Guralnik, C. R. Hagen, and T. W. Kibble. Global Conservation Laws and Massless Particles. *Physical Review Letters*, 13:585–587, November 1964.

[23] Steven Weinberg. A Model of Leptons. *Phys.Rev.Lett.*, 19:1264–1266, 1967.

[24] Antonio Pich. The Standard model of electroweak interactions. 2007.

[25] Georges Aad et al. Observation of a new particle in the search for the Standard Model Higgs boson with the ATLAS detector at the LHC. *Phys.Lett.*, B716:1–29, 2012.

[26] Serguei Chatrchyan et al. Observation of a new boson at a mass of 125 GeV with the CMS experiment at the LHC. *Phys.Lett.*, B716:30–61, 2012.

[27] David J. Gross and Frank Wilczek. Ultraviolet Behavior of Nonabelian Gauge Theories. *Phys.Rev.Lett.*, 30:1343–1346, 1973.

[28] H. David Politzer. Reliable Perturbative Results for Strong Interactions? *Phys.Rev.Lett.*, 30:1346–1349, 1973.

[29] Gerard 't Hooft. Naturalness, chiral symmetry, and spontaneous chiral symmetry breaking. *NATO Adv.Study Inst.Ser.B Phys.*, 59:135, 1980.

[30] Sergey Troitsky. Unsolved problems in particle physics. *Phys.Usp.*, 55:72–95, 2012.

[31] Gary Steigman and Michael S. Turner. Cosmological Constraints on the Properties of Weakly Interacting Massive Particles. *Nucl.Phys.*, B253:375, 1985.

[32] Gianfranco Bertone, Dan Hooper, and Joseph Silk. Particle dark matter: Evidence, candidates and constraints. *Phys.Rept.*, 405:279–390, 2005.

[33] Adrian Signer. ABC of SUSY. *J.Phys.*, G36:073002, 2009.

[34] Stephen P. Martin. A Supersymmetry primer. 1997.

[35] Daniele Bertolini, Jesse Thaler, and Zachary Thomas. TASI 2012: Super-Tricks for Superspace. 2013.

[36] Savas Dimopoulos and Howard Georgi. Softly Broken Supersymmetry and SU(5). *Nucl.Phys.*, B193:150, 1981.

[37] D.J. Miller and A.P. Morais. Supersymmetric SU(5) Grand Unification for a Post Higgs Boson Era. *JHEP*, 1310:226, 2013.

[38] Jonathan L. Feng, Konstantin T. Matchev, and Takeo Moroi. Focus points and naturalness in supersymmetry. *Phys.Rev.*, D61:075005, 2000.

[39] John R. Ellis, K. Enqvist, Dimitri V. Nanopoulos, and F. Zwirner. Observables in Low-Energy Superstring Models. *Mod.Phys.Lett.*, A1:57, 1986.

[40] Riccardo Barbieri and G.F. Giudice. Upper Bounds on Supersymmetric Particle Masses. *Nucl.Phys.*, B306:63, 1988.

[41] S. Dimopoulos and G.F. Giudice. Naturalness constraints in supersymmetric theories with nonuniversal soft terms. *Phys.Lett.*, B357:573–578, 1995.

[42] B. de Carlos and J.A. Casas. One loop analysis of the electroweak breaking in supersymmetric models and the fine tuning problem. *Phys.Lett.*, B309:320–328, 1993.

[43] B. de Carlos and J.A. Casas. The Fine tuning problem of the electroweak symmetry breaking mechanism in minimal SUSY models. 1993.

[44] Piotr H. Chankowski, John R. Ellis, and Stefan Pokorski. The Fine tuning price of LEP. *Phys.Lett.*, B423:327–336, 1998.

[45] K. Agashe and M. Graesser. Improving the fine tuning in models of low-energy gauge mediated supersymmetry breaking. *Nucl.Phys.*, B507:3–34, 1997.

[46] David Wright. Naturally nonminimal supersymmetry. 1998.

[47] Gordon L. Kane and S.F. King. Naturalness implications of LEP results. *Phys.Lett.*, B451:113–122, 1999.

[48] M. Bastero-Gil, Gordon L. Kane, and S.F. King. Fine tuning constraints on supergravity models. *Phys.Lett.*, B474:103–112, 2000.

[49] B.C. Allanach, J.P.J. Hetherington, Michael Andrew Parker, and B.R. Webber. Naturalness reach of the large hadron collider in minimal supergravity. *JHEP*, 0008:017, 2000.

[50] Radovan Dermisek and John F. Gunion. Escaping the large fine tuning and little hierarchy problems in the next to minimal supersymmetric model and h —¿ aa decays. *Phys.Rev.Lett.*, 95:041801, 2005.

[51] Riccardo Barbieri and Lawrence J. Hall. Improved naturalness and the two Higgs doublet model. 2005.

[52] B.C. Allanach. Naturalness priors and fits to the constrained minimal supersymmetric standard model. *Phys.Lett.*, B635:123–130, 2006.

[53] Ben Gripaios and Stephen M. West. Improved Higgs naturalness with or without supersymmetry. *Phys.Rev.*, D74:075002, 2006.

[54] Radovan Dermisek, John F. Gunion, and Bob McElrath. Probing NMSSM Scenarios with Minimal Fine-Tuning by Searching for Decays of the Upsilon to a Light CP-Odd Higgs Boson. *Phys.Rev.*, D76:051105, 2007.

[55] Riccardo Barbieri, Lawrence J. Hall, and Vyacheslav S. Rychkov. Improved naturalness with a heavy Higgs: An Alternative road to LHC physics. *Phys.Rev.*, D74:015007, 2006.

[56] Tatsuo Kobayashi, Haruhiko Terao, and Akito Tsuchiya. Fine-tuning in gauge mediated supersymmetry breaking models and induced top Yukawa coupling. *Phys.Rev.*, D74:015002, 2006.

[57] Maxim Perelstein and Bibhushan Shakya. XENON100 Implications for Naturalness in the MSSM, NMSSM and lambda-SUSY. 2012.

[58] Stefan Antusch, Lorenzo Calibbi, Vinzenz Maurer, Maurizio Monaco, and Martin Spinrath. Naturalness of the Non-Universal MSSM in the Light of the Recent Higgs Results. *JHEP*, 01:187, 2013.

[59] Taoli Cheng, Jinmian Li, Tianjun Li, Xia Wan, You kai Wang, et al. Toward the Natural and Realistic NMSSM with and without R-Parity. 2012.

[60] Matthew W. Cahill-Rowley, JoAnne L. Hewett, Ahmed Ismail, and Thomas G. Rizzo. The Higgs Sector and Fine-Tuning in the pMSSM. *Phys.Rev.*, D86:075015, 2012.

[61] Graham G. Ross, Kai Schmidt-Hoberg, and Florian Staub. The Generalised NMSSM at One Loop: Fine Tuning and Phenomenology. *JHEP*, 1208:074, 2012.

[62] Tanushree Basak and Subhendra Mohanty. Triplet-Singlet Extension of the MSSM with a 125 Gev Higgs and Dark Matter. *Phys.Rev.*, D86:075031, 2012.

[63] Zhaofeng Kang, Jinmian Li, and Tianjun Li. On Naturalness of the MSSM and NMSSM. *JHEP*, 1211:024, 2012.

[64] Greg W. Anderson and Diego J. Castano. Measures of fine tuning. *Phys.Lett.*, B347:300–308, 1995.

[65] Greg W. Anderson and Diego J. Castano. Naturalness and superpartner masses or when to give up on weak scale supersymmetry. *Phys.Rev.*, D52:1693–1700, 1995.

[66] Greg W. Anderson and Diego J. Castano. Challenging weak scale supersymmetry at colliders. *Phys.Rev.*, D53:2403–2410, 1996.

[67] Greg W. Anderson, Diego J. Castano, and Antonio Riotto. Naturalness lowers the upper bound on the lightest Higgs boson mass in supersymmetry. *Phys.Rev.*, D55:2950–2954, 1997.

[68] Paolo Ciafaloni and Alessandro Strumia. Naturalness upper bounds on gauge mediated soft terms. *Nucl.Phys.*, B494:41–53, 1997.

[69] Kwok Lung Chan, Utpal Chattopadhyay, and Pran Nath. Naturalness, weak scale supersymmetry and the prospect for the observation of supersymmetry at the Tevatron and at the CERN LHC. *Phys.Rev.*, D58:096004, 1998.

[70] Riccardo Barbieri and Alessandro Strumia. About the fine tuning price of LEP. *Phys.Lett.*, B433:63–66, 1998.

[71] Leonardo Giusti, Andrea Romanino, and Alessandro Strumia. Natural ranges of supersymmetric signals. *Nucl.Phys.*, B550:3–31, 1999.

[72] J.A. Casas, J.R. Espinosa, and I. Hidalgo. The MSSM fine tuning problem: A Way out. *JHEP*, 0401:008, 2004.

[73] J.A. Casas, J.R. Espinosa, and I. Hidalgo. A Relief to the supersymmetric fine tuning problem. pages 76–85, 2004.

[74] J.A. Casas, J.R. Espinosa, and I. Hidalgo. Implications for new physics from fine-tuning arguments. 1. Application to SUSY and seesaw cases. *JHEP*, 0411:057, 2004.

[75] J.A. Casas, J.R. Espinosa, and I. Hidalgo. Expectations for LHC from naturalness: modified versus SM Higgs sector. *Nucl.Phys.*, B777:226–252, 2007.

[76] Ryuichiro Kitano and Yasunori Nomura. A Solution to the supersymmetric fine-tuning problem within the MSSM. *Phys.Lett.*, B631:58–67, 2005.

[77] Peter Athron and D.J. Miller. A New Measure of Fine Tuning. *Phys.Rev.*, D76:075010, 2007.

[78] Howard Baer, Vernon Barger, Peisi Huang, Azar Mustafayev, and Xerxes Tata. Radiative natural SUSY with a 125 GeV Higgs boson. *Phys.Rev.Lett.*, 109:161802, 2012.

[79] Philipp Grothaus, Manfred Lindner, and Yasutaka Takanishi. Naturalness of Neutralino Dark Matter. *JHEP*, 1307:094, 2013.

[80] M. Maniatis. The Next-to-Minimal Supersymmetric extension of the Standard Model reviewed. *Int.J.Mod.Phys.*, A25:3505–3602, 2010.

[81] Ulrich Ellwanger, Cyril Hugonie, and Ana M. Teixeira. The Next-to-Minimal Supersymmetric Standard Model. *Phys.Rept.*, 496:1–77, 2010.

[82] D.J. Miller, R. Nevzorov, and P.M. Zerwas. The Higgs sector of the next-to-minimal supersymmetric standard model. *Nucl.Phys.*, B681:3–30, 2004.

[83] A. Dedes, C. Hugonie, S. Moretti, and K. Tamvakis. Phenomenology of a new minimal supersymmetric extension of the standard model. *Phys.Rev.*, D63:055009, 2001.

[84] JoAnne L. Hewett and Thomas G. Rizzo. Low-Energy Phenomenology of Superstring Inspired E(6) Models. *Phys.Rept.*, 183:193, 1989.

[85] E. Keith and Ernest Ma. Generic consequences of a supersymmetric U(1) gauge factor at the TeV scale. *Phys.Rev.*, D56:7155–7165, 1997.

[86] Serguei Chatrchyan et al. Observation of a new boson with mass near 125 GeV in pp collisions at $\sqrt{s} = 7$ and 8 TeV. *JHEP*, 1306:081, 2013.

[87] Eldad Gildener and Steven Weinberg. Symmetry breaking and scalar bosons. *Phys. Rev. D*, 13:3333–3341, Jun 1976.

[88] Leonard Susskind. Dynamics of Spontaneous Symmetry Breaking in the Weinberg-Salam Theory. *Phys.Rev.*, D20:2619–2625, 1979.

[89] Search for supersymmetry in hadronic final states using MT2 with the CMS detector at sqrt(s) = 8 TeV. Technical Report CMS-PAS-SUS-13-019, CERN, Geneva, 2014.

[90] Jonathan L. Feng. Naturalness and the Status of Supersymmetry. *Ann.Rev.Nucl.Part.Sci.*, 63:351–382, 2013.

[91] Nathaniel Craig. The State of Supersymmetry after Run I of the LHC. 2013.

[92] M. Bastero-Gil, C. Hugonie, S.F. King, D.P. Roy, and S. Vempati. Does LEP prefer the NMSSM? *Phys.Lett.*, B489:359–366, 2000.

[93] Ulrich Ellwanger, Gregory Espitalier-Noel, and Cyril Hugonie. Naturalness and Fine Tuning in the NMSSM: Implications of Early LHC Results. *JHEP*, 1109:105, 2011.

[94] Doyoun Kim, Peter Athron, Csaba Balzs, Benjamin Farmer, and Elliot Hutchison. Bayesian naturalness of the C(N)MSSM. 2013.

[95] S.F. King and P.L. White. Nonminimal supersymmetric Higgs bosons at LEP-2. *Phys.Rev.*, D53:4049–4062, 1996.

[96] M. Masip, R. Munoz-Tapia, and A. Pomarol. Limits on the mass of the lightest Higgs in supersymmetric models. *Phys.Rev.*, D57:R5340, 1998.

[97] Riccardo Barbieri, Lawrence J. Hall, Anastasios Y. Papaioannou, Duccio Pappadopulo, and Vyacheslav S. Rychkov. An Alternative NMSSM phenomenology with manifest perturbative unification. *JHEP*, 0803:005, 2008.

[98] S.F. King, M. Muhlleitner, and R. Nevzorov. NMSSM Higgs Benchmarks Near 125 GeV. *Nucl.Phys.*, B860:207–244, 2012.

[99] Lawrence J. Hall, David Pinner, and Joshua T. Ruderman. A Natural SUSY Higgs Near 126 GeV. *JHEP*, 1204:131, 2012.

[100] Alexander Vilenkin. Cosmic Strings and Domain Walls. *Phys.Rept.*, 121:263, 1985.

[101] Jonathan P. Hall and Stephen F. King. NMSSM+. *JHEP*, 1301:076, 2013.

[102] James C. Callaghan, Stephen F. King, and George K. Leontaris. Gauge coupling unification in E_6 F-theory GUTs with matter and bulk exotics from flux breaking. *JHEP*, 1312:037, 2013.

[103] H. Nishino et al. Search for Proton Decay via p —¿ e+ pi0 and p —¿ mu+ pi0 in a Large Water Cherenkov Detector. *Phys.Rev.Lett.*, 102:141801, 2009.

[104] Edward Hardy. Is Natural SUSY Natural? *JHEP*, 1310:133, 2013.

[105] Asimina Arvanitaki, Masha Baryakhtar, Xinlu Huang, Ken Van Tilburg, and Giovanni Villadoro. The Last Vestiges of Naturalness. 2013.

[106] Kamila Kowalska, Leszek Roszkowski, Enrico Maria Sessolo, and Sebastian Trojanowski. Low fine tuning in the MSSM with higgsino dark matter and unification constraints. 2014.

[107] Anna Kaminska, Graham G. Ross, Kai Schmidt-Hoberg, and Florian Staub. A precision study of the fine tuning in the DiracNMSSM. 2014.

[108] Anna Kaminska, Graham G. Ross, and Kai Schmidt-Hoberg. Non-universal gaugino masses and fine tuning implications for SUSY searches in the MSSM and the GNMSSM. 2013.

[109] Celine Boehm, P. S. Bhupal Dev, Anupam Mazumdar, and Ernestas Pukartas. Naturalness of Light Neutralino Dark Matter in pMSSM after LHC, XENON100 and Planck Data. *JHEP*, 1306:113, 2013.

[110] Zygmunt Lalak and Marek Lewicki. Fine-tuning in GGM and the 126 GeV Higgs particle. *JHEP*, 1305:125, 2013.

[111] Sylvain Fichet. Quantified naturalness from Bayesian statistics. *Phys.Rev.*, D86:125029, 2012.

[112] Tony Gherghetta, Benedict von Harling, Anibal D. Medina, and Michael A. Schmidt. The Scale-Invariant NMSSM and the 126 GeV Higgs Boson. *JHEP*, 02:032, 2013.

[113] Kaustubh Agashe, Yanou Cui, and Roberto Franceschini. Natural Islands for a 125 GeV Higgs in the scale-invariant NMSSM. *JHEP*, 1302:031, 2013.

[114] Peter Athron, Maien Binjonaid, and Stephen F. King. Fine Tuning in the Constrained Exceptional Supersymmetric Standard Model. *Phys.Rev.*, D87:115023, 2013.

[115] Ulrich Ellwanger and Cyril Hugonie. NMSPEC: A Fortran code for the sparticle and Higgs masses in the NMSSM with GUT scale boundary conditions. *Comput.Phys.Commun.*, 177:399–407, 2007.

[116] Stephen P. Martin and Michael T. Vaughn. Two loop renormalization group equations for soft supersymmetry breaking couplings. *Phys.Rev.*, D50:2282, 1994.

[117] Florian Staub. Automatic Calculation of supersymmetric Renormalization Group Equations and Self Energies. *Comput.Phys.Commun.*, 182:808–833, 2011.

[118] G. Belanger, F. Boudjema, A. Pukhov, and A. Semenov. micrOMEGAs$_3$: A program for calculating dark matter observables. *Comput.Phys.Commun.*, 185:960–985, 2014.

[119] Florian Domingo and Ulrich Ellwanger. Constraints from the Muon g-2 on the Parameter Space of the NMSSM. *JHEP*, 0807:079, 2008.

[120] S. Schael et al. Search for neutral MSSM Higgs bosons at LEP. *Eur.Phys.J.*, C47:547–587, 2006.

[121] R. Barate et al. Search for the standard model Higgs boson at LEP. *Phys.Lett.*, B565:61–75, 2003.

[122] Searches for invisible Higgs bosons: Preliminary combined results using LEP data collected at energies up to 209-GeV. 2001.

[123] Y. Amhis et al. Averages of B-Hadron, C-Hadron, and tau-lepton properties as of early 2012. 2012.

[124] R Aaij et al. First Evidence for the Decay $B_s^0 \to \mu^+\mu^-$. *Phys.Rev.Lett.*, 110(2):021801, 2013.

[125] I. Adachi et al. Evidence for $B^- \to \tau^- \bar{\nu}_\tau$ with a Hadronic Tagging Method Using the Full Data Sample of Belle. *Phys.Rev.Lett.*, 110(13):131801, 2013.

[126] G. Belanger, B. Dumont, U. Ellwanger, J.F. Gunion, and S. Kraml. Global fit to Higgs signal strengths and couplings and implications for extended Higgs sectors. *Phys.Rev.*, D88:075008, 2013.

[127] Search for squarks and gluinos in events with isolated leptons, jets and missing transverse momentum at $\sqrt{s} = 8$ tev with the atlas detector. Technical Report ATLAS-CONF-2013-062, CERN, Geneva, Jun 2013.

[128] Genevieve Belanger, Ulrich Ellwanger, John F. Gunion, Yun Jiang, Sabine Kraml, et al. Higgs Bosons at 98 and 125 GeV at LEP and the LHC. *JHEP*, 1301:069, 2013.

[129] P.A.R. Ade et al. Planck 2013 results. XVI. Cosmological parameters. *Astron.Astrophys.*, 571:A16, 2014.

[130] Ulrich Ellwanger and Cyril Hugonie. The semi-constrained NMSSM satisfying bounds from the LHC, LUX and Planck. *JHEP*, 1408:046, 2014.

[131] Georges Aad et al. Search for a heavy top-quark partner in final states with two leptons with the ATLAS detector at the LHC. *JHEP*, 1211:094, 2012.

[132] Georges Aad et al. Hunt for new phenomena using large jet multiplicities and missing transverse momentum with ATLAS in 4.7 fb^{-1} of $\sqrt{s} = 7$ TeV proton-proton collisions. *JHEP*, 1207:167, 2012.

[133] D.J.H. Chung, L.L. Everett, G.L. Kane, S.F. King, Joseph D. Lykken, et al. The Soft supersymmetry breaking Lagrangian: Theory and applications. *Phys.Rept.*, 407:1–203, 2005.

[134] S. Cassel and D.M. Ghilencea. A Review of naturalness and dark matter prediction for the Higgs mass in MSSM and beyond. *Mod.Phys.Lett.*, A27:1230003, 2012.

[135] Dumitru M. Ghilencea, Hyun Min Lee, and Myeonghun Park. Tuning supersymmetric models at the LHC: A comparative analysis at two-loop level. *JHEP*, 1207:046, 2012.

[136] S.F. King, S. Moretti, and R. Nevzorov. Theory and phenomenology of an exceptional supersymmetric standard model. *Phys.Rev.*, D73:035009, 2006.

[137] S.F. King, S. Moretti, and R. Nevzorov. Exceptional supersymmetric standard model. *Phys.Lett.*, B634:278–284, 2006.

[138] Ulrich Ellwanger, Michel Rausch de Traubenberg, and Carlos A. Savoy. Particle spectrum in supersymmetric models with a gauge singlet. *Phys.Lett.*, B315:331–337, 1993.

[139] Ulrich Ellwanger, Michel Rausch de Traubenberg, and Carlos A. Savoy. Higgs phenomenology of the supersymmetric model with a gauge singlet. *Z.Phys.*, C67:665–670, 1995.

[140] Ulrich Ellwanger. Radiative corrections to the neutral Higgs spectrum in supersymmetry with a gauge singlet. *Phys.Lett.*, B303:271–276, 1993.

[141] P.N. Pandita. Radiative corrections to the scalar Higgs masses in a nonminimal supersymmetric Standard Model. *Z.Phys.*, C59:575–584, 1993.

[142] T. Elliott, S.F. King, and P.L. White. Radiative corrections to Higgs boson masses in the next-to-minimal supersymmetric Standard Model. *Phys.Rev.*, D49:2435–2456, 1994.

[143] S.F. King and P.L. White. Resolving the constrained minimal and next-to-minimal supersymmetric standard models. *Phys.Rev.*, D52:4183–4216, 1995.

[144] F. Franke and H. Fraas. Neutralinos and Higgs bosons in the next-to-minimal supersymmetric standard model. *Int.J.Mod.Phys.*, A12:479–534, 1997.

[145] Serguei Chatrchyan et al. Search for narrow resonances in dilepton mass spectra in pp collisions at $\sqrt{s} = 7$ TeV. *Phys.Lett.*, B714:158–179, 2012.

[146] P. Athron, S.F. King, D.J. Miller, S. Moretti, and R. Nevzorov. LHC Signatures of the Constrained Exceptional Supersymmetric Standard Model. *Phys.Rev.*, D84:055006, 2011.

[147] Peter Athron, Jonathan P. Hall, Richard Howl, Stephen F. King, D.J. Miller, et al. Aspects of the exceptional supersymmetric standard model. *Nucl.Phys.Proc.Suppl.*, 200-202:120–129, 2010.

[148] P. Athron, S.F. King, D.J. Miller, S. Moretti, and R. Nevzorov. The Constrained Exceptional Supersymmetric Standard Model. *Phys.Rev.*, D80:035009, 2009.

[149] P. Athron, S.F. King, D.J. Miller, S. Moretti, and R. Nevzorov. Predictions of the Constrained Exceptional Supersymmetric Standard Model. *Phys.Lett.*, B681:448–456, 2009.

[150] P. Athron, S.F. King, D.J. Miller, S. Moretti, and R. Nevzorov. Constrained Exceptional Supersymmetric Standard Model with a Higgs Near 125 GeV. *Phys.Rev.*, D86:095003, 2012.

[151] Peter Athron, Dominik Stockinger, and Alexander Voigt. Threshold Corrections in the Exceptional Supersymmetric Standard Model. *Phys.Rev.*, D86:095012, 2012.

[152] James C. Callaghan and Stephen F. King. E6 Models from F-theory. *JHEP*, 1304:034, 2013.

[153] R. Howl and S.F. King. Exceptional Supersymmetric Standard Models with non-Abelian Discrete Family Symmetry. *JHEP*, 0805:008, 2008.

[154] R. Howl and S.F. King. Solving the Flavour Problem in Supersymmetric Standard Models with Three Higgs Families. *Phys.Lett.*, B687:355–362, 2010.

[155] Alexander Belyaev, Jonathan P. Hall, Stephen F. King, and Patrik Svantesson. Novel gluino cascade decays in E_6 inspired models. *Phys.Rev.*, D86:031702, 2012.

[156] Alexander Belyaev, Stephen F. King, and Patrik Svantesson. Little Z models. *Phys.Rev.*, D88(3):035015, 2013.